

AD-A248 495



(2)

**COMPUTER-CONTROLLED ION BEAM SPUTTER-DEPOSITION
OF SUPERCONDUCTING OXIDE FILMS**

DARPA Contract No. N00014-88-K-0525

Final project report
Covering the period July 1, 1988 - Dec. 31, 1991

DTIC
S **ELECTE** **D**
APR 9 1992
C

Principal Investigators:

Orlando H. Auciello*

Angus I. Kingon

Robert F. Davis

North Carolina State University
Department of Materials Science and Engineering
Raleigh, NC 27695-7907
(919) 515-2347

*also Microelectronics Center of North Carolina
Research Triangle Park, NC

Report prepared in collaboration with Dr. Daniel J. Lichtenwalner, post-doctoral
research associate

The views and conclusions contained in this document are those of the
authors and should not be interpreted as necessarily representing the
official policies, either expressed or implied, of the Defense Advanced
Research Projects Agency or the U.S. Government.

EXCLUDED FROM AUTOMATIC DECLASSIFICATION

Approved for public release;
Distribution Unlimited

92 4 06 09 8

92-08861



TABLE OF CONTENTS

Project summary.....	4
1. Introduction to $\text{YBa}_2\text{Cu}_3\text{O}_{7-\delta}$ materials issues.....	7
2. Deposition system design and development.....	10
2.1 Deposition chamber.....	11
2.2 System configuration and design of internal components.....	14
2.3 Computer control system.....	21
3. Fundamental studies of the sputter-deposition process.....	25
3.1 Sputtering yield studies.....	25
3.2 Scattering yield studies.....	27
3.3 Conclusions.....	33
4. Summary of properties of <i>in situ</i> deposited $\text{YBa}_2\text{Cu}_3\text{O}_{7-\delta}$ thin films.....	34
4.1 Sputtering from single $\text{YBa}_2\text{Cu}_3\text{O}_{7-\delta}$ target.....	34
4.1.1 Electrical properties	
4.1.2 Microstructural properties	
4.2 Sputtering from multiple targets (Y, BaF, and Cu).....	46
4.2.1 Electrical properties	
4.2.2 Microstructural properties	
4.3 Conclusions.....	50
5. Effects of ion beam energy on <i>in situ</i> $\text{YBa}_2\text{Cu}_3\text{O}_{7-\delta}$ film properties.....	52
5.1 Experimental.....	52
5.2 Electrical properties.....	53
5.3 Microstructural properties.....	54
5.4 Conclusions.....	56

Accession For	
NTIS GR&I	<input checked="" type="checkbox"/>
DTIC TAB	<input type="checkbox"/>
Unannounced	<input type="checkbox"/>
Justification	
By AD-A213921	
Distribution/	
Availability Codes	
Dist	Avail and/or Special
A-1	



6.	Effects of substrate temperature and oxygen pressure on <i>in situ</i> YBa ₂ Cu ₃ O _{7-δ} film properties.....	59
6.1	Experimental.....	52
6.2	Electrical properties.....	60
6.3	Microstructural properties.....	63
6.4	Surface morphology study.....	65
6.5	Conclusions.....	73
7.	Multilayered film structures.....	74
7.1	YBa ₂ Cu ₃ O _{7-δ} / MgO / YBa ₂ Cu ₃ O _{7-δ} layered structures on MgO substrates.....	74
7.2	YBa ₂ Cu ₃ O _{7-δ} / KNbO ₃ layers on MgO substrates.....	77
7.3	YBa ₂ Cu ₃ O _{7-δ} / YSZ / Si ₃ N ₄ on silicon substrates.....	81
7.4	Conclusions.....	84
8.	Demonstration of uniform YBa ₂ Cu ₃ O _{7-δ} deposition over 4" diam (unheated) silicon wafers.....	85
8.1	Experimental.....	85
8.2	Results and discussion.....	87
8.3	Conclusions.....	93
9.	Project summary and conclusions.....	94
10.	Acknowledgments.....	96
11.	References.....	97
12.	Publication and presentation list.....	100

PROJECT SUMMARY

This is the final report covering our 3-year DARPA contract # N00014-88-K-0525. The original program goals included:

- 1) the development of a new method for the fabrication of superconducting oxide thin films (computer-controlled ion beam sputter-deposition),
- 2) the fabrication of quality $\text{YBa}_2\text{Cu}_3\text{O}_{7-\delta}$ thin films using this technique, while studying fundamental aspects of the film growth process, and
- 3) the demonstration of feasibility of growing $\text{YBa}_2\text{Cu}_3\text{O}_{7-\delta}$ / insulator / $\text{YBa}_2\text{Cu}_3\text{O}_{7-\delta}$ structures for fabricating Josephson junction devices for digital superconducting electronics.

ACCOMPLISHMENTS

Presented here is a summary of project accomplishments, which are described in detail in this report.

- 1) **Development of an automated ion-beam sputter-deposition system.** The system developed can be used to produce multicomponent and/or multilayered structures. Computer-controlled growth of multicomponent materials can be accomplished by sequentially sputtering from elemental targets. Layered structures can be obtained by sequentially sputtering from different multicomponent targets. Sputtering targets are mounted on a motor-driven rotating holder for sequential, *in situ* positioning in front of the ion beam. The thickness of each individual material layer is monitored by a quartz crystal resonator. The computer program uses feedback control from the quartz crystal monitor to turn the ion beam on and off, and to position the appropriate target in front of the ion beam. This system can be utilized in three basic configurations:

A: with multiple elemental (or single cation) targets, for growing multicomponent oxide films (multiple cations) of any chosen composition, e.g. Y, Cu, and BaF targets for $\text{YBa}_2\text{Cu}_3\text{O}_{7-\delta}$ film growth;

B: with multiple elemental or compound targets, for growing multiple film layers, such as $\text{YBa}_2\text{Cu}_3\text{O}_{7-\delta}$ / MgO layers;

C with a single multicomponent target, continuously or periodically rotated to minimize or eliminate ion-bombardment-induced surface topography (one of the difficulties with multicomponent targets is a change in the surface during time, resulting in changes in the sputtered flux distribution).

2) **Fabrication of high quality *in situ* $\text{YBa}_2\text{Cu}_3\text{O}_{7-\delta}$ films, while gaining an understanding of the deposition process.** We have produced *in situ* epitaxial, c-axis oriented $\text{YBa}_2\text{Cu}_3\text{O}_{7-\delta}$ films on (100) MgO substrates heated to $\sim 700^\circ\text{C}$. The films have a superconducting critical temperature (T_c) of 85 K, and a critical current density (J_c) of 1×10^7 A/cm² at 12 K. The J_c values have been obtained on 25 μm wide lines, successfully patterned using conventional photolithographic techniques.

We have observed significant effects on the film properties due to changes in the ion beam energy, substrate temperature, and oxygen pressure during film growth. Observed property changes include effects on film orientation, surface morphology, c-axis length, and T_c . We have been the first group to observe the spiral-type growth mode on ion beam sputter-deposited $\text{YBa}_2\text{Cu}_3\text{O}_{7-\delta}$ thin films using scanning tunneling microscopy.

3) **Deposition of multilayered structures.** With this system we have demonstrated growth of c-axis oriented $\text{YBa}_2\text{Cu}_3\text{O}_{7-\delta}$ / MgO / $\text{YBa}_2\text{Cu}_3\text{O}_{7-\delta}$ structures having an 80 Å MgO layer, as a proof-of-capability of the technique to produce multilayered structures for Josephson junction fabrication. We have also produced epitaxial $\text{YBa}_2\text{Cu}_3\text{O}_{7-\delta}$ films on epitaxial (100) KNbO_3 films on (100) MgO substrates, which demonstrates the possibility of integrating superconducting and ferroelectric or electrooptic devices on a single

chip. We have also succeeded in depositing c-axis oriented $\text{YBa}_2\text{Cu}_3\text{O}_{7-\delta}$ films on polycrystalline YSZ / Si_3N_4 / Si substrates, with properties sufficient for use as bolometers at 77 K.

4) **Demonstration of uniform deposition of YBCO over large areas.** Depositing from a single $\text{YBa}_2\text{Cu}_3\text{O}_{7-\delta}$ target onto an unheated 4" diam Si wafer, we have demonstrated a coating thickness uniformity of $\pm 4.7\%$, and an average compositional spread of only about $\pm 5\%$ over the entire 4" diam area. This is one very promising aspect of ion-beam sputter-deposition, because coating large areas is a concern for nearly all types of films being considered for use in microelectronic devices, and especially so for superconducting films used for passive microwave applications. We are one of the few groups that have demonstrated the capability for depositing uniform films over large-area substrates.

Chapter 1

Introduction to $\text{YBa}_2\text{Cu}_3\text{O}_{7-\delta}$ materials issues

We have concentrated our efforts in this project on the preparation of $\text{YBa}_2\text{Cu}_3\text{O}_{7-\delta}$ thin films. There are several reasons why $\text{YBa}_2\text{Cu}_3\text{O}_{7-\delta}$ has become the material of choice for many device applications; there are also several aspects of this material system which make it challenging to produce high-quality devices. These aspects will be discussed briefly here as an introduction to important $\text{YBa}_2\text{Cu}_3\text{O}_{7-\delta}$ materials issues.

The high-temperature superconductor $\text{YBa}_2\text{Cu}_3\text{O}_{7-\delta}$ has several properties which make it a promising candidate for many applications. It has a critical temperature (T_c) as high as ~ 93 K [Wu et al.¹], above liquid nitrogen temperature. Thin films of $\text{YBa}_2\text{Cu}_3\text{O}_{7-\delta}$ have been produced which have critical current densities (J_c) greater than 2×10^7 A/cm² at 4.2 K, remaining as high as 5×10^6 A/cm² at 77 K [Ref. 2]. These J_c values are higher than can be obtained with any of the low- T_c materials, and at least as good the J_c of the Tl-based high- T_c materials. The Bi-based high- T_c materials generally have lower J_c 's due to flux creep problems. Another advantage of $\text{YBa}_2\text{Cu}_3\text{O}_{7-\delta}$ over the Tl- or Bi-based superconductors is that $\text{YBa}_2\text{Cu}_3\text{O}_{7-\delta}$ has 'only' three cations in its structure, as opposed to the four or more needed in the Tl- or Bi-structures. A larger number of cations makes film preparation much more difficult.

Presently, there has been much more success in obtaining single phase, epitaxial $\text{YBa}_2\text{Cu}_3\text{O}_{7-\delta}$ thin films than there has been with other high- T_c materials. The microwave losses of $\text{YBa}_2\text{Cu}_3\text{O}_{7-\delta}$ at 77 K now rival that of Nb at 4.2 K, and microwave filters have been demonstrated³. Other devices that have been proven are S/N/S junctions⁴ and bolometers.⁵

Despite their good electrical properties, all of these high- T_c materials have other properties which make them difficult to work with. Here we focus on some of the difficulties involved with the $\text{YBa}_2\text{Cu}_3\text{O}_{7-\delta}$

compound.

Major concerns about $\text{YBa}_2\text{Cu}_3\text{O}_{7-\delta}$ include its thermodynamic stability, its ability to easily diffuse oxygen in and out of the structure, and its reactivity with water vapor and carbon-containing gases. It has been established that for thermodynamic stability of $\text{YBa}_2\text{Cu}_3\text{O}_{7-\delta}$ at growth temperatures ($\geq 700^\circ\text{C}$), very high oxygen pressures are required (≥ 5 mTorr), much higher than that required for most other oxide materials.⁶ This requires that any hot deposition system components be oxidation resistant. Some processes, such as evaporation, require system modifications at these pressures.⁷

The oxygen content of the films during deposition is only O_6 or slightly above, meaning that the films have a tetragonal, nonsuperconducting structure. During film cooling, the oxygen pressure is increased (to >50 Torr by 500°C), and the oxygen content rises to nearly O_7 . At this stage, the film has converted to the orthorhombic, superconducting structure. The potential problem is that oxygen diffusion occurs readily at fairly low temperatures, even as low as 400°C .⁸ A film could then lose superconductivity in a warm, low oxygen pressure environment. $\text{YBa}_2\text{Cu}_3\text{O}_{7-\delta}$ is also very reactive with water,⁹ resulting in a breakdown of the superconducting phase at the surface. Samples that are not fully dense will also be degraded internally.

Another observed property of $\text{YBa}_2\text{Cu}_3\text{O}_{7-\delta}$ is that the superconducting properties across high-angle grain boundaries are very poor.¹⁰ The J_c drops by more than an order of magnitude across high-angle boundaries compared to boundaries of only a few degrees. Therefore, films must be nearly single crystal to have the best electrical properties (and so substrates must be nearly single crystal). This puts restrictions on device designs. Recently, these grain boundary properties have been advantageously used for the fabrication of weak-link junctions.¹¹ So, the properties of well designed boundaries can be useful, even if to a limited extent.

The properties of $\text{YBa}_2\text{Cu}_3\text{O}_{7-\delta}$ are anisotropic due to its structure. Electrical properties are much better in the a- and b- directions than in the c- direction. The coherence length (~length over which

superconducting pairs interact) is also anisotropic, being about 15 Å in the a- and b- directions, while only 7 Å in the c- direction.¹² This limits the thickness of the insulating barrier layer that could be used in a superconductor-insulator-superconductor (S/I/S) Josephson junction. For c-axis oriented films, a sandwich junction structure would require a continuous insulator layer of ≤ 7 Å, clearly a difficult task. With a-axis oriented films, this distance is slightly larger, but has still not been demonstrated as being feasible. This material property constraint (plus the reactivity of the $\text{YBa}_2\text{Cu}_3\text{O}_{7-\delta}$ surfaces) have so far made it impossible to obtain true S/I/S junctions.

Many device applications of $\text{YBa}_2\text{Cu}_3\text{O}_{7-\delta}$ ultimately require a good quality film that is uniform over a large substrate area. This has proven very difficult for a variety of reasons. This must also be achieved in order to integrate superconductor and semiconductor devices on the same chip.

In summary then, $\text{YBa}_2\text{Cu}_3\text{O}_{7-\delta}$ has superconducting properties which are good enough for many thin film device applications. Many properties of $\text{YBa}_2\text{Cu}_3\text{O}_{7-\delta}$ make it favorable as a material of choice compared to the Bi- or Tl- based superconductors. More complicated S/I/S devices have not yet been achieved by any group, although S/N/S devices for use in SQUIDS have been demonstrated. The fabrication of electronic devices that will operate over long periods of time in diverse operating conditions remains a challenge, due to some current limitations in the properties of $\text{YBa}_2\text{Cu}_3\text{O}_{7-\delta}$.

Chapter 2

Deposition system design and development

The deposition chamber we have developed allows computer-controlled, sequential growth from multiple sputtering targets to produce multicomponent oxide films. Presently, the system operates with up to 3 sputtering targets, held on a motorized rotating holder. The film composition is controlled by adjusting the film thickness deposited from each sputtering target. The layer thickness is monitored using a quartz crystal resonator. The computer program reads the real-time thickness of each layer, and when the setpoint thickness is reached, turns off the ion beam, rotates the next target into position, and begins depositing the next material layer.

Besides this capability for layer-by-layer growth, this system can also be utilized to deposit multilayer thin film structures. For example, $\text{YBa}_2\text{Cu}_3\text{O}_{7-\delta}$ / MgO / $\text{YBa}_2\text{Cu}_3\text{O}_{7-\delta}$ multilayers can be grown using $\text{YBa}_2\text{Cu}_3\text{O}_{7-\delta}$ and Mg sputtering targets. A third system configuration is to sputter from a single $\text{YBa}_2\text{Cu}_3\text{O}_{7-\delta}$ target, employing target rotation during deposition. There are two major advantages to using ion beam sputtering over conventional sputtering techniques when sputtering from a single multicomponent target. First, the sputtering target is not biased during deposition, so energetic negative ion bombardment is not present. Secondly, by bombarding at an oblique angle and rotating the target during sputtering, we are able to minimize the development of a rough surface morphology (which can lead to changes in the sputtered flux distribution over time).

These different system configurations make this a very flexible deposition system. The only real disadvantage of using ion beam sputter-deposition as compared to more conventional techniques is that the maximum system pressure is limited to a couple millitorr, as opposed to hundreds of millitorr.

2.1 Deposition chamber

An ultra-high vacuum chamber has been developed as part of this research effort aimed at producing ion beam sputter-deposited $\text{YBa}_2\text{Cu}_3\text{O}_{7-\delta}$ thin films. The essential features of the vacuum chamber are shown in the schematic drawings in Fig. 2.1, which show a top view and front view of the system. The essential features to note are: the motorized manipulator for substrate positioning, the independently pumped load-lock chamber, and the magnetically coupled linear motion transfer rod which is used to introduce and retrieve substrates into the deposition chamber through the load-lock chamber. A photograph of the deposition chamber (opened) is shown in Fig. 2.2.

A 16" diam spherical main chamber design was selected as this symmetry allows access ports to be easily aimed towards the system center. For example, 14 of the 29 ports have a direct relationship to the substrate when properly aligned for a deposition sequence. Ports are available to accommodate a variety of deposition equipment and analytical instruments, including: a 3-cm Kaufman-type ion source; electrical feedthroughs for the rotating multiple-target assembly; a precision manipulator with substrate heater; a load-lock connection; a RHEED ion source and screen; a quartz crystal rate monitor; a second ion source or oxygen plasma source; appropriate vacuum gauges; and a residual gas analyzer. The chamber is pumped to high vacuum using a 330 l/s Balzers turbomolecular pump, backed by a rotary vane mechanical pump. Both pumps operate with Fomblin pump oil, making them compatible for operation with oxygen gas or ozone vapor.

Note that the chamber is constructed in two halves, allowing separation along the centerline. The chamber seal can be made using either a reusable viton O-ring (10^{-8} Torr minimum possible pressure) or a copper wire seal (10^{-9} Torr minimum pressure). We have found that the use the viton seal gives acceptable background pressures. A motorized hoist system utilizing a permanent magnet motor and a variable speed SCR controller is used to lift the top half of the chamber when performing internal system maintenance.

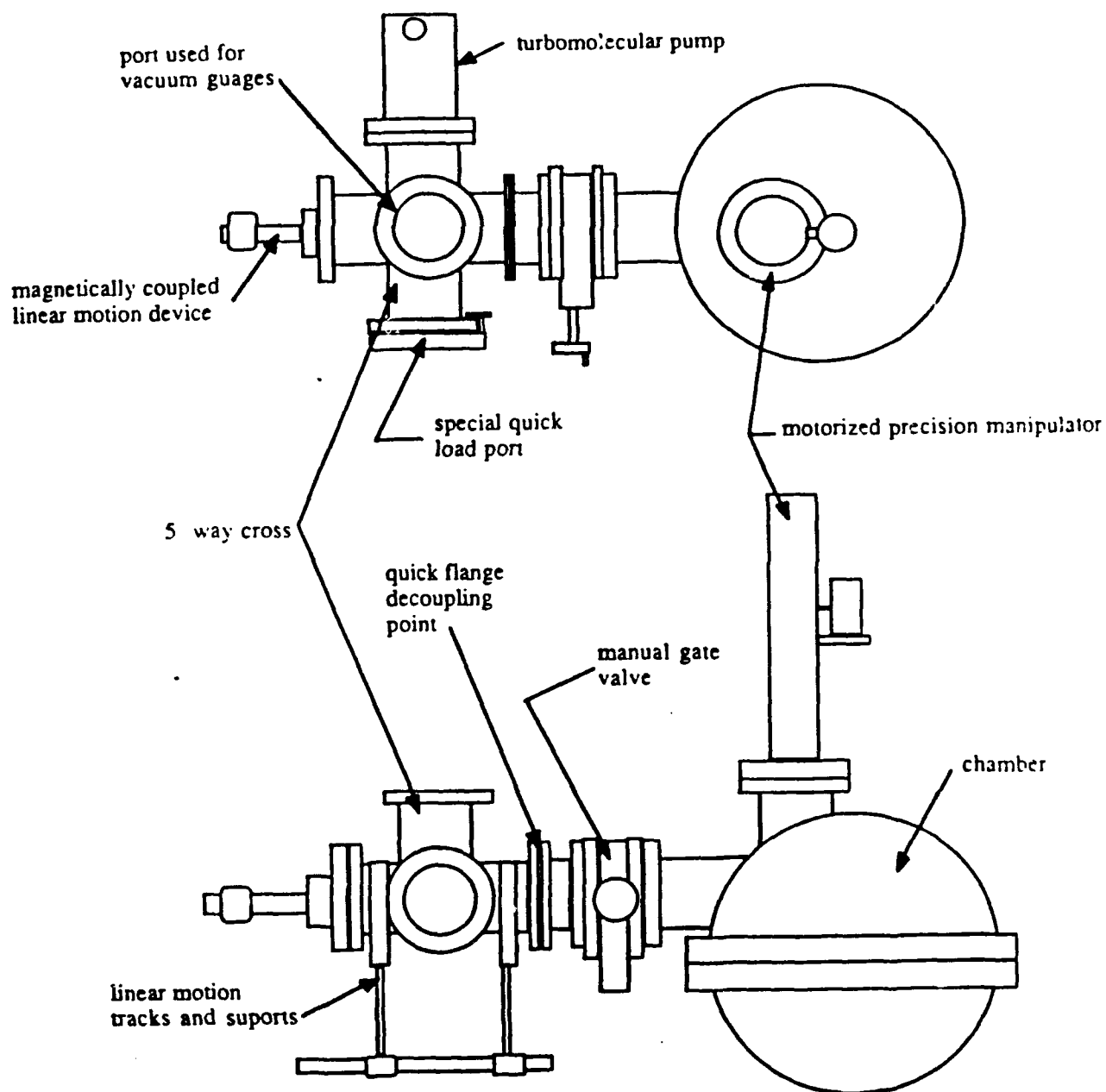


Figure 2.1. Schematic representation of the vacuum chamber and load-lock chamber designed for the ion-beam sputter deposition of $\text{YBa}_2\text{Cu}_3\text{O}_{7-\delta}$ thin films.

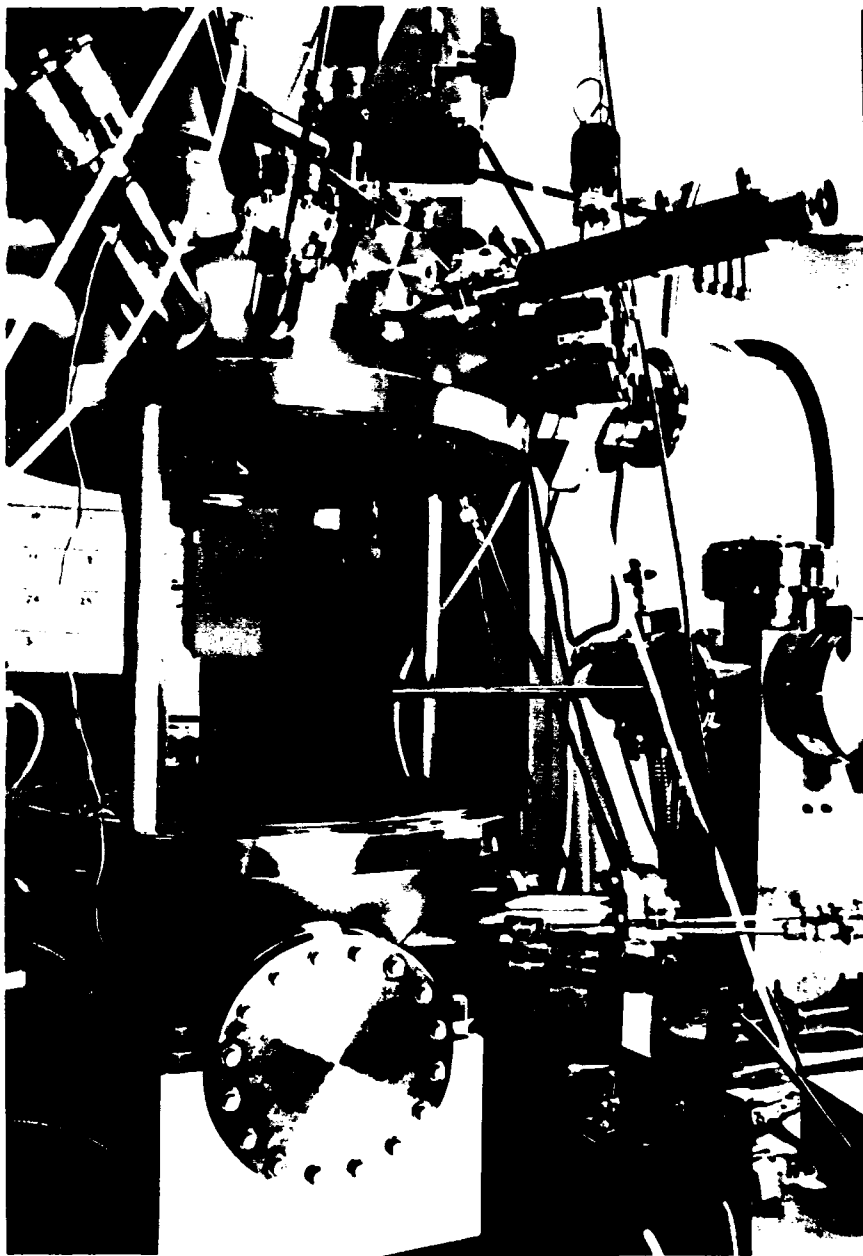


Figure 2.2. Photograph of the deposition system (opened), showing the substrate heater and the load-lock transfer mechanism.

Substrate loading and removal after deposition is performed using the load-lock system (included schematically in Fig. 2.1). The transfer of substrates between chambers is accomplished by opening the manual gate valve isolating the two chambers, and using the magnetically-coupled linear transfer arm to move the substrate holder back and forth. The transfer arm attaches to the substrate holder via a threaded rod, which is screwed into the substrate holder by simply rotating the transfer arm (which has both linear and rotational freedom of motion).

2.2 System configuration and design of internal components

The essential internal components of the sputtering chamber include: 1) the ion source; 2) the substrate heater; the 3) quartz crystal deposition rate monitor; and 4) the rotating target holder assembly.

The basic sputtering system geometry for sequential multi-target sputtering is shown schematically in Fig. 2.3. The 3-cm diam ION TECH ion source is located about 9 cm from the sputtering target, with the beam incident normal to the target. The substrate is located about 40° from the target normal, at a distance of about 13 cm from the target center. The quartz rate monitor, which serves as the feedback signal for the computer control, is located at the opposite side of the ion source, symmetrically opposed to the substrate. Therefore, the rate monitor and the substrate receive the same flux of depositing species.

The basic sputtering system geometry for the single-target sputtering is shown schematically in Fig. 2.4. The 3-cm diam ION TECH ion source is located about 9 cm from the sputtering target, and at about a 20° angle from the target normal. The substrate is located about 30° to the opposite side of the target normal (the angle between beam and substrate-normal is about 50°) at a distance of about 13 cm from the target center. The quartz rate monitor is located in the vicinity of the substrate. Although the rate monitor and substrate will not receive the exact same deposition flux, they will be linearly proportional to each other.

The ion source and the quartz rate monitor are commercially

ROTATING TARGET ASSEMBLY

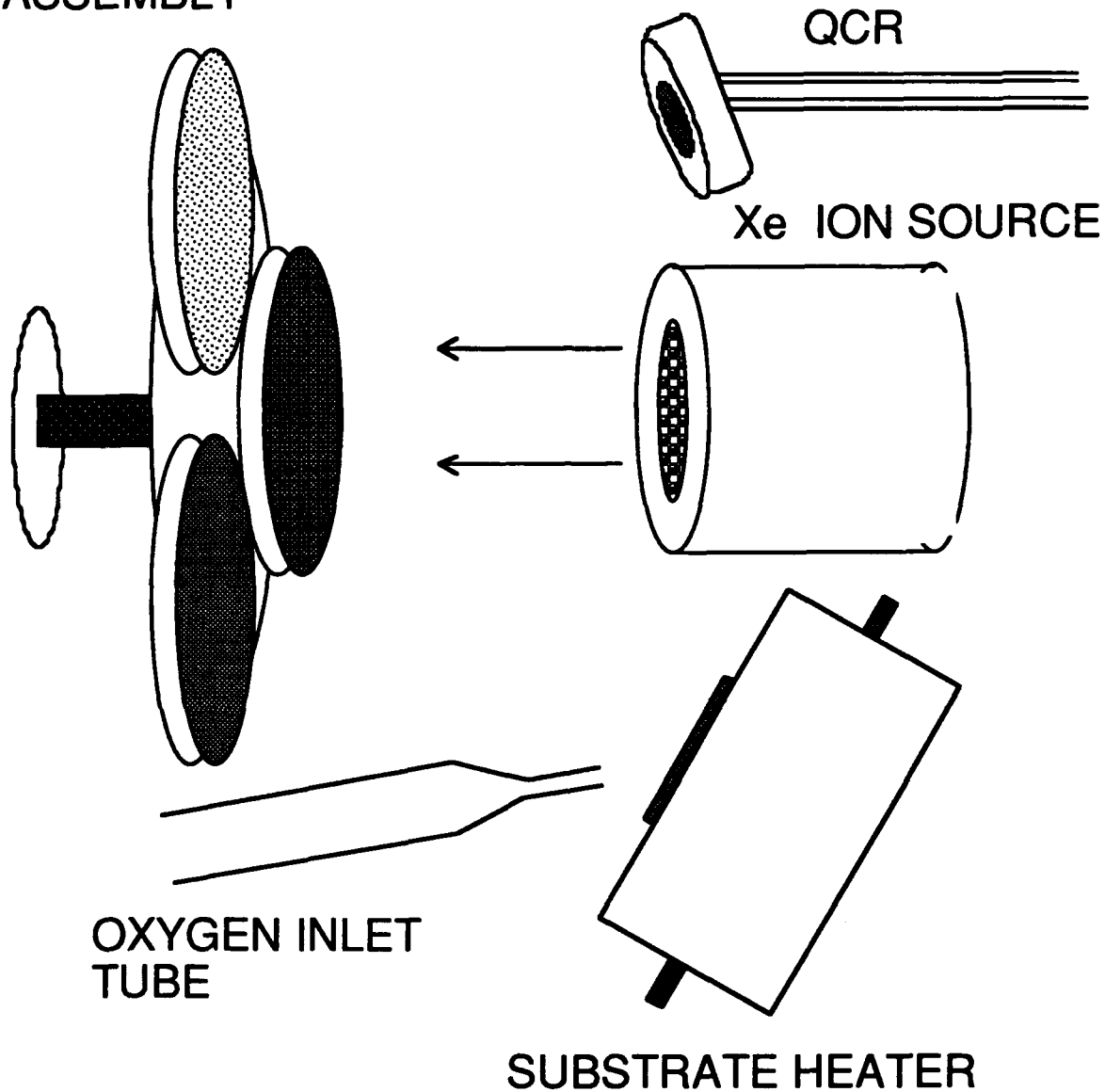


Figure 2.3. System configuration for ion-beam sputter-deposition from multiple elemental targets (Y, Cu, and BaF).

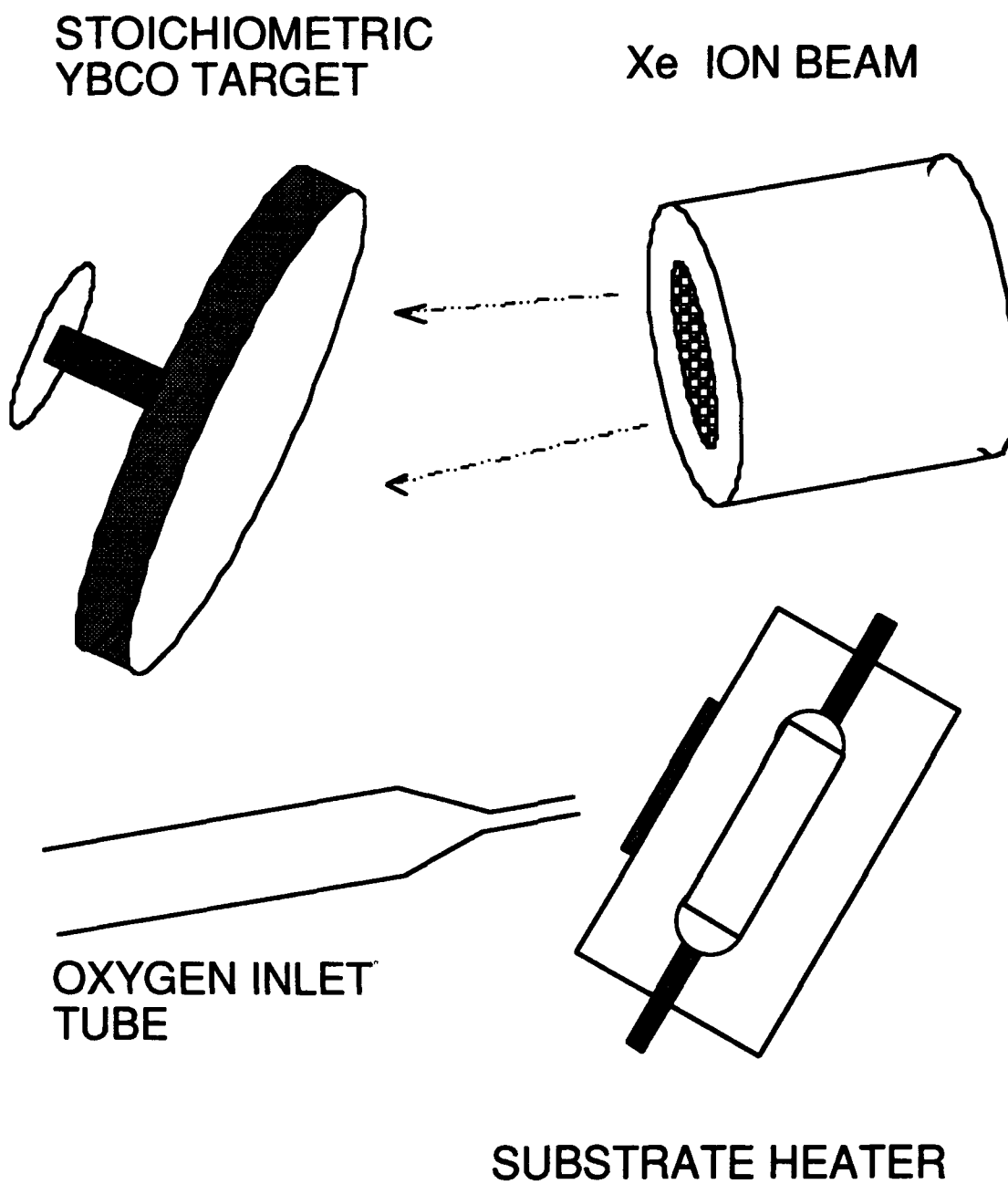
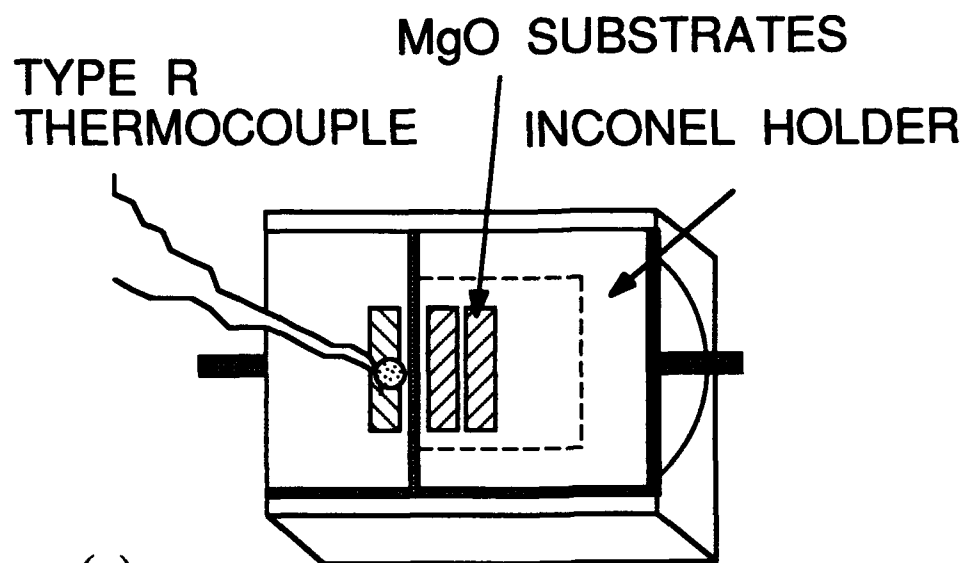


Figure 2.4. System configuration for ion-beam sputter-deposition from a single $\text{YBa}_2\text{Cu}_3\text{O}_{7-\delta}$ target.

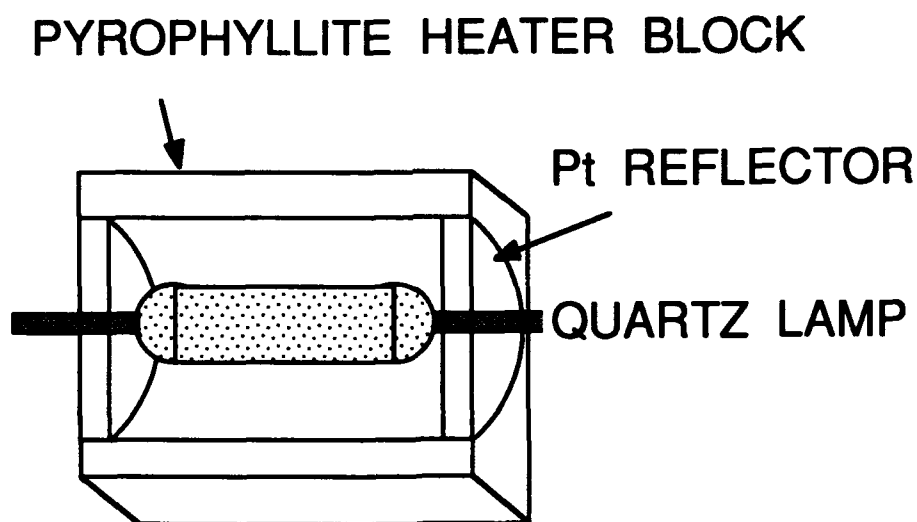
available (and so their principles of operation will not be discussed here). The 3-cm ION TECH ion source is capable of operating with energies between about 400 - 1200 eV, beam currents up to about 50 mA, and at pressures from 8×10^{-5} to $\sim 2 \times 10^{-3}$ Torr. The upper pressure is limited by electrical breakdown across the pyrolytic graphite ion extraction grids, which are ~ 1 mm apart. Operation of this source in high oxygen pressures requires periodic maintenance, due to reaction of oxygen with the tungsten cathode filament. The Leybold-Heraeus Inficon quartz crystal thickness monitor is a specially designed version which has a 0.01 \AA thickness resolution. A joint collaboration between Inficon and our group resulted in the development of this new, high sensitivity QCR, which has recently been introduced into the market. This instrument was still being developed at the time our work started, and we served as an initial test site (β -site) for this product.

The substrate heater and target holder assemblies were designed and built in-house. The substrate heater was designed with the following criteria in mind: it must have the ability to withstand high temperature (up to 900°C) in the presence of high oxygen pressures (200 Torr O_2 at 500°C ; less at higher temperatures), and be compatible with the sample transfer mechanism. The heater must also include a temperature measuring sensor which can withstand these operating conditions. (The high-temperature superconductors require much higher oxygen pressures for thermodynamic stability than most oxides, which is one of the main challenges in fabricating these materials).

The substrate heater that we have designed and implemented is shown schematically in Fig. 2.5. The heater body and sides are made from pyrophyllite, a high temperature ceramic which can be shaped while in the green state, and then fired for curing purposes. Therefore, no final machining of the ceramic is required. Heating is performed radiatively using a 500 W quartz-lamp heater. The key advantage of using a quartz lamp is that the hot filament is isolated from the oxygen in the sputtering atmosphere, and so the heater lifetime is relatively long. Directly behind the heater lamp is a Pt foil reflector, which serves to increase the heater efficiency. The heater temperature is controlled



(a)



(b)

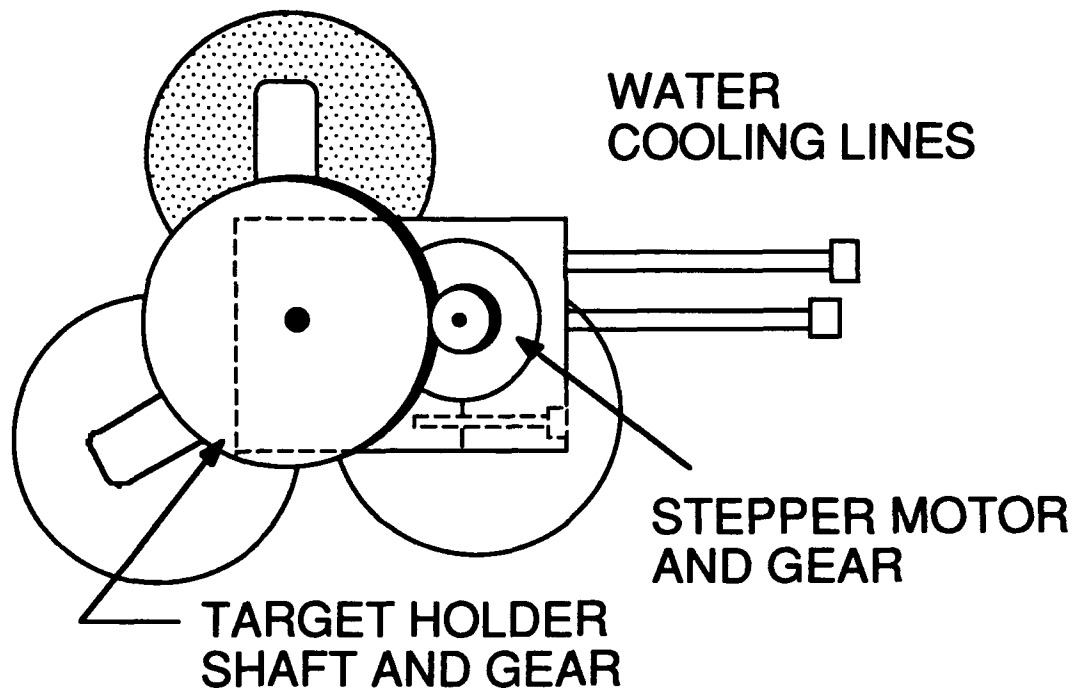
Figure 2.5. Schematic drawings of the substrate heater; (a) with the substrates and thermocouple in place, and (b) with only the lamp and backing pieces shown.

by a Yokagawa programmable PID controller connected to a Eurotherm power supply.

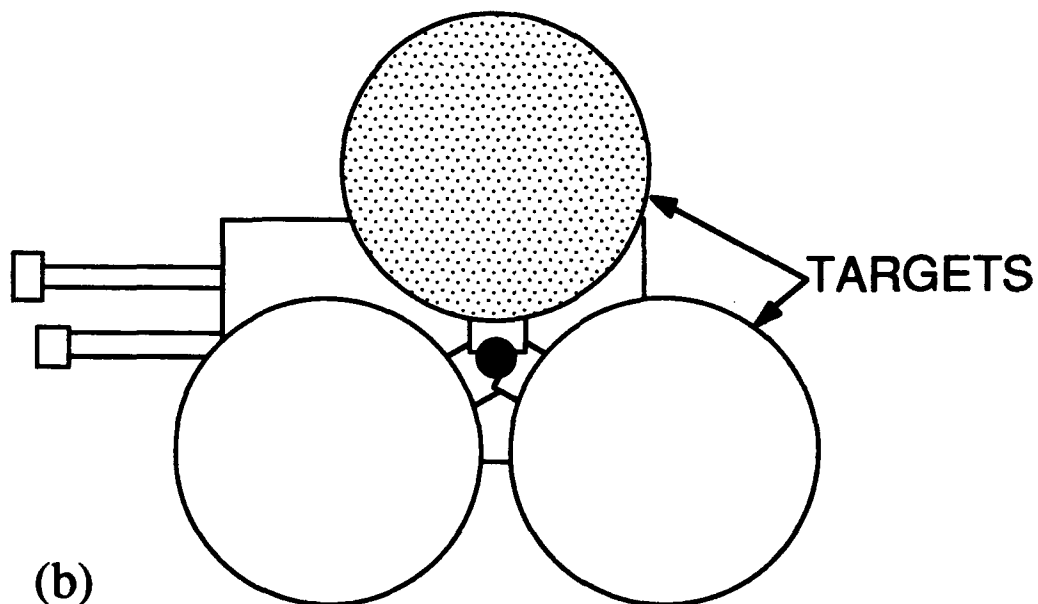
The heater temperature is monitored using a Pt-Pt(13%Rh) thermocouple (type R). This thermocouple type is the best suited for the high temperature, high oxygen pressure growth conditions. The thermocouple is mounted (using a high temperature silver epoxy) to an Inconel holder mounted on the front-left of the heater block. Again, Inconel is chosen because of its resistance to the highly oxidizing operating conditions. Substrates are mounted on an Inconel holder using a colloidal silver "paint" to provide good heat transfer from the Inconel holder. Inconel clips hold the substrate holder in place, and allow it to be slid in and out of the heater for sample transfer purposes.

The design of our rotating target holder assembly is shown in Fig. 2.6. The design features a vacuum compatible stepper motor connected to the target shaft via a set of drive gears (the gear ratio proportioned to minimize load on the motor). The motor is mounted in a water-cooled holder to avoid overheating. The vacuum compatible stepper motor, manufactured by Princeton Research Instruments, gives added system flexibility compared to a drive shaft run through a vacuum feedthrough. A set of bearings on the target shaft allows smooth rotation of this assembly. The rotation is computer controlled, with a holding torque applied at the end of each rotation cycle to eliminate any rotational drift.

Oxygen can be supplied to the growing film using a number of different sources. Molecular oxygen gas (O_2), ozone vapor (O_3), low energy (50 - 300 eV) oxygen ions (O_2^+ , with O_2 present), and sub-eV atomic oxygen (O, with O_2 present) have all been investigated as oxygen sources. Use of atomic oxygen and oxygen ions was not sufficiently studied to warrant discussion here. For most experiments, O_2 or O_3 jets were directed at the substrate through a 1.8 mm I.D. glass tube positioned about 8 mm from the substrate surface. The local O_2 pressure at the substrate has been measured using the stagnation tube method¹³ and is about 20 times greater than the background pO_2 . The local O_3 flux has been measured using a coated quartz crystal rate



(a)



(b)

Figure 2.6. Schematic drawing of the rotating target holder assembly. Drawing (a) reveals the gear mechanism and water-cooled holder (rear view), and (b) shows the target arrangement from the front.

monitor, as described by Kucera et al.¹⁴

The generation and collection of liquid ozone, which served as our ozone source, was performed as described by Berkley et al.¹⁵ A schematic of the O₃ generation system is shown in Fig. 2.7. Passing O₂ gas through an a.c. discharge produces a gas containing a few percent of O₃ in O₂. This O₃ is condensed by passing it through a liquid-nitrogen-cooled condenser tube which is filled with silica gel particles. The O₂ is removed by pumping with a mechanical pump (so the pressure is about 10 Torr during O₃ collection). Ozone vapor can then be generated by heating the condenser tubes. The heating is accomplished by passing current through a Ni-Cr wire wrapped around the tube. The O₃ pressure is controlled by feeding back the signal from a capacitance manometer to the heater power supply. This type of O₃ system is capable of delivering nearly pure O₃ with a very small O₂ component.

2.3 Computer control system

The design and implementation of the computer software which drives the ion-beam sputter-deposition system marks a major achievement in the program. The computer software and associated hardware interfaces play a crucial role in determining the flexibility of the system both as a research tool and as a prototype for potential upgrading to a manufacturing system. This computer-controlled operation is essential for composition control when sputtering sequentially from multiple elemental targets. The following section describes the computer-related portions of the deposition system, including unique features in both the software and hardware.

The computer used to drive the system is a Macintosh II, which has a 40 kilobyte internal hard drive, 25kB external back-up drive (from Jasmine), and an internal floppy disk. The system has been upgraded to 2 megabytes of random access memory. This system was chosen for its ease of programming, speed of operation, and user-friendliness.

Equipment interfacing is performed using a National Instruments

OZONE VAPOR JET SYSTEM SCHEMATIC

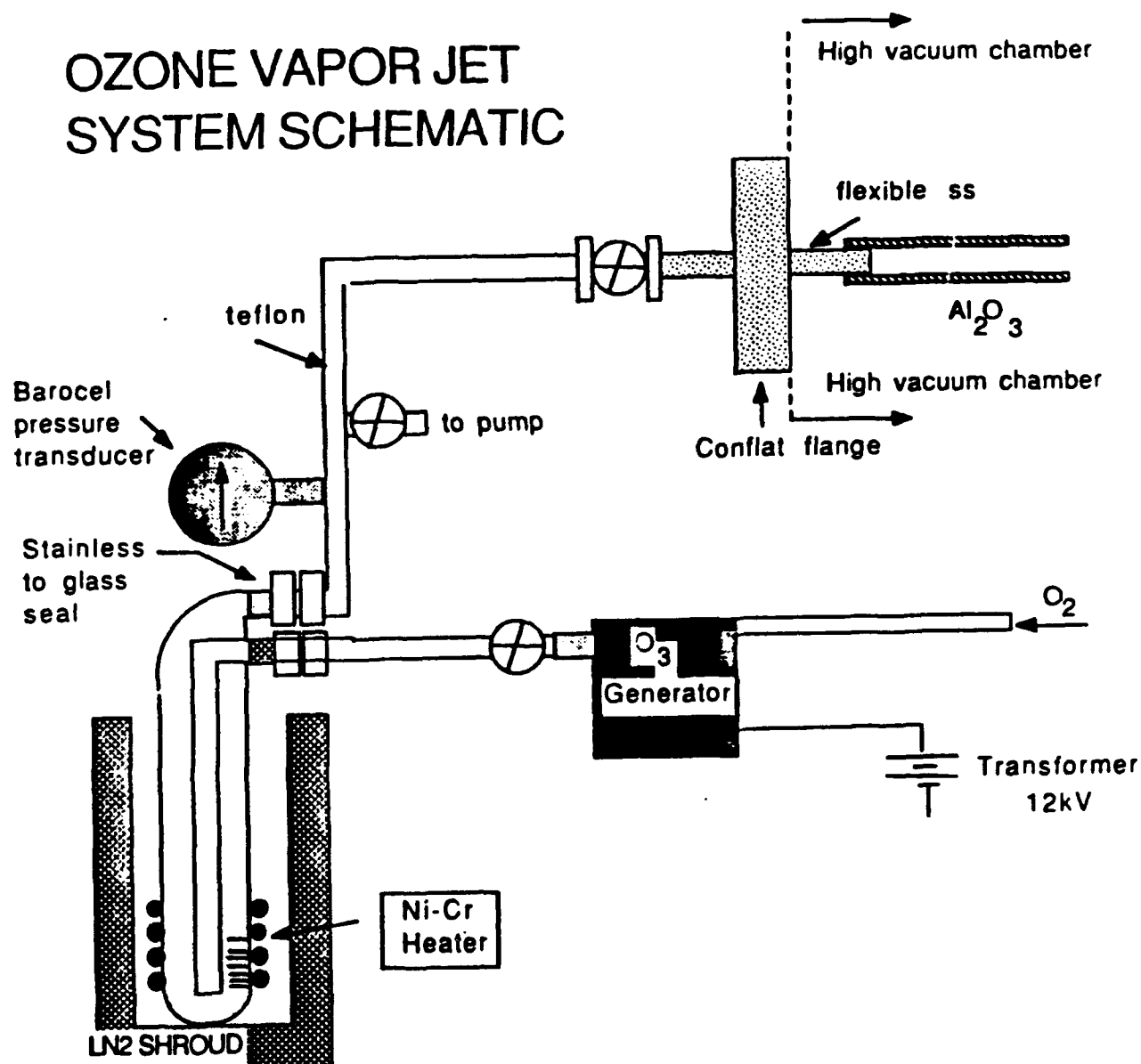


Figure 2.7. Schematic of the ozone generation, collection, and vaporization system.

data acquisition board that features analog-to-digital, digital-to-analog, timing, and digital I/O ports, as well as a communications port (RS-232). The current system utilizes all of the features described above. The board can easily be configured and controlled through two software languages, either BASIC or through LABVIEW, a National Instruments software package. In this research program, we have utilized the LABVIEW 'language' for computer control of the deposition process.

For the deposition of multicomponent films from elemental targets, the computer control software is described as follows. First, the following parameters are introduced into the computer program: (a) the number of sputtering targets used to produce a multicomponent film; (b) the density of each layer deposited; (c) the thickness of each layer to be deposited; and (d) the desired ion beam current and voltage (power) for each target. Upon starting the program, the computer rotates the first target into position in front of the ion beam. The quartz crystal resonator (QCR), used for dynamic monitoring of the film thickness, has the desired film density input, and the thickness is set to zero. The computer then turns on the ion beam to the specified current and voltage (gas flows are established prior to this). The computer monitors the QCR readings, and when the desired thickness setpoint is reached, the beam is turned off, the next target is rotated into position, and the process is repeated. Each deposited layer is very thin ($>10 \text{ \AA}$), and interdiffusion of the elements occurs during growth to give the desired multicomponent phase (under proper temperature and oxidizing conditions). This sequential deposition process is repeated until the final overall programmed film thickness is reached. This experimental setup allows films of virtually any composition to be deposited.

Figure 2.8 shows the virtual instrument 'panel' created by LABVIEW to drive the system. The target density, z-ratio, setpoint thickness, beam voltage, and beam current are input by the user. The other panels show the output from the QCR (thickness and deposition rate) during each cycle. Additional instrument control can also be added if desired.

This computer control capability can also be utilized for the

deposition of multilayer structures, such as $\text{YBa}_2\text{Cu}_3\text{O}_{7-\delta}$ / MgO / $\text{YBa}_2\text{Cu}_3\text{O}_{7-\delta}$ sandwich structures, or even more exotic structures such as $\text{Pb}(\text{Zr}_x\text{Ti}_{1-x})\text{O}_3$ / $\text{YBa}_2\text{Cu}_3\text{O}_{7-\delta}$ / MgO (on Si substrates, for instance). In these cases, appropriate multicomponent targets could be used, and the thickness of each film layer would be input into the computer program.

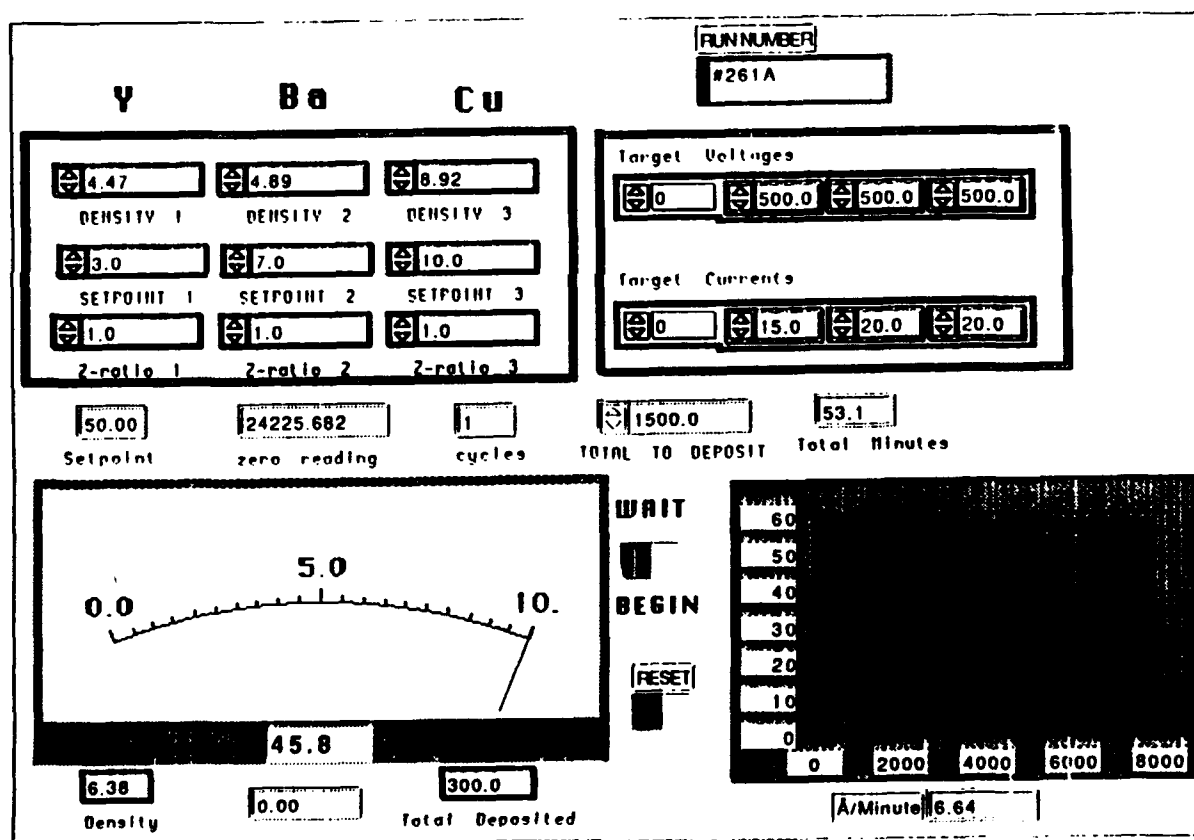


Figure 2.8. LABVIEW instrument panel into which control setpoints are entered, and from which process information is displayed during deposition.

Chapter 3

Fundamental studies of the sputter-deposition process

Although many groups have been using various sputtering techniques to deposit $\text{YBa}_2\text{Cu}_3\text{O}_{7-\delta}$ thin films, little information is available concerning the basic particle interaction processes occurring when the ion beam impacts the target, which may be relevant to film growth (i.e., sputtering yields, scattered-ion yields, preferential sputtering effects, ion energy effects,...). The need for a better understanding of the sputtering process was made clear in the case of plasma sputter-deposition by early studies by Shah and Carcia,¹⁶ who found that when sputtering from $\text{YBa}_2\text{Cu}_3\text{O}_{7-\delta}$ compound targets, energetic bombardment by sputtered negative ions caused severe resputtering of Ba from $\text{YBa}_2\text{Cu}_3\text{O}_{7-\delta}$ films. Therefore, typical sputtering geometries proved ineffective for the deposition of good quality $\text{YBa}_2\text{Cu}_3\text{O}_{7-\delta}$ thin films.

For the case of ion-beam sputter-deposition, early studies in this research program also revealed the need for a better understanding of the sputtering process. For example, initial experiments were performed using 1200 eV Ar^+ ions. Although Cu and Y films could easily be deposited, Ba films could not. During sputtering from the Ba target, substrates were actually *etched*. This led to experimental and theoretic studies of the main processes occurring during sputtering: *sputtering* of target material and *scattering* of incident ions from the target.

3.1 Sputtering yield studies

The sputtering yields of the various target materials give an indication of the deposition rate which may be obtained from each target. Although we have performed experimental studies relating the sputtering yields of Y, Cu, and Ba,¹⁷ here we will only present the results of our computer simulations using the TRIM.SP code.¹⁸ The results of

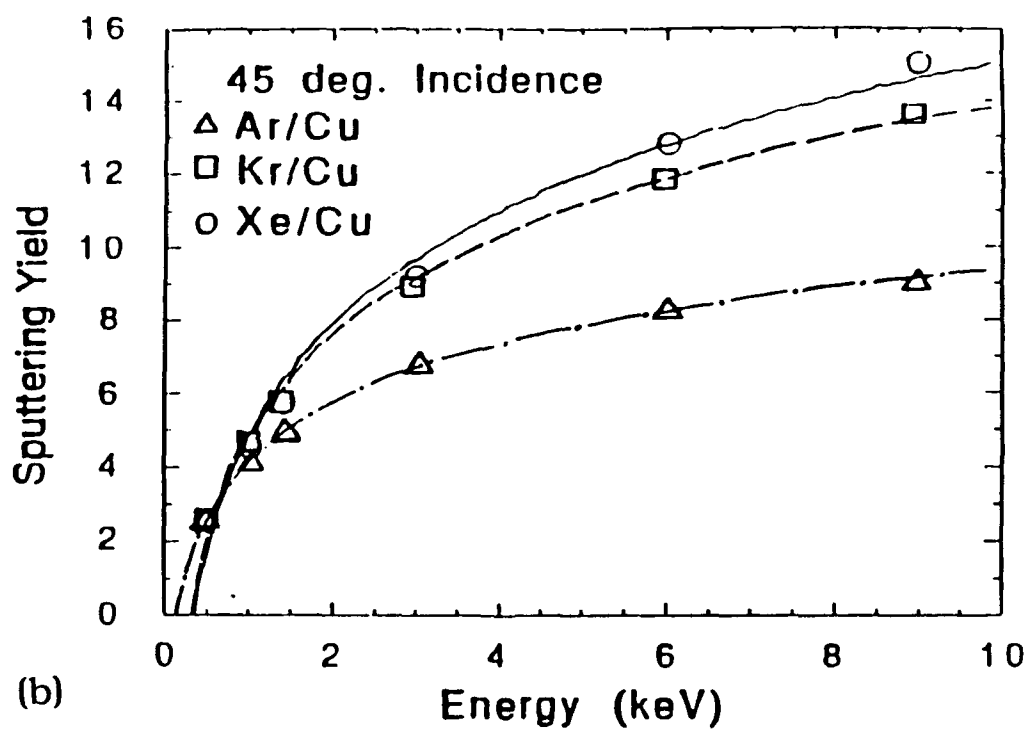
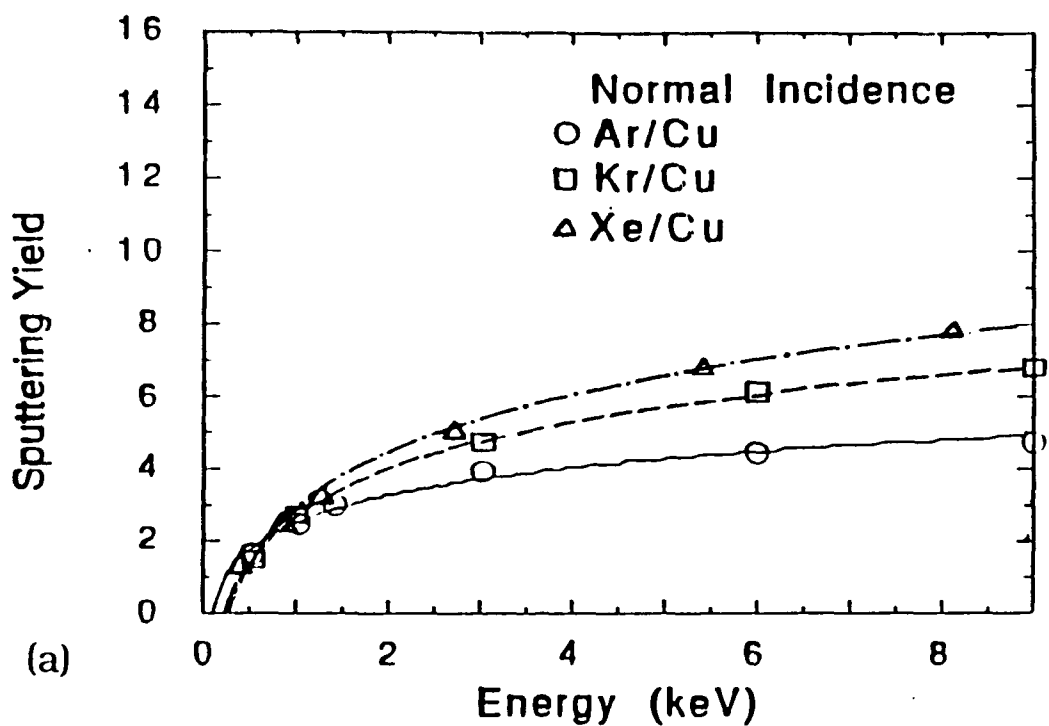


Figure 3.1. Calculated sputtering yields of Cu under either Ar^+ , Kr^+ , or Xe^+ bombardment as a function of incident energy. In (a) the incident ion beam is normal to the target surface, and in (b) the beam is incident 45° from the target normal.

extensive calculations have been included in our first-year report; here only a summary of important results will be included.

Figure 3.1 shows the calculated sputtering yield of Cu atoms under Ar^+ , Kr^+ , and Xe^+ ion bombardment as a function of the incident ion energy. In Fig. 3.1(a) the ion beam is at normal incidence to the target, and in Fig. 3.1(b) the beam is incident at 45° from the target normal. It can be observed that the sputtering yield increases with increasing ion energy, with increasing target angle (away from the normal), and with increasing mass of the incident ion. These results alone would tend to indicate that all these factors which increase the deposition rate would be beneficial; however, we have found that this is not the case, as will be revealed shortly.

3.2 Scattering yield studies

During sputtering, ions incident on the target may either (a) implant into the target, or (b) scatter from the target surface. The ratio of the scattered species to the total number of incident ions is called the scattering yield (also called the reflection coefficient). These scattered species can be very energetic, and can affect final film properties. This has been shown for other ion beam sputtered materials, such as Niobium.¹⁹ Resputtering caused by these scattered species can also alter the composition of multicomponent films. Therefore, we have studied the ion scattering process both experimentally and theoretically.

The experimental setup used to measure the relative amounts of ion scattering is shown in Fig. 3.2. The ion-beam is incident to the target at a 45° angle, and substrates are positioned at total scattering angles of 90° , 120° , and 150° . Films are then deposited using either Ar^+ , Kr^+ , or Xe^+ gases of 1200 eV beam energy. Using SIMS, the relative amounts of implanted gases in the films are measured. (This is not an absolute measure of ion scattering, but only a relative measure.) This allows the effects of both the scattering angle and the mass of the ions to be compared.

Figure 3.3 shows the gas incorporation measured in Cu films

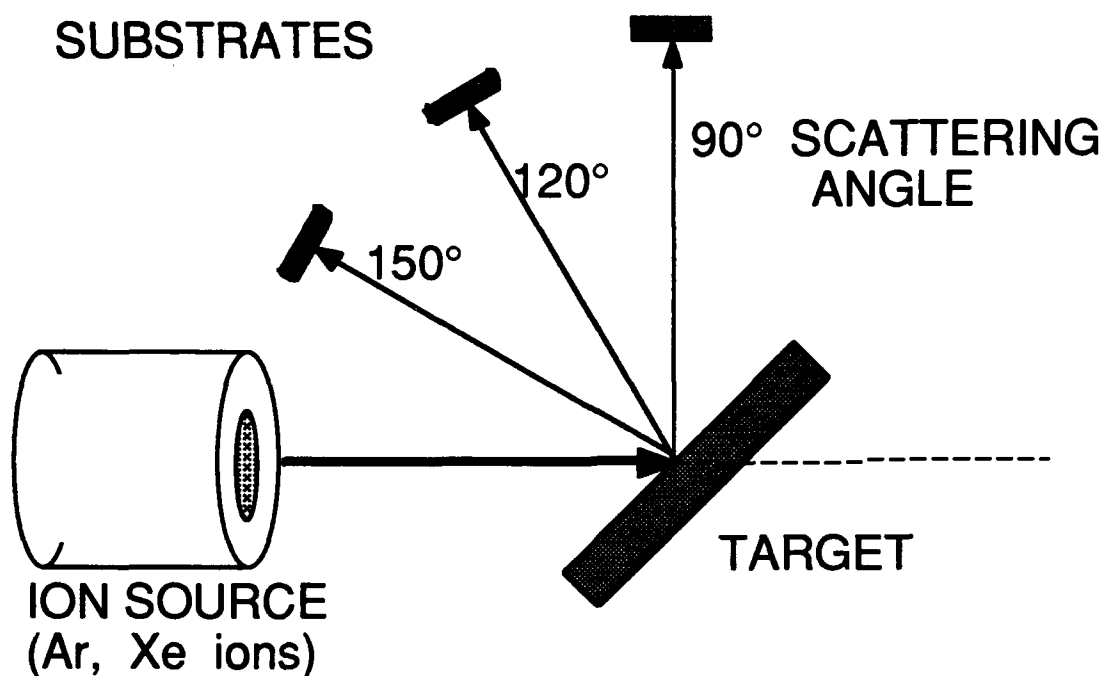


Figure 3.2. Experimental set-up used to measure relative amounts of ion scattering, at scattering angles of 90°, 120°, and 150°.

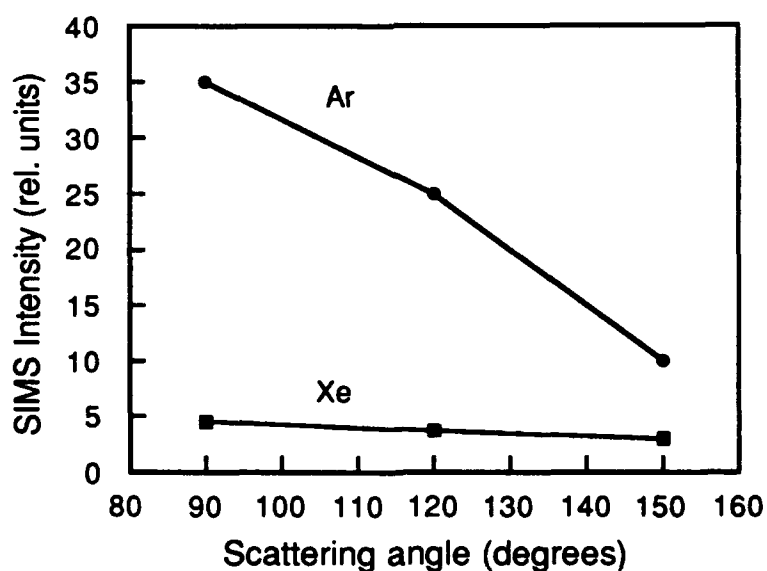


Figure 3.3. Relative Ar and Xe incorporation into Cu films, measured using secondary-ion mass spectrometry (SIMS).

deposited using either Ar^+ or Xe^+ ions. Note that much more gas incorporation was measured when using Ar ions than when using Xe, and the amount of gas incorporation decreases with increasing scattering angles. This implies that to minimize bombardment by scattered species during film growth, a heavy (high mass) sputtering gas should be used, and the substrates should be positioned such that the total scattering angle is as large as possible.

Theoretical calculations of the scattering process confirm these results. The TRIM.SP program has been used to study the scattering process as a function of ion beam energy, ion mass, target mass, and beam incidence angle to the target. The angular distribution of scattered species, and their energy distributions have also been examined. A summary of the most pertinent results are presented here.

The calculated scattering yields of Ar, Kr, and Xe ions from Cu and Ba targets are shown as a function of the incident ion energy in Figs. 3.4 (a) and (b). For these calculations, the ion beam is incident along the target normal. In Figs. 3.5 (a) and (b) similar calculations are shown, except that the ion beam incidence angle has been changed to 45° . These figures reveal several important relationships. Notice that the scattering yield *increases* with: (1) decreasing ion mass, (2) increasing target mass (Cu to Ba), and (3) increasing angle of incidence of the ion beam from the target normal.

The calculated energy distributions of scattered Ar and Xe (from a Ba target) are shown in Figs. 3.6 (a) and (b). Notice that the energy and amount of scattered species increases with decreasing ion mass, and the energy increases as the ion beam angle from the target normal increases. Although not shown here, it is also known that the energy of the scattered species increases with increasing ion beam energy.

In order to minimize bombardment by energetic scattered species during growth, the ion-to-target mass ratio should be as large as possible, the ion beam incidence direction should be close to the target normal, and the ion beam energy should be kept low.

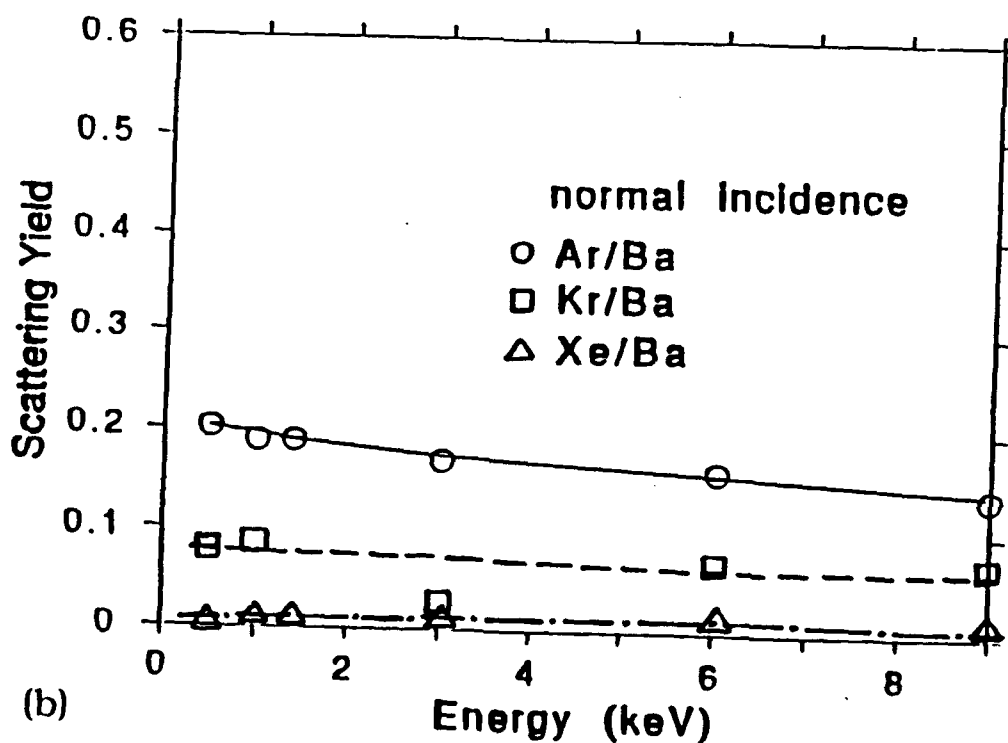
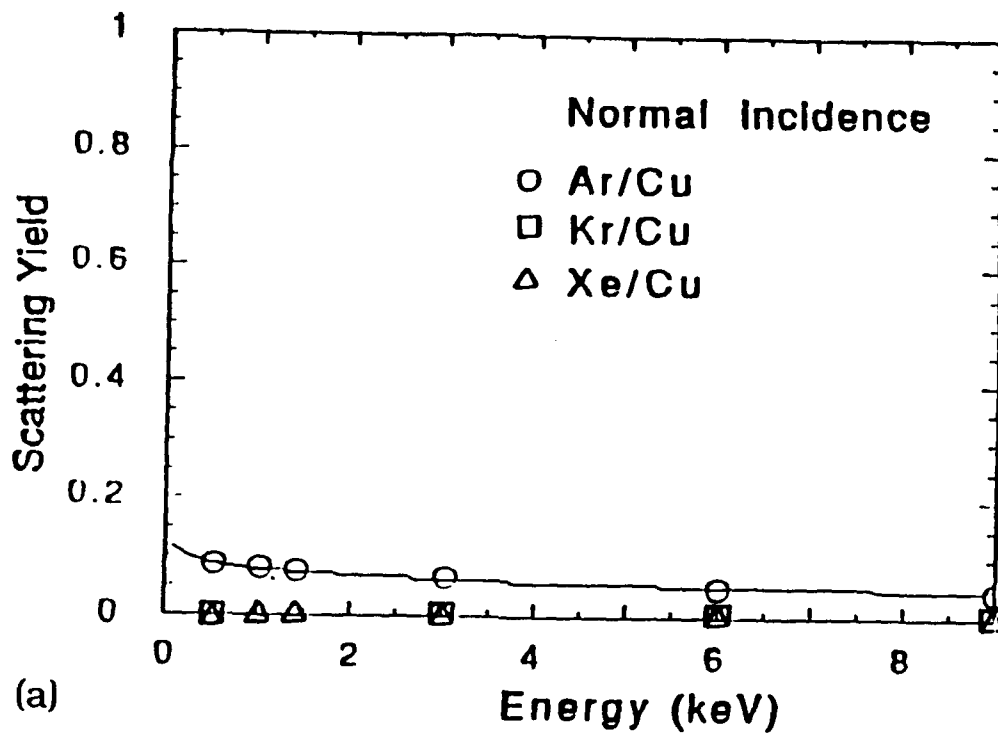


Figure 3.4. Calculated scattering yields of Ar, Kr, and Xe from (a) Cu and (b) Ba targets, with a normal-incidence ion beam.

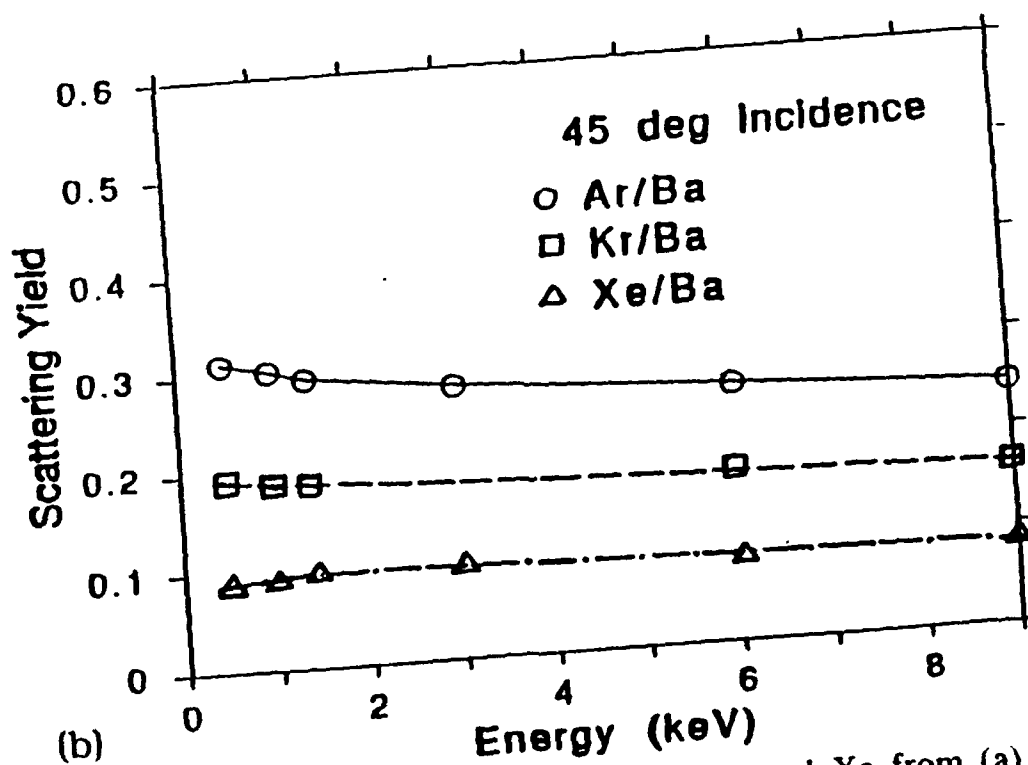
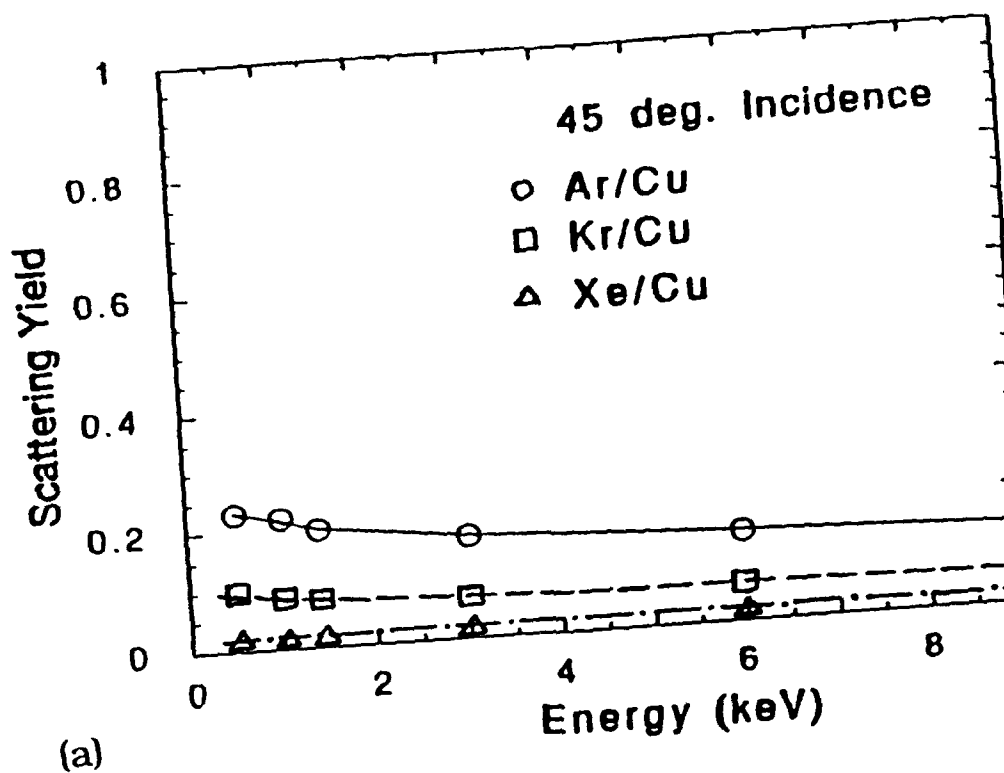


Figure 3.5. Calculated scattering yields of Ar, Kr, and Xe from (a) Cu and (b) Ba targets, with a ion-beam incidence angle of 45°.

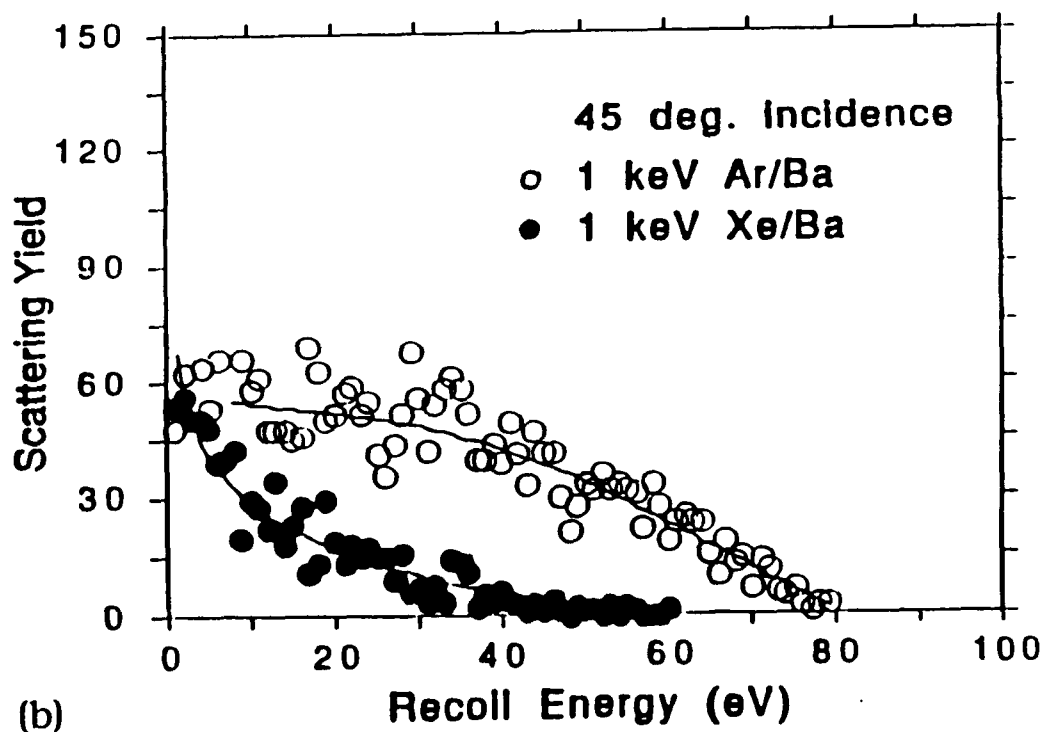
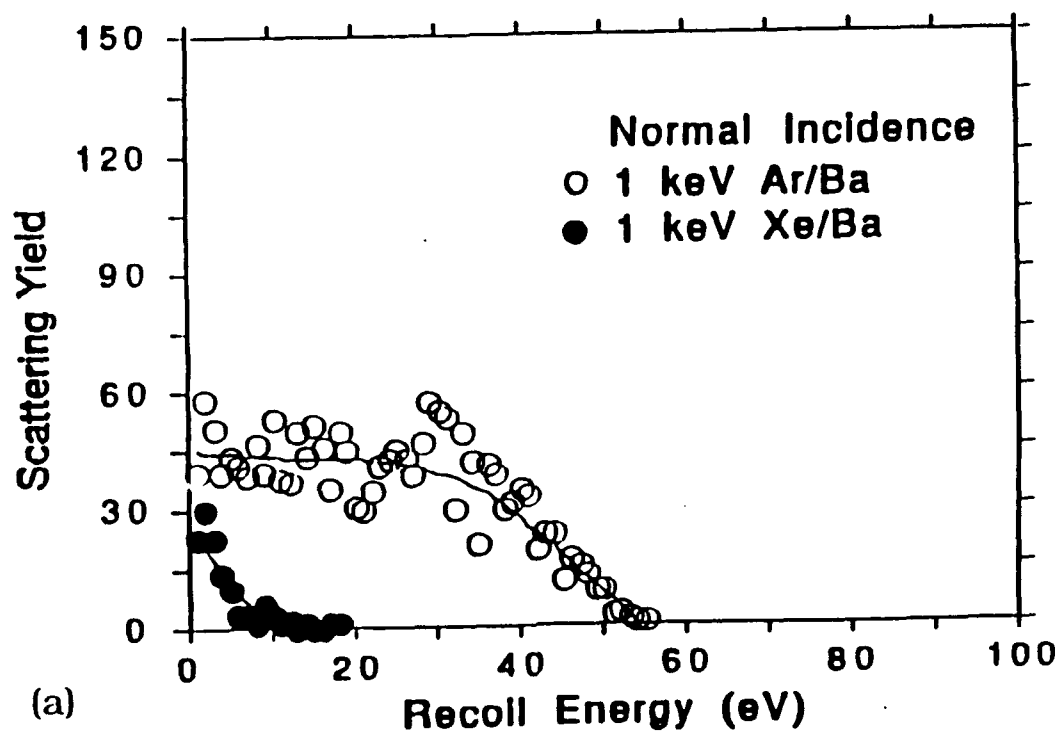


Figure 3.6. Calculated energy distribution of scattered Ar and Xe from a Ba target, sputtering with a 1 keV beam energy. The incident ion beam is either (a) normal to the target, or (b) 45° from the normal.

3.3 Conclusions

The studies of the sputtering and scattering phenomena show that, for the most part, factors which increase the sputtering yield (good) also increase the scattering yield (not good). Therefore, a balance must be struck in these cases. The ion beam incidence angle and the ion-beam energy are two examples. One factor which does increase the sputtering yield while decreasing the scattering yield is a large ion mass (such as Xenon). Therefore, most of our experiments have been performed using Xe ion beams, generally at the lowest possible energy (~500 eV).

Chapter 4

Summary of properties of *in situ* deposited $\text{YBa}_2\text{Cu}_3\text{O}_{7-\delta}$ thin films

In this chapter, the properties of $\text{YBa}_2\text{Cu}_3\text{O}_{7-\delta}$ films deposited during the course of this study using both a) single target and b) multi-target sputtering are reviewed. The single target approach has proven useful for studying the effects of deposition parameters (such as substrate temperature and oxygen pressure) on film properties. The single target approach is therefore most useful for studying fundamental aspects of the deposition process, while the multi-target approach (using Y, BaF, and Cu targets) is more versatile, allowing deposition of any given film composition. Based on the experience gained from this research program, the pros and cons of each technique will be described at the end of this chapter.

4.1 Sputtering from a single $\text{YBa}_2\text{Cu}_3\text{O}_{7-\delta}$ target

Ion-beam sputter-deposited films produced *in situ* by sputtering from a single $\text{YBa}_2\text{Cu}_3\text{O}_{7-\delta}$ target are discussed in this section. The experimental setup has been shown schematically in Fig. 2.4. Xenon is typically used as the sputtering gas, with either O_2 or O_3 supplied during growth via a tube directed at the substrate. This tube provides a pressure at the substrate which is about 20 times that of the background gas. This was measured using the stagnation-tube method.¹³ The 3-cm ion source is usually operated with a beam energy of 500 eV and a current of 20 mA (see Chap. 5 about effects of ion-beam parameters). Typical deposition temperatures and oxygen pressures resulting in the best film properties range from 680°C, 1 mTorr O_2 to 720°C, 5 mTorr O_2 . Film thicknesses are generally about 1500 Å (for the films discussed here), deposited at a rate of about 15 Å/min. After deposition, the films are slowly (~30 min.) cooled to 500°C while the O_2 pressure is increased to 200 Torr. The film is held at 500°C, 200 mTorr O_2 for 30 min., and then cooled to room temperature in about 2 hrs.

Most films have been deposited on (100) MgO substrates, although (100) SrTiO₃ has also been used to a limited extent. MgO substrates have the advantage of having superior high-frequency dielectric properties, which are important for microwave devices.²⁰

Single target ion-beam sputter-deposition has several important differences compared to other single target sputtering techniques. Because the target is not biased during ion-beam sputtering, the emission of energetic negative ions is eliminated. (These energetic negative ions can cause severe nonuniform resputtering of the film¹⁶ during magnetron or diode sputtering.) The independence of the ion beam and the target allows the target to be rotated throughout the deposition (with the beam slightly away from the target normal), which ensures that the target surface morphology remains smooth. A rough surface would otherwise develop, causing changes in the sputtered flux and its distribution.²¹

4.1.1 Electrical properties

Epitaxial, c-axis oriented YBa₂Cu₃O₇₋₈ thin films with optimized properties were deposited using substrate temperatures from 680 - 720°C and O₂ pressures from 1 - 5 mTorr. The resistivity versus temperature curve is shown in Fig. 4.1 for a film deposited at 720°C with 5 mTorr O₂ on (100) MgO. This film has a resistivity ratio (ρ_{300}/ρ_{100}) of 2.23, and a resistivity of 192 $\mu\Omega$ -cm at 100 K. The superconducting onset occurs at 87 K, with the zero resistance temperature (T_c) at ~83 K. The superconducting transition as measured by the change in the ac susceptibility is shown in Figs. 4.2 (a) and (b), for films on MgO and (100) SrTiO₃, respectively. Both films have been deposited at 720°C with 5 mTorr O₂. In both cases, the transition is fairly sharp. The T_c 's obtained from this measurement are 85 K on MgO, and 85.5 K on SrTiO₃.

The J_c has been measured using the conventional four-point arrangement used to measure the transport J_c . The transport J_c is generally more meaningful than values obtained using magnetization techniques. A 25 μ m wide, 2 mm long YBa₂Cu₃O₇₋₈ line was patterned using standard photolithographic techniques, and etched in a weak

phosphoric acid spray. The patterned line is shown in an SEM micrograph in Fig. 4.3. The J_c measured as a function of temperature (for a film deposited on MgO at 680°C with 1 mTorr O₂) is shown in Fig. 4.4. At 12 K, the J_c is 1×10^7 A/cm², and remains above 1×10^6 A/cm² up to 60 K. We saw no significant difference in the electrical properties of films on SrTiO₃, compared to those on MgO.

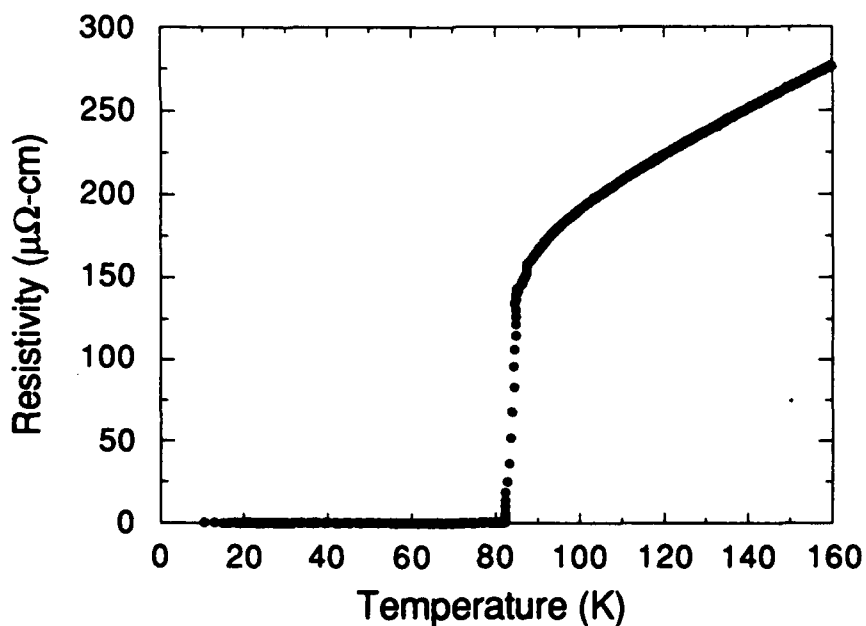


Figure 4.1 Resistance versus temperature of YBa₂Cu₃O_{7.8} film deposited on (100) MgO at 720°C, with 5 mTorr O₂.

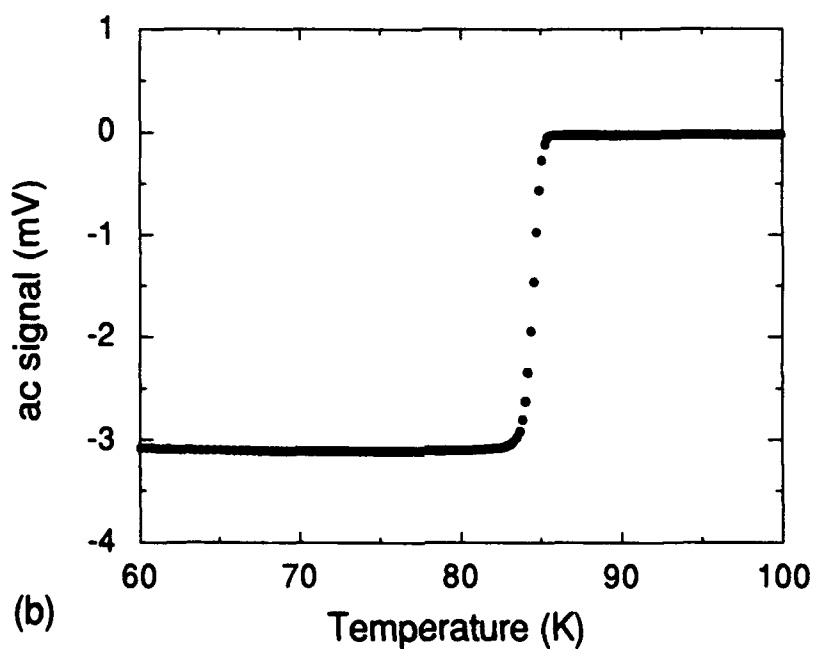
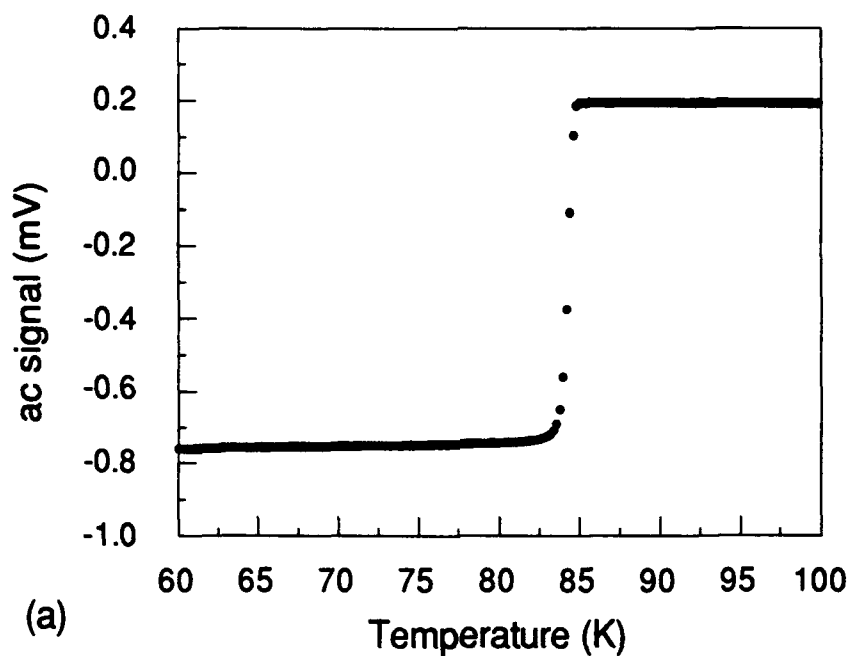


Figure 4.2. Susceptibility measurement of the superconducting transition for YBa₂Cu₃O_{7-δ} films deposited on (a) (100) MgO and (b) (100) SrTiO₃ at 720° with 5 mTorr O₂.

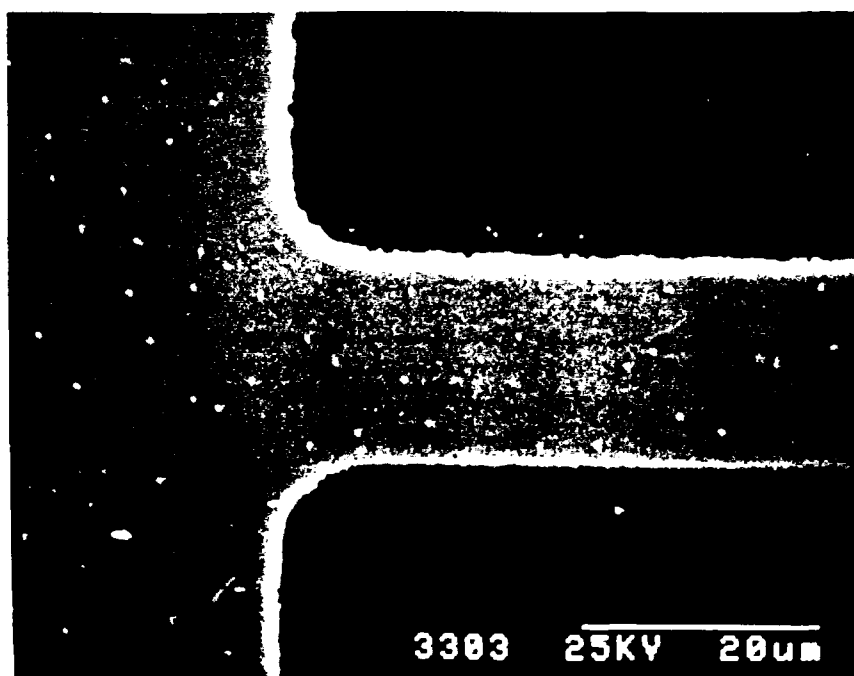
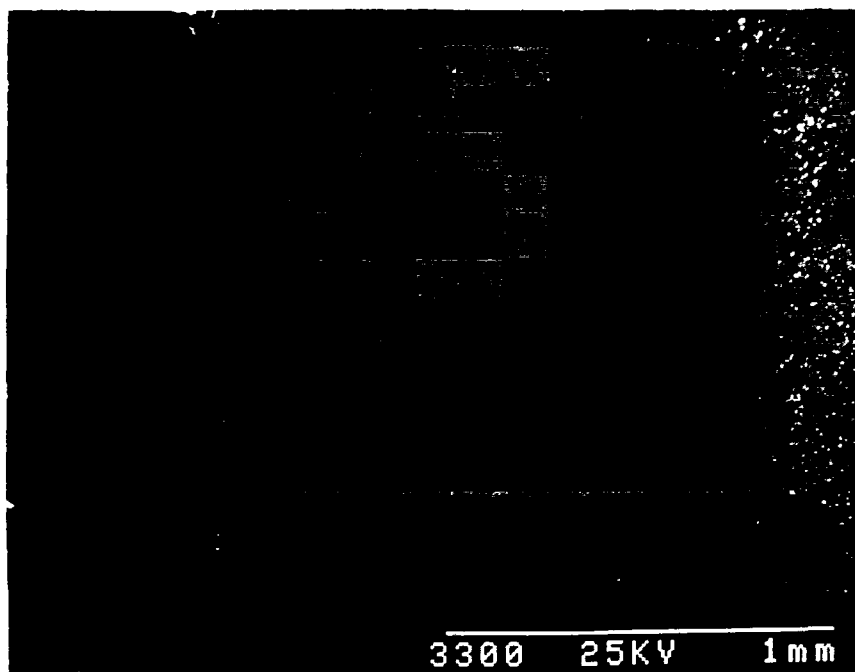


Figure 4.3. SEM micrograph of a 2 mm long, 25 μm wide $\text{YBa}_2\text{Cu}_3\text{O}_{7-\delta}$ line on MgO .

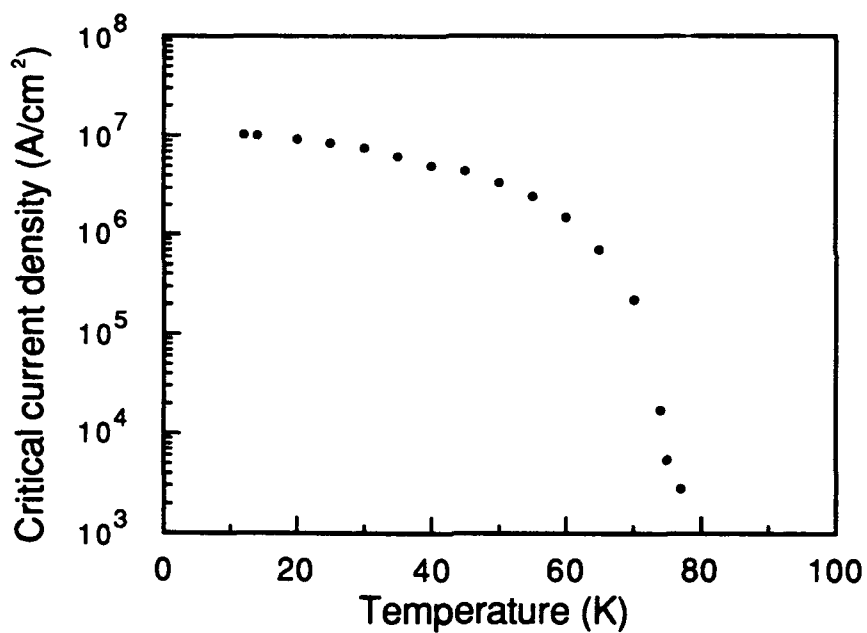


Figure 4.4. Critical current density of a 533 Å thick, 25 μm wide $\text{YBa}_2\text{Cu}_3\text{O}_{7.8}$ line as a function of temperature. This film was deposited at 680°C, with 1 mTorr O_2 .

4.1.2 Microstructural properties

Film structure and composition have been examined using X-ray diffraction, transmission electron microscopy (TEM), and Rutherford backscattering spectroscopy (RBS). X-ray diffraction patterns of films deposited on MgO and SrTiO₃ at 720°C with 5 mTorr O₂ are shown in Figs. 4.5 (a) and (b). In both cases, films are c-axis oriented, with the c-axis parameters 11.712 Å on MgO, and 11.706 Å on SrTiO₃ (the bulk value is 11.68 Å). A slightly expanded c-lattice is typical of *in situ* deposited films.²²

Figure 4.6 shows an RBS spectrum of a typical film on MgO. Through use of a simulation program, the film thickness (1710 Å) and cation composition (1.12:1.93:2.94) are revealed. Films deposited from the YBa₂Cu₃O_{7-δ} target are typically rich in Y and deficient in Ba. This occurs because the sticking coefficient of each element is different. It is expected that all of the Y atoms stick, but some of the Cu and much of the Ba does not stick. This results in an overall cation composition which is rich in Y and deficient in Ba compared to the ideal 1:2:3 composition.

Extensive microstructural characterization has been performed using TEM. Figure 4.7 shows an electron diffraction pattern and bright-field micrograph (both plan-view) of a YBa₂Cu₃O_{7-δ} film on MgO at 720°C. The diffraction pattern reveals that the film growth is epitaxial. The bright-field micrograph reveals the presence of various defects, mostly twin boundaries and low-angle grain boundaries. The twin boundaries form as a result of the tetragonal to orthorhombic transition which occurs during the cooling of the film in oxygen immediately after growth. The low angle boundaries are (at least partially) due to the lattice mismatch between YBa₂Cu₃O_{7-δ} and MgO.

Scanning tunneling microscopy (STM) and scanning electron microscopy (SEM) have both been used to study the surface morphology of these films. An STM scan of a 1 μm x 1 μm area is shown in Fig. 4.8(a). Note the stepped surface appearance, with an indication of spiral-type growth peaks. The height of each step is about 12 Å, ~equal to the c-lattice distance. This is similar to the surface structure observed by Hawley et al.²³ on off-axis sputtered YBa₂Cu₃O_{7-δ} thin films, and later by

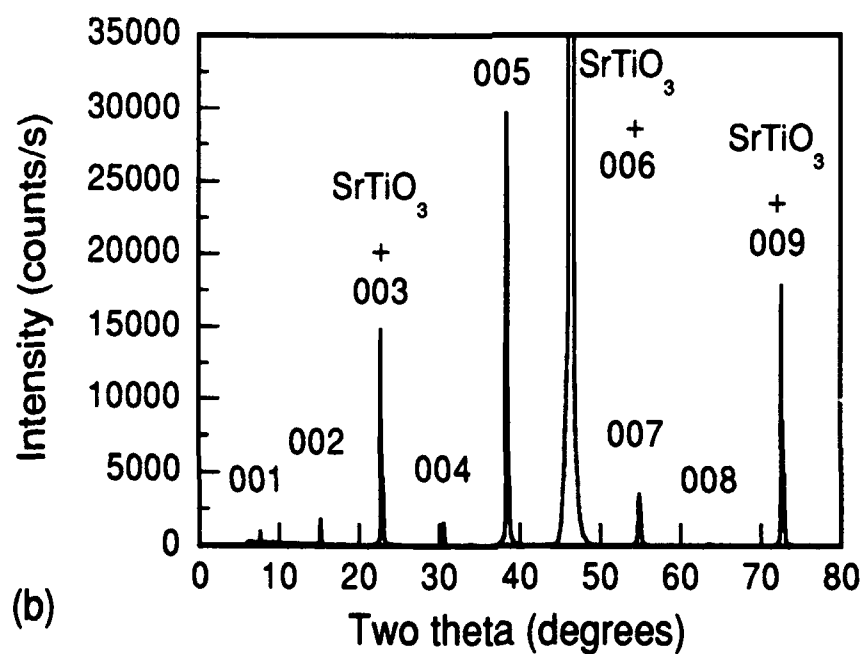
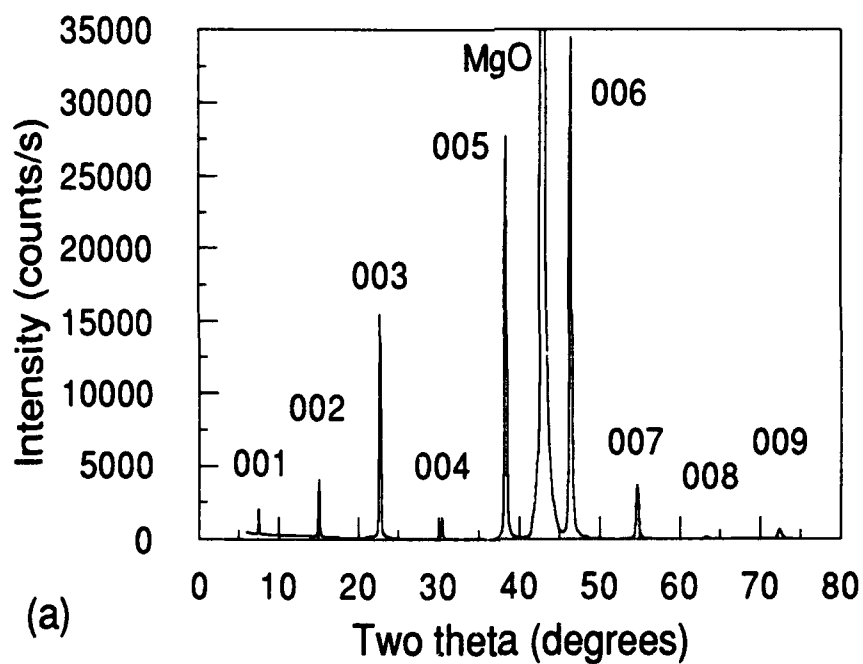


Figure 4.5. X-ray diffraction patterns of $\text{YBa}_2\text{Cu}_3\text{O}_{7-\delta}$ films deposited on (a) MgO and (b) SrTiO_3 substrates at 720°C with 5 mTorr O_2 .

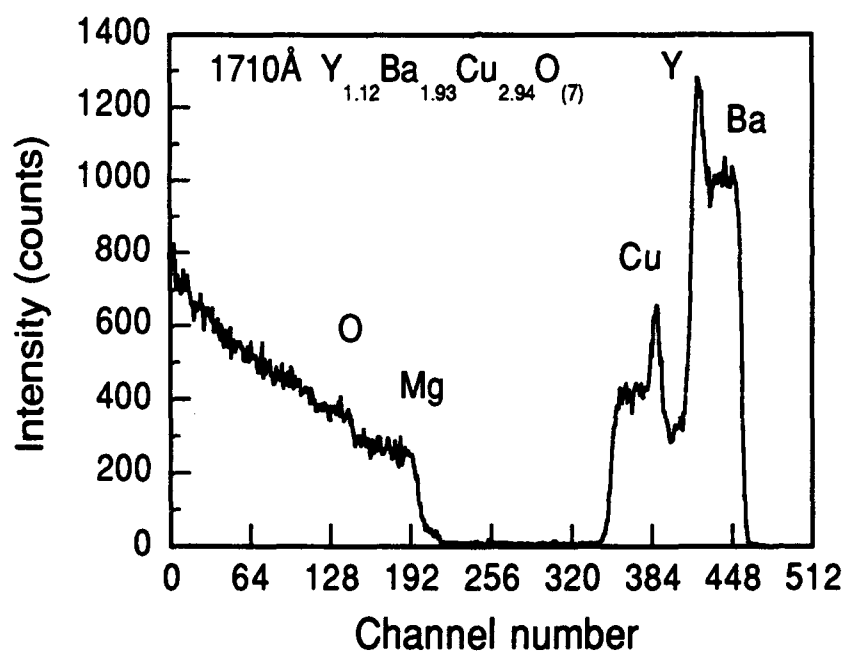


Figure 4.6. RBS spectrum of $\text{YBa}_2\text{Cu}_3\text{O}_{7-\delta}$ film on MgO , deposited at 720°C with 5 mTorr O_2 .

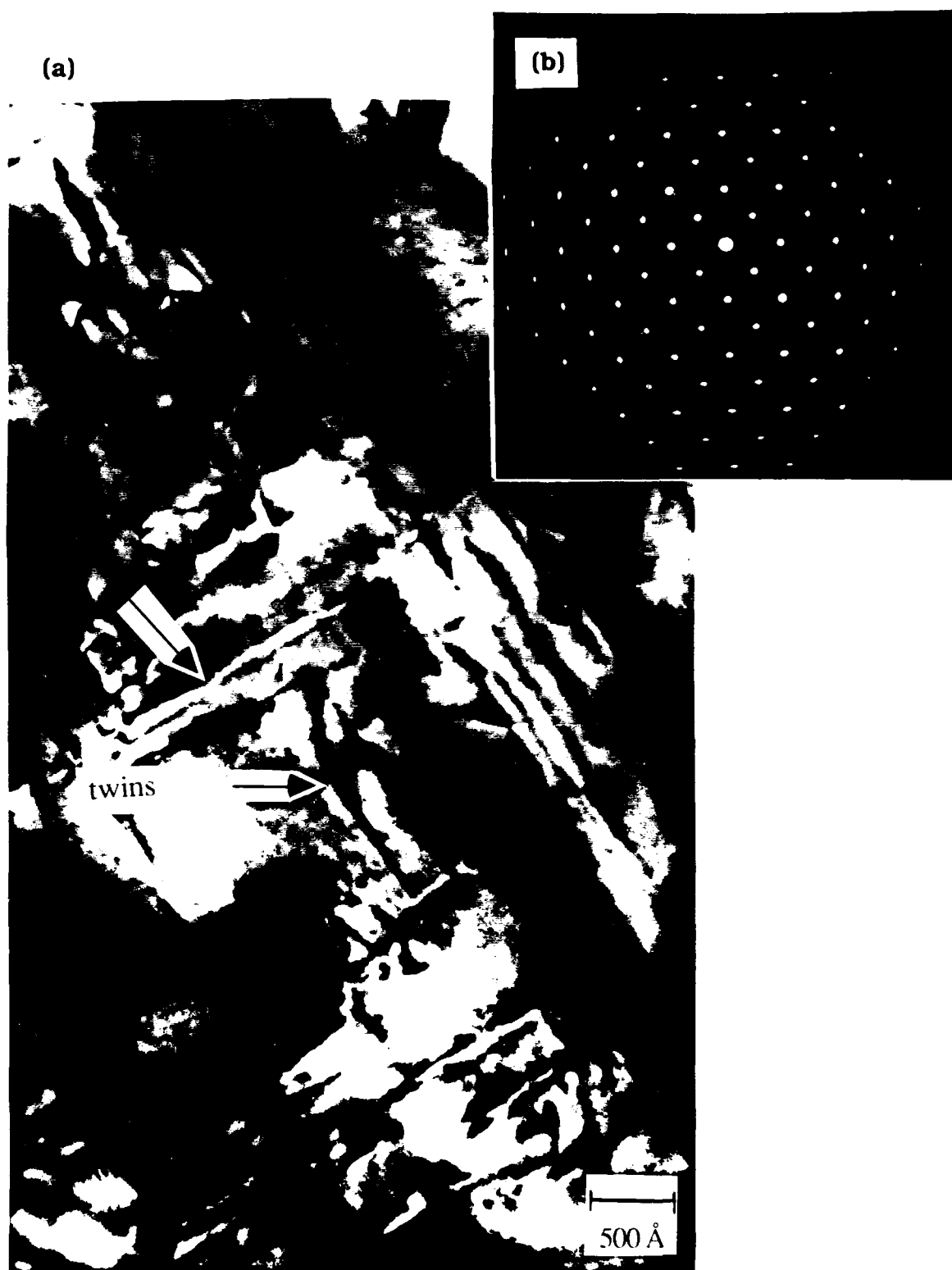
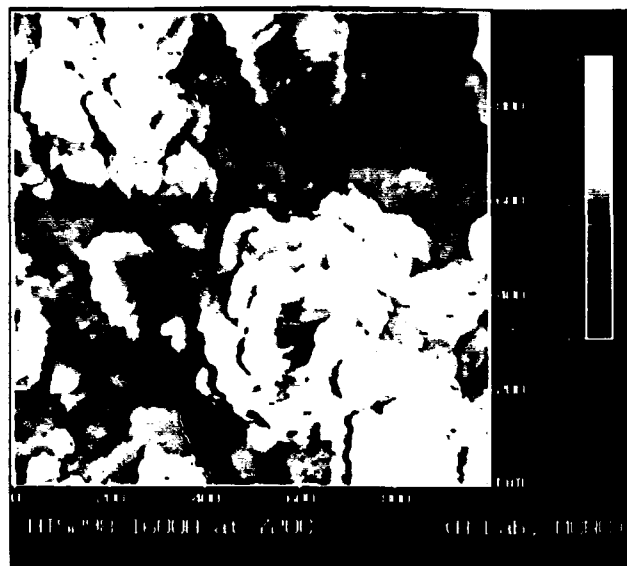


Figure 4.7. Plan-view TEM analysis showing (a) bright-field micrograph and (b) electron diffraction pattern obtained from a $\text{YBa}_2\text{Cu}_3\text{O}_{7-\delta}$ film deposited at 720°C .

(a)



(b)

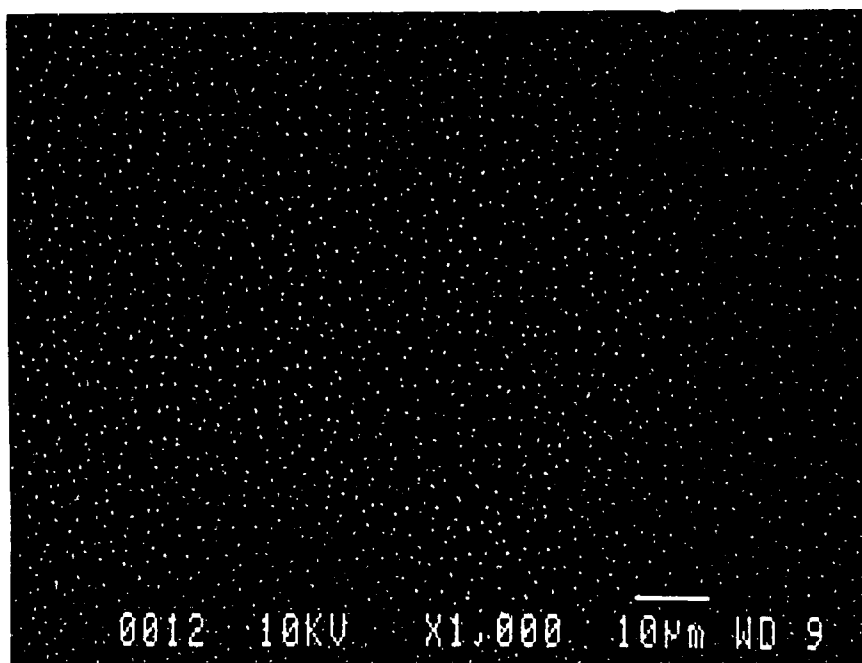


Figure 4.8. Surface morphology of YBa₂Cu₃O_{7-δ} films measured using (a) STM and (b) SEM analyses.

Krebs et al.²⁴ on laser ablated films. However, our films appear to have a smaller density of surface steps, and so the surface is smoother.

The SEM image of a larger surface area is shown in Fig. 4.8(b). Scattered across the film surface are Cu-rich precipitates, as determined using energy-dispersive x-ray analysis. We have been able to link the precipitate size and density with the deposition conditions, as will be discussed in Chapter 6. Precipitate growth is a common problem with *in situ* deposited films,²⁵ and needs to be eliminated.

All of the $\text{YBa}_2\text{Cu}_3\text{O}_{7-\delta}$ films described to this point have been c-axis oriented, deposited with O_2 during growth. When depositing with O_3 (ozone) vapor instead of O_2 , and lowering the deposition temperature to 640°C , we have been able to obtain *a*-axis oriented films on (100) MgO substrates, as shown in the X-ray diffraction pattern in Fig. 4.9 (some c-axis orientation remains). However, these films have depressed T_c 's (70 K) due to the lower deposition temperature. The conditions we used to obtain *a*-axis films are in agreement with those observed by other groups;

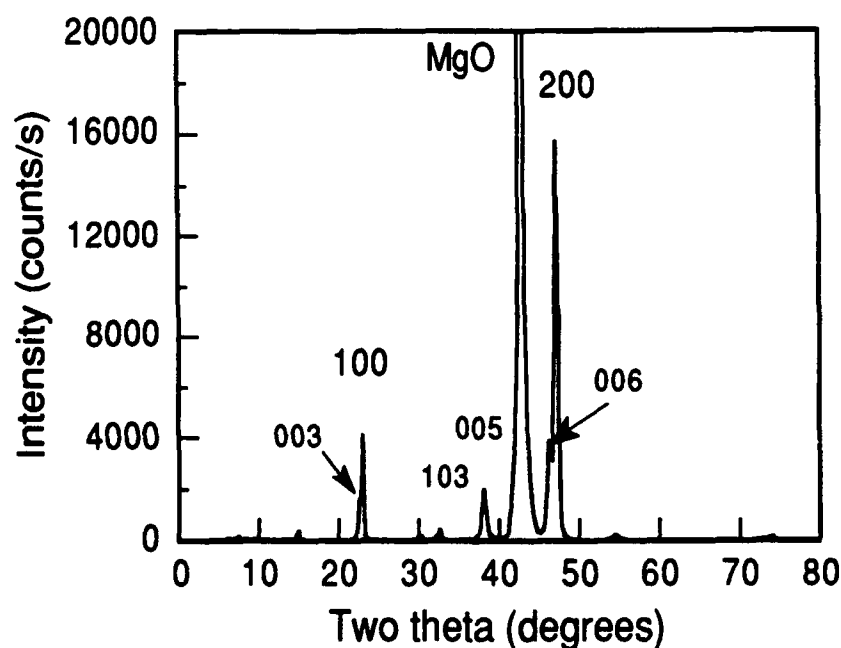


Figure 4.9. X-ray diffraction pattern of predominantly *a*-axis oriented $\text{YBa}_2\text{Cu}_3\text{O}_{7-\delta}$ film on (100) MgO at 640°C with ozone vapor.

namely, that lower deposition temperatures and/or higher oxygen pressures (activity) tend to favor a-axis growth.²² A-axis oriented films have potential applications for Josephson junctions, because the coherence length is longer in the a-direction than in the c-direction.¹²

4.2 Sputtering from multiple targets

The system geometry shown in Figure 2.3 is that used for the computer-controlled sequential deposition from Y, BaF, and Cu targets. As described earlier, layer thicknesses are controlled using feedback from a quartz crystal rate monitor. The deposition sequence used for most experiments was Y, Ba(F), and Cu. Therefore, this is not a true layer-by-layer growth process (which may be possible using the sequence Y-Cu-Ba-Cu-Ba-Cu).

The films described in this section were deposited using 1200 eV Kr ions, with a 20 mA beam current. A substrate temperature of 760°C was used, with O₃ vapor as the oxidant. Molecular oxygen was unable to provide a high enough oxygen activity during growth. (In the single-target case, much of the (reactive) oxygen is supplied by the sputtering target, as we discovered later in the research program; see chapter 6.) After deposition, films are cooled to 500°C in 40 min. while increasing the O₂ pressure to 200 Torr. The films are held at 500°C for 30 min., and then cooled to room temperature in about 90 min. (the same post-processing used for the single-target deposition).

4.2.1 Electrical properties

The resistance versus temperature of a sequentially-deposited YBa₂Cu₃O_{7-δ} thin film on (100) MgO is shown in Fig. 4.10. The film shows metallic behavior, with a superconducting onset of 82 K, and a T_c(R=0) of 60 K. (The depression of the T_c is likely caused by the high beam energy (1200 eV) used in these experiments. It was later discovered that the beam energy has significant effects on the electrical properties; see Chap. 5.)

4.2.2 Microstructural properties

An X-ray diffraction pattern of a film on MgO is shown in Fig. 4.11. The superconducting film is c-axis oriented, as would be expected, with a c-axis parameter of 11.77 Å. Note also that oriented BaF is present in this film, revealing that F incorporation does occur, and can be a potential problem. An RBS spectrum of a typical film is shown in Fig. 4.12. Fitting this spectrum with a simulation program reveals a film thickness of 950 Å, and a cation composition of 1.13:2.15:2.72 .

The plan-view TEM diffraction pattern shown in Fig. 4.13 reveals that the $\text{YBa}_2\text{Cu}_3\text{O}_{7.8}$ film is epitaxially oriented to the MgO substrate. The multiple spot pattern around each main spot is mainly due to double diffraction (from the $\text{YBa}_2\text{Cu}_3\text{O}_{7.8}$ and MgO underneath). Some second-phase Cu_2O and BaF is also evident from this diffraction pattern.

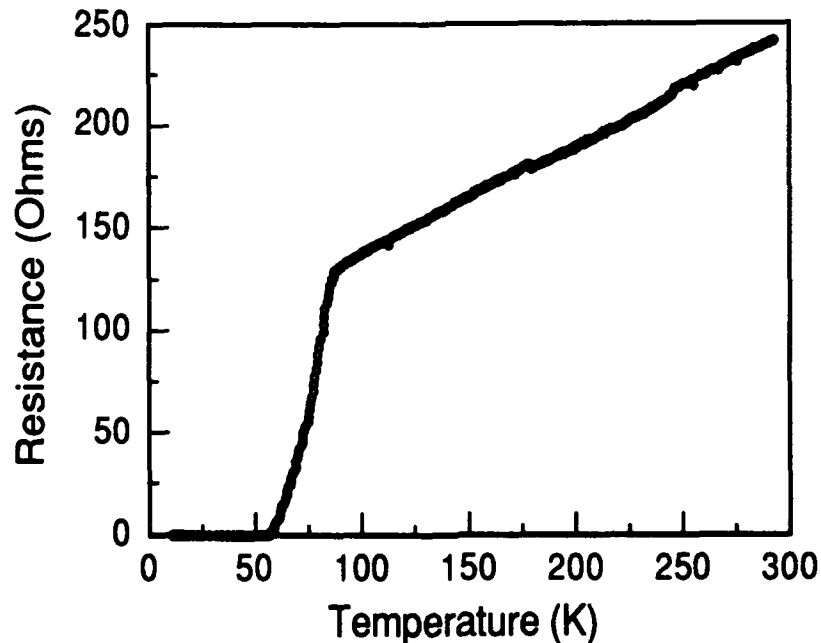


Figure 4.10. Resistance versus temperature of a $\text{YBa}_2\text{Cu}_3\text{O}_{7.8}$ film on (100) MgO deposited sequentially from multiple, elemental targets.

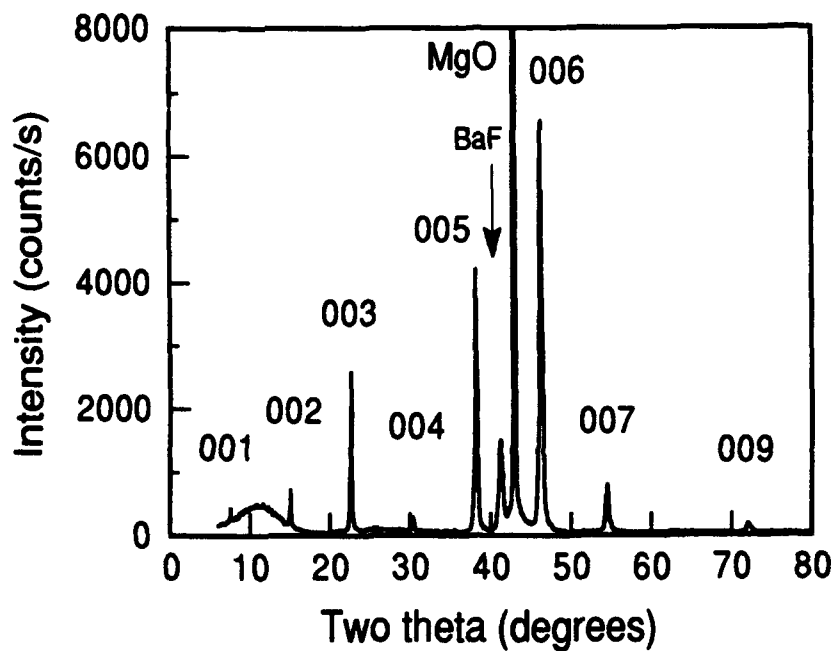


Figure 4.11. X-ray diffraction pattern of a $\text{YBa}_2\text{Cu}_3\text{O}_{7-\delta}$ film on MgO, deposited sequentially from elemental targets.

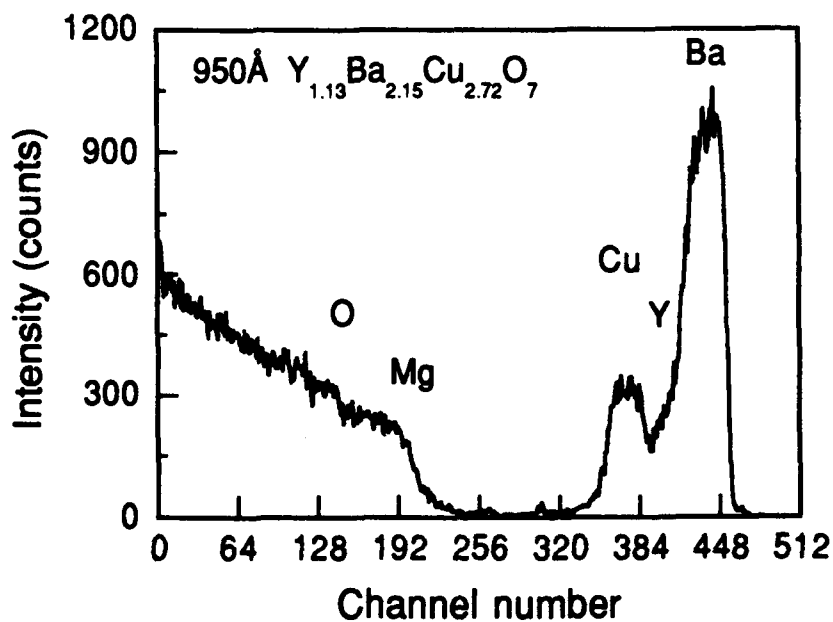


Figure 4.12. RBS spectrum of a $\text{YBa}_2\text{Cu}_3\text{O}_{7-\delta}$ film on MgO, deposited sequentially from elemental targets.

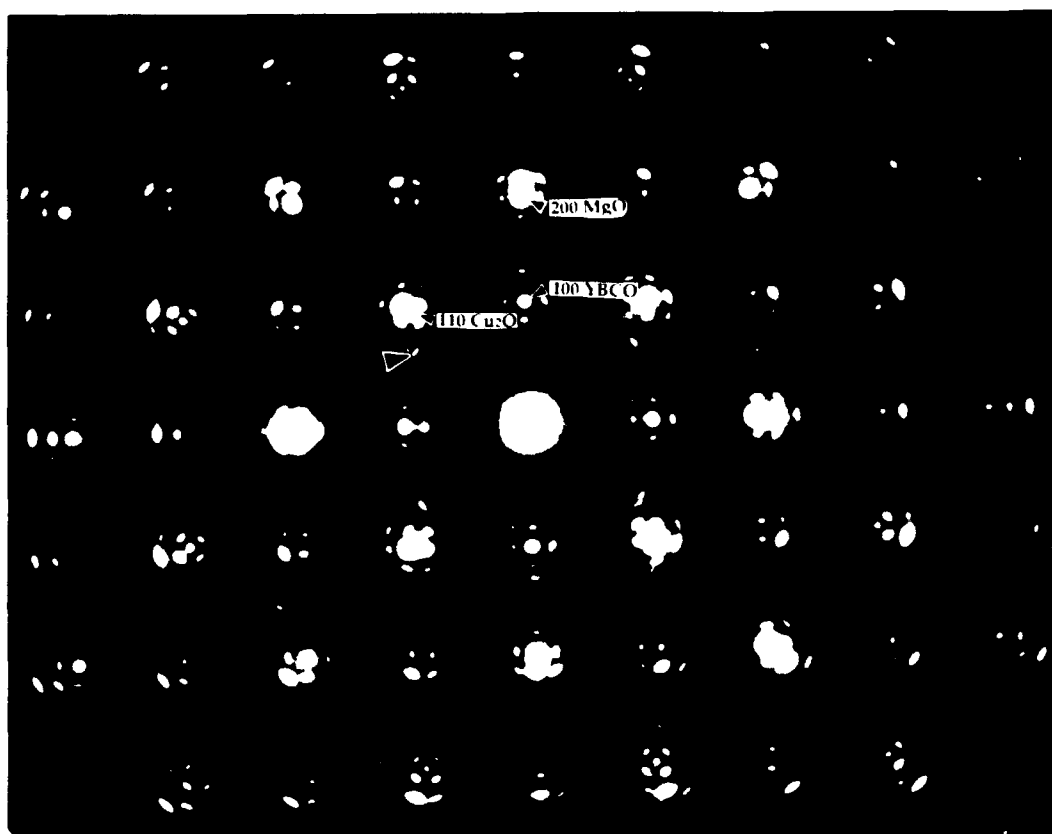


Figure 4.13. Plan-view TEM diffraction pattern of $\text{YBa}_2\text{Cu}_3\text{O}_{7-\delta}$ on MgO . The multiple spots are mainly due to double-diffraction (from the MgO layer below the $\text{YBa}_2\text{Cu}_3\text{O}_{7-\delta}$), and also to Cu_2O and BaF second phases.

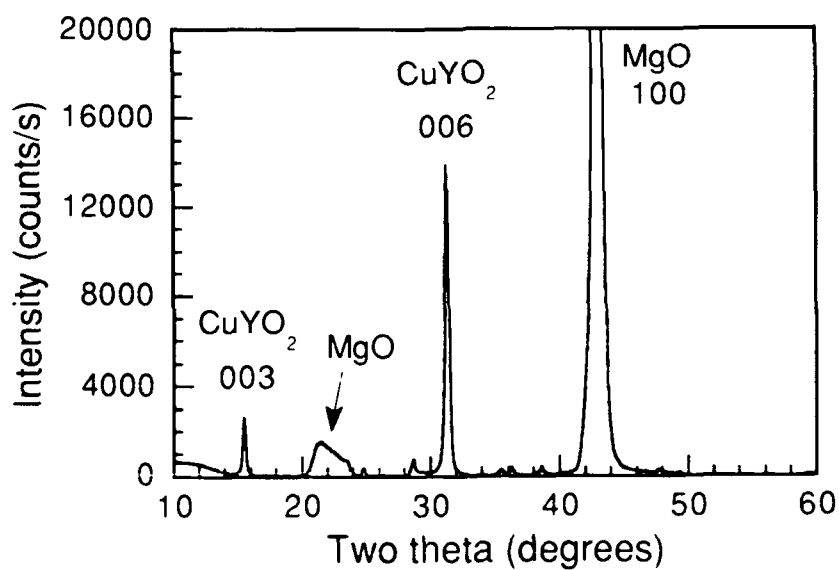


Figure 4.14. X-ray diffraction pattern of an oriented CuYO_2 film.

Using this multiple target setup, other phases can also be obtained if desired. For example, by sputtering from only Y and Cu targets (with O_3 present), we have obtained oriented $CuYO_2$ insulating films. This is shown by the X-ray diffraction pattern in Fig. 4.14. Sputtering from only the Cu target (with O_3 present) produces oriented CuO films. These examples show the versatility of this technique.

4.3 Conclusions

Under the proper operating conditions, use of the single-target approach results in films having good electrical and structural properties. Furthermore, run-to-run consistency is very good. However, film properties are slightly inferior to those deposited using either off-axis sputtering²⁵ or laser-ablation deposition.² To date, no group using ion beam sputtering has produced films with properties equivalent to those produced using these other techniques. (However, James et al.²⁶ have produced films on $SrTiO_3$ with T_C 's of ~ 89 K, although the J_C 's are about equal to what we obtain on MgO .) The exact reasons for this have yet to be determined, and should be overcome once understood. Ion beam sputtering does have the advantage of being able to coat large areas (see Chap. 8), and so the technique should be investigated further.

The use of sequential deposition from multiple targets to produce $YBa_2Cu_3O_{7-\delta}$ films has been shown to be feasible. This technique has also been applied in our laboratory to deposit epitaxial $Pb(Zr_xTi_{1-x})O_3$ ferroelectric thin films²⁷ and $KNbO_3$ electrooptic thin films.²⁸ For the growth of $YBa_2Cu_3O_{7-\delta}$, this technique has proven difficult for a number of reasons. These difficulties have to do mainly with the material properties of $YBa_2Cu_3O_{7-\delta}$ itself, and not the deposition technique per se. Because Ba is very reactive in its elemental form, a compound target must be used for the Ba source, such as BaF , BaO , $BaCO_3$, or a Ba-Cu compound. We have mainly used BaF , but this often results in BaF second phase in the films. BaO is fairly reactive with water vapor, and $BaCO_3$ can potentially result in C contamination, which can drastically reduce T_C .²⁹ Ba-Cu compounds have been used by some groups, but this eliminates the possibility of depositing in a true layer-by-layer fashion.

The other major difficulty is the high oxygen activity needed to stabilize the superconducting phase. The chamber pressure during ion beam sputtering must be kept below about 2 mTorr (whereas the pressure may be as high as hundreds of mTorr in magnetron sputtering systems and laser ablation systems). This has required the use of O_3 as an oxidant. Because there is some oxidation of the Y and Cu targets during processing, the oxygen flux to the substrate is different when the beam is on or off (during target rotation). Some effects on film properties are expected due to this variable oxygen flux. Because of the many possible oxide phases that can form between Y, Ba, and Cu, it is also very important that individual layers be very thin so that surface diffusion enables proper mixing of the components.

Chapter 5

Effects of ion beam energy on *in situ* $\text{YBa}_2\text{Cu}_3\text{O}_{7-\delta}$ film properties

We examined the effects of ion beam energy on film properties for a variety of reasons. Our earlier studies of ion scattering and sputtering yields (Chap. 3) revealed that use of a heavy sputtering gas would maximize the sputtering yield while minimizing the amount of energetic scattered ions. Therefore, we used Xe gas or Kr for most experiments. However, the effects of the beam energy on the scattering had not been clarified. For example, the scattering yield slightly decreases with increasing energy, although the energy of these scattered species will increase. Because the $\text{YBa}_2\text{Cu}_3\text{O}_{7-\delta}$ structure is rather sensitive to ion bombardment damage,³⁰ we felt it was necessary to thoroughly investigate the effects of ion beam energy. The effects of beam energy on the properties of other materials deposited using ion beam sputtering can be found in Ref. [31].

5.1 Experimental

A series of experiments were performed using a $\text{YBa}_2\text{Cu}_3\text{O}_{7-\delta}$ composite target, and Xe sputtering gas. Figure 2.4 shows the basic system geometry used in these experiments. The ion beam energy was varied from 500 eV to 1200 eV in order to determine the effects of the beam energy on film properties. The beam current was lowered when using higher beam energies to keep the total power (and therefore deposition rate) constant. Either molecular oxygen or ozone was used as an oxidant in these experiments. Substrate temperatures were in the range of 720° to 780°C. (In this range of oxidizing conditions and substrate temperatures, the effects on film properties are minimal, see Chap. 6). All films were deposited on polished (100) MgO substrates (with no further surface treatments).

5.2 Electrical properties

The most dramatic effect of the beam energy is its influence on the T_C . The T_C (as measured by the ac susceptibility) is shown as a function of the ion beam energy in Fig. 5.1. Notice the clear trend of increasing T_C with decreasing beam energy. This trend implies that, even though Xe gas is used, there is still significant film bombardment when using a 1200 eV beam, resulting in a T_C of only about 70 K. The T_C rises to 83-85 K when the beam voltage is lowered to 500 eV. We have performed experiments with beam energies of 400 eV and 250 eV (although the ion source grids are not really designed to be used at these low voltages) and observed no further increase in the T_C , so a 500 eV beam energy appears to be an optimum value. Because the sputtered species themselves are fairly energetic when operating in this low pressure regime,³² their energy may be limiting the T_C to the 85 K we obtain (which is independent of whether we use MgO or SrTiO₃). The fact that this trend of T_C with ion beam energy holds when using a variety of substrate

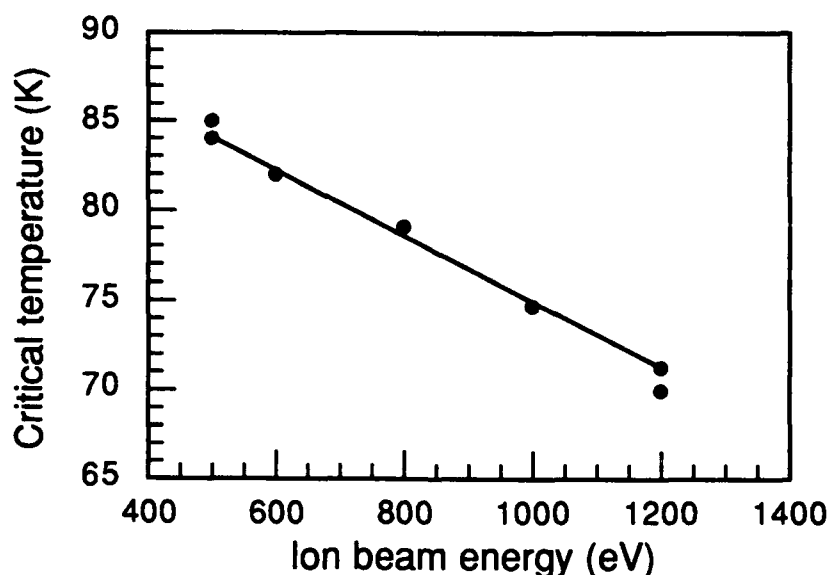


Figure 5.1. Transition temperature of YBa₂Cu₃O_{7.8} films on MgO as a function of the Xe⁺ ion-beam energy.

temperatures (above 720°C) and oxidizing conditions gives further proof of its importance. (Many films were deposited using a 1200 eV beam energy under a variety of temperature and oxygen conditions; none had a T_c greater than 70 K.)

We have also measured the critical current density J_c of films deposited at 500 eV and 1200 eV using a Xe ion beam. A typical graph showing the J_c versus temperature for a film deposited using a 500 eV ion beam has been shown in Fig. 4.4. As expected, the J_c of a 1200 eV film is significantly lower. The J_c is about 3 times lower at low temperatures, and falls to a couple orders of magnitude lower at higher temperatures, due to the lower T_c .

5.3 Microstructural properties

X-ray diffraction patterns of films deposited with 500 eV and 1200 eV Xe ions look virtually identical. Both show c-axis oriented films; however, the c-lattice parameter is different, being 11.71 Å at 500 eV and 11.75 Å at 1200 eV (although both show some scatter depending on the substrate temperature). The expanded c-lattice is an indication of either atomic disorder or oxygen deficiency.³⁰

Compositional analysis of films deposited at 500 eV and 1200 eV were performed using Rutherford backscattering spectroscopy (RBS). The results indicated film compositions of 1.10:1.98:2.92 and 1.15:1.96:2.88 for films deposited at 500 eV and 1200 eV, respectively. This is not a large enough difference to significantly affect the properties of *in situ* YBa₂Cu₃O_{7-δ} thin films.⁷

Microstructural differences are revealed using plan view transmission electron microscopy (TEM). Figure 5.2(a) shows an electron diffraction pattern and a bright field micrograph of a YBa₂Cu₃O_{7-δ} film deposited using a 500 eV beam. The diffraction pattern indicates that the film is epitaxial with respect to the MgO substrate. The micrograph reveals the presence of many twin boundaries (short straight lines running in perpendicular directions), as well as very low-angle boundaries. The twins form as a result of the tetragonal to orthorhombic transition which occurs upon cooling the film in oxygen after deposition.

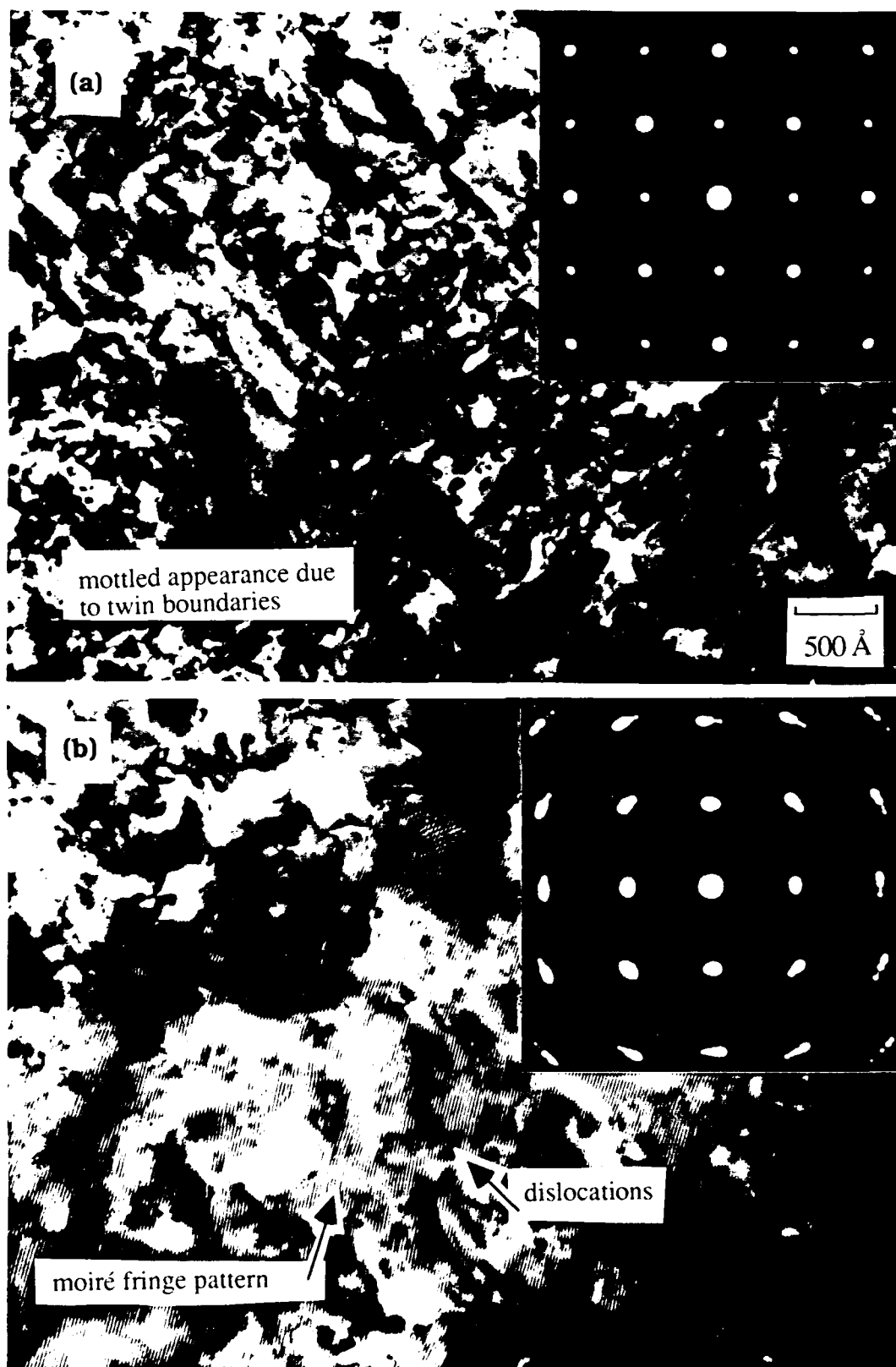


Figure 5.2. Plan-view TEM bright-field micrographs and diffraction patterns of films deposited using either (a) 500 eV or (b) 1200 eV Xe^+ .

The TEM diffraction pattern and bright field micrograph of a film deposited with a 1200 eV beam are shown in Fig. 5.2(b). The diffraction pattern reveals that this film is made up of c-axis oriented grains, with a rotation between grains on the order of 10° ($\pm 5^\circ$ of twist with respect to the substrate). The bright-field micrograph reveals these boundaries between grains; however, there is no indication of any twin boundaries as are seen in Fig. 5.2(a). This is an indication that the film deposited with a 1200 eV ion beam is not (fully) orthorhombic.

A study of the film surface structure has been performed using scanning tunneling microscopy (STM). In figure 5.3, STM images of the surfaces of films deposited using (a) 500 eV and (b) 1200 eV ion beams are shown. These films were deposited with a substrate temperature of 720°C , and 5 mTorr O_2 . Notice that both films show a terraced surface structure, with some indication of the spiral growth pattern observed by Hawley et al.²³ Note that the density of surface 'peaks' and steps is highest for the film deposited with a 1200 eV beam energy. This could be interpreted as a result of excess bombardment during growth, which could serve as nucleation sites for the growing 'spirals'. The film deposited with a 500 eV Xe beam is much smoother (each surface step is about 1.2 nm, or one c-lattice spacing), which could be important for multilayer structures requiring thin continuous layers.

5.4 Conclusions

The data presented in this chapter reveals that the ion beam energy has significant effects on ion-beam sputter-deposited $\text{YBa}_2\text{Cu}_3\text{O}_{7-\delta}$ thin films. This is observed when using Xe sputtering gas, which would result in less scattering events than if Kr or Ar gas were used. The measured T_c 's, the c-lattice parameters obtained using x-ray diffraction, and the TEM microstructures indicate that the films are not fully orthorhombic when deposited using a 1200 eV Xe ion beam. This is most likely a result of lattice disorder occurring during growth, which makes it

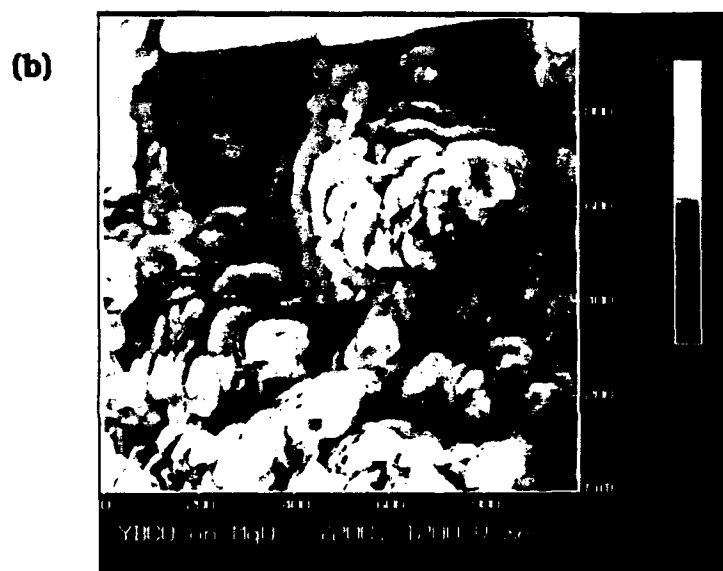
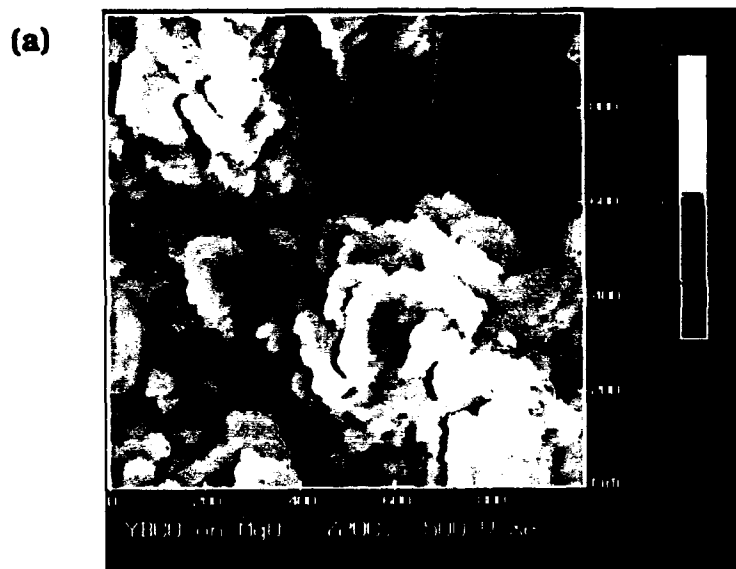


Figure 5.3. STM images of the $\text{YBa}_2\text{Cu}_3\text{O}_{7-8}$ film surface (on MgO substrates) when depositing with (a) 500 eV and (b) 1200 eV Xe^+ .

impossible for the tetragonal to orthorhombic transition to go to completion. The exact disorder mechanism causing this effect has not been determined.

Many early studies have revealed how bombardment during sputter deposition can drastically affect film compositions. We now clearly show that excess bombardment can also degrade film properties even if no significant compositional changes are observed. It is expected that bombardment energies greater than about 50 eV are responsible for defect creation. Atoms with energies less than this may actually be beneficial in some ways; such as by increasing surface mobilities, allowing for deposition at lower temperatures.

Chapter 6

Effects of substrate temperature and oxygen pressure on properties of *in situ* YBa₂Cu₃O_{7-δ} thin films

A complete study of the YBa₂Cu₃O_{7-δ} film growth process requires an examination of the role of substrate temperature and oxygen pressure on film properties. This is especially important for YBa₂Cu₃O_{7-δ}, because of its thermodynamic properties.⁶ Using various *in situ* film growth techniques, researchers have observed that substrate temperature and oxygen pressure play a role in determining nearly all film properties, both electrical and structural.^{22,25} Because of the energetics of the ion-beam sputtering process (as discussed in chapters 3 and 5), the temperature-O₂ pressure relationships to film properties may be significantly different than with other lower-energy deposition techniques. For example, energetic bombardment could produce effects such as lowering the temperature required to produce epitaxial films. Presently, no complete studies of this type have been carried out using ion beam sputtering.

6.1 Experimental

In order to enable a study in which only the substrate temperature and oxygen pressure are varied, a composite YBa₂Cu₃O_{7-δ} target was sputtered using fixed ion-beam parameters. The system geometry is as shown in Fig. 2.4. The target is rotated throughout the deposition in order to maintain a smooth target surface morphology. A 500 eV, 20 mA Xe ion beam was used, with O₂ gas directed at the substrate using a quartz nozzle. The use of the O₂ nozzle allowed substrate O₂ pressures to be as high as 20 mTorr, while the background O₂ pressure is only 1 mTorr (the local substrate pressure has been measured using the stagnation tube method¹³). Oxygen pressures investigated range from 1 mTorr to 15 mTorr. The substrate temperatures examined in this study range from 640°C to 760°C. Substrate temperatures have been calibrated using an optical pyrometer (to measure the temperature of a

silicon substrate). The MgO substrates are mounted using a silver paste, ensuring good thermal contact with the holder.

After film deposition, the oxygen pressure is kept low (< 1 Torr) as the films are cooled to 500°C (~ 30 min.), then the oxygen pressure is increased to 600 Torr. The film is held at 500°C for 30 min., and then slowly cooled (> 60 min.) to room temperature. (This post-processing is different than we have used for other experiments, but resulted in similar film properties. This seems to disprove what some groups have postulated; namely, that the exact manner in which the O_2 pressure is increased while cooling to room temperature is very important.³³)

A complete discussion of the deposition conditions used here, and the film property results, has been presented by Soble.³⁴

6.2 Electrical properties

The superconducting transition temperature of films deposited in this study have been obtained by measuring the ac susceptibility change versus temperature. At a deposition temperature of 760°C , the effects of varying the O_2 pressure are clearly seen, as shown by the susceptibility curves in Fig. 6.1. Note that with 1 mTorr O_2 , there is practically no transition; with 5 mTorr, the transition is fairly sharp (onset 83.8 K, 6.4 K width); and by 15 mTorr, the transition is very sharp (onset 83 K, 1.2 K width). This is in general agreement with the findings of researchers using other deposition techniques. At lower deposition temperatures ($\leq 720^{\circ}\text{C}$), 1 mTorr was sufficient to produce films having fairly sharp transitions, and the transition was not as dependent on the O_2 pressure. This implies that sufficient O_2 was present in these cases. A complete listing of the properties of all films are given in Table 6.1. Note that at a deposition temperature of 640°C , the transition width begins to broaden. This is an effect caused by the low substrate temperature (and not the O_2 pressure), limiting the atom mobilities during deposition.

The temperatures and O_2 pressures under which $\text{YBa}_2\text{Cu}_3\text{O}_{7-\delta}$ is thermodynamically stable have been well studied.⁶ In Fig. 6.2, the stability line of tetragonal $\text{YBa}_2\text{Cu}_3\text{O}_6$ is shown (along with the stability line of CuO). To the left of this line, $\text{YBa}_2\text{Cu}_3\text{O}_6$ decomposes into other

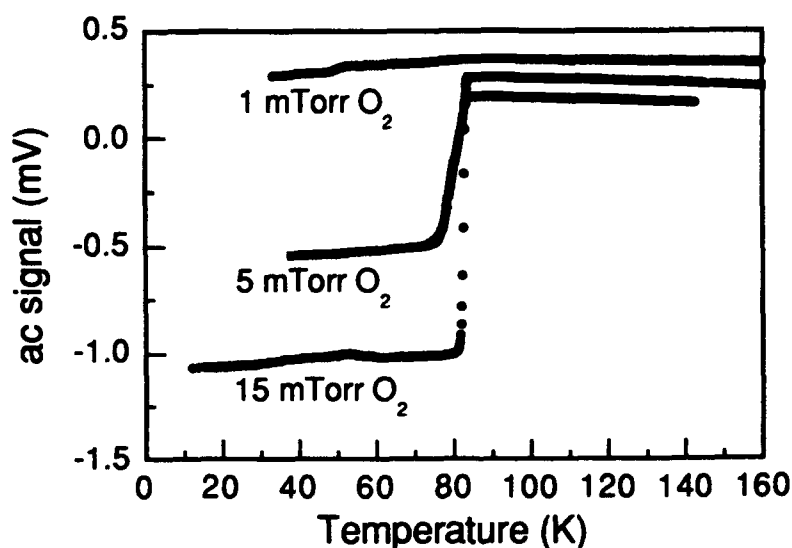


Figure 6.1. Superconducting transitions shown for YBa₂Cu₃O_{7-δ} films deposited on MgO at 760°C with either 1, 5, or 15 mTorr O₂.

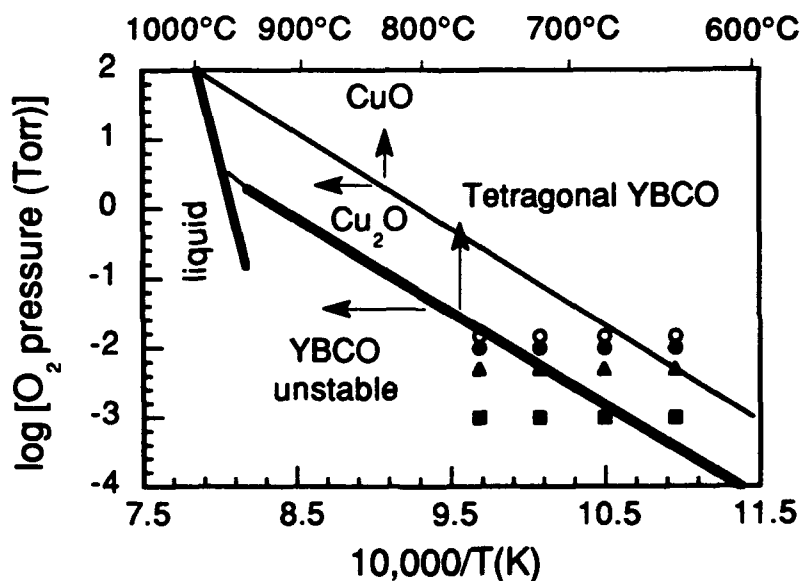


Figure 6.2. Thermodynamic stability diagram of YBa₂Cu₃O_{7-δ}. The heavy line marks the stability limit of the tetragonal YBa₂Cu₃O₆ phase, while the other line marks the Cu₂O-CuO stability line. The conditions under which the films studied here were deposited are shown by the circles, triangles, and squares.

Table 6.1 Listing of film properties as a function of substrate temperature and oxygen pressure. The T_c shown is the onset of the susceptibility transition, as is standard. The c-lattice parameter shown is for the 007 diffraction peak. All films are deposited on MgO substrates.

Substrate temp. (°C)	pO ₂ (mTorr)	T _c (K)	δT_c (10%-90% width) (K)	c-lattice constant (Å)	RBS cation ratios (Y:Ba:Cu)
760	1	~80	37	11.708	
760	5	83.8	6.4	11.704	1.12:1.92:2.96
760	10	83.3	1.7	11.697	1.22:1.76:3.01
760	15	83.0	1.3	11.714	1.14:1.78:3.08
720	1	84.4	5.0		1.12:1.80:3.08
720	5	84.8	0.9	11.712	1.13:1.92:2.94
720	10	84.0	2.3		1.14:1.86:2.97
720	15	83.8	0.9		1.13:1.87:3.00
680	1	84.7	1.7		1.14:1.93:2.93
680	5	83.8	1.3	11.726	
680	10	83.9	1.6		
680	15	84.2	2.4		1.15:1.91:2.94
640	1	81.3	3.4	11.731	1.11:1.89:3.00
640	5	79.4	5.2	11.729	
640	10	78.3	6.8	11.719	
640	15	81.6	5.0	11.717	1.16:1.82:2.82

phases (such as Y_2BaCuO_5 and Cu_2O). The conditions under which the films were deposited in this study are included in this diagram as individual points. Note that four of the film growth conditions are clearly in the region where $\text{YBa}_2\text{Cu}_3\text{O}_6$ is unstable, yet they all contain the superconducting phase (X-ray diffraction of the film grown at 760°C with 1 mTorr O_2 shows the presence of the superconducting phase). This is evidence that oxygen sputtered from the target is greatly contributing to the total oxygen flux at the substrate. It is also possible that the energetic conditions during growth are enhancing the O_2 activity. The $\text{YBa}_2\text{Cu}_3\text{O}_6$ stability line has then effectively been brought down one order of magnitude in $p\text{O}_2$. This becomes important when scaling up to cover larger substrate areas, because the chamber pressure during ion-beam sputtering must be less than ~ 2 mTorr. It is much more difficult to locally increase the substrate pressure when a large area must be uniformly covered with O_2 . Because film growth is possible at $\sim 700^\circ\text{C}$ with only 1 mTorr of O_2 , this will not be a problem (as long as an oxidized target is used).

6.3 Microstructural properties

The structural properties examined in this study include the film composition, film orientation, microstructure, lattice parameters, and surface morphology. The results of film properties obtained using RBS, X-ray diffraction, and TEM are presented in this section. Studies of the film surface morphology (using STM and SEM) will be discussed separately in the following section.

The composition of selected films was examined using Rutherford backscattering spectroscopy (RBS), with the results listed in table 6.1. Note that all films are rich in Y compared to the 1:2:3 target composition. Assuming that the sticking coefficient of the sputtered Y is one, this reveals that the sticking coefficients of Ba and Cu are less than one (on average, about 0.80 for Ba, and 0.86 for Cu). There does not appear to be any significant trend in the film composition as substrate temperature and oxygen pressure are varied (although it is expected that some trend would exist).

X-ray diffraction was used to examine the film orientation and lattice parameters of selected films. All films examined were c-axis oriented, except for the film deposited at 760°C with 1 mTorr O₂, which had a mixed orientation. The c-lattice parameters measured from the 007 diffraction peak are listed in Table 6.1. Although there is some scatter in the data, two trends are present. The c-axis parameter tends to decrease (towards the bulk value of 11.68 Å) as the temperature and oxygen pressure are increased. This is clearly shown in Fig. 6.3, in which the c-axis parameter is plotted as a function of substrate temperature, at an oxygen pressure of 5 mTorr. We believe that the higher surface diffusion rates at the higher temperatures allow a better ordering of the cations. This minimizes the amount of defects (of as yet unknown type) which contribute to the lattice expansion.

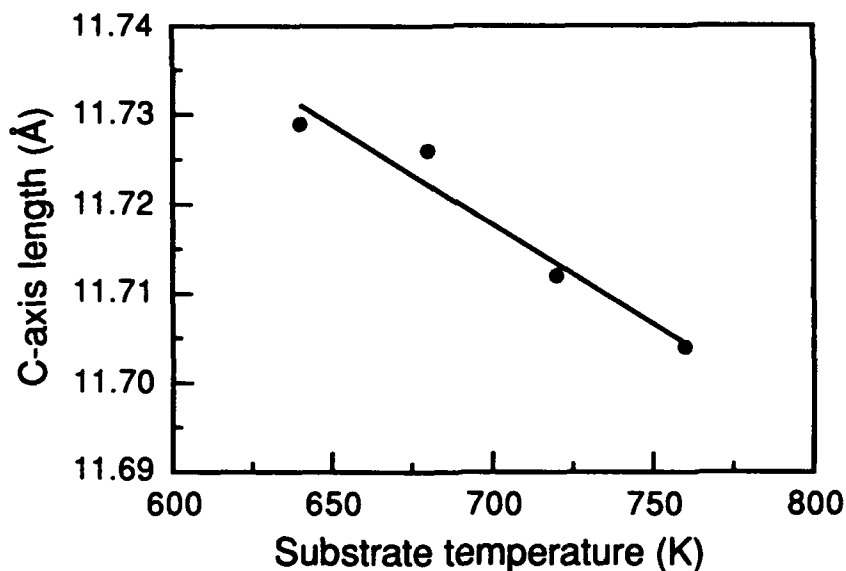


Figure 6.3. C-axis length (measured from the 007 diffraction peak) as a function of the substrate temperature. All films have been deposited using 5 mTorr O₂.

The film microstructures have been examined in more detail using transmission electron microscopy (TEM). Bright field micrographs and electron diffraction patterns are shown in Fig. 6.4 for films deposited at (a) 720°C, (b) 680°C, and (c) 640°C, with 5 mTorr oxygen. The bright-field micrographs reveal twins in all samples, and low-angle grain boundaries, but we are not able to make any quantitative comparisons between the microstructures of these samples. The electron diffraction patterns do reveal some differences between these films. The diffraction patterns reveal that the film deposited at 720°C is epitaxial. As the substrate temperature is lowered, the degree of epitaxy worsens, as indicated by the rotational spreading of the diffraction spots. This is an indication that the surface mobility during growth is not sufficient for complete ordering with respect to the substrate.

Analysis of the electrical and structural properties indicate that 680 - 720°C is the optimal growth temperature regime for YBCO films on MgO. Film properties are noticeably degraded when the substrate temperature is lowered to 640°C.

6.4 Surface morphology study

The surface morphology of ion-beam sputter-deposited $\text{YBa}_2\text{Cu}_3\text{O}_{7-\delta}$ thin films has been examined using scanning electron microscopy (SEM) and scanning tunneling microscopy (STM). Films examined have been deposited on (100) MgO substrates at temperatures of 720°C, 680°C, and 640°C, with a local O_2 pressure of 1 mTorr. Films of thickness 1600 Å and 200 Å have been analyzed.

A smooth surface is important for superconducting films used in microwave devices or in Josephson junctions. Obtaining smooth film surfaces is difficult when depositing multicomponent oxide thin films. A common problem related to the *in situ* synthesis of YBCO thin films is the appearance of second phase precipitates scattered across the film surface. These precipitates are present in both laser-ablation deposited films³⁵ and off-axis sputtered films.²⁵

Scanning electron microscopy (SEM) has been used to investigate the surface structure on a large scale, to reveal the presence and areal

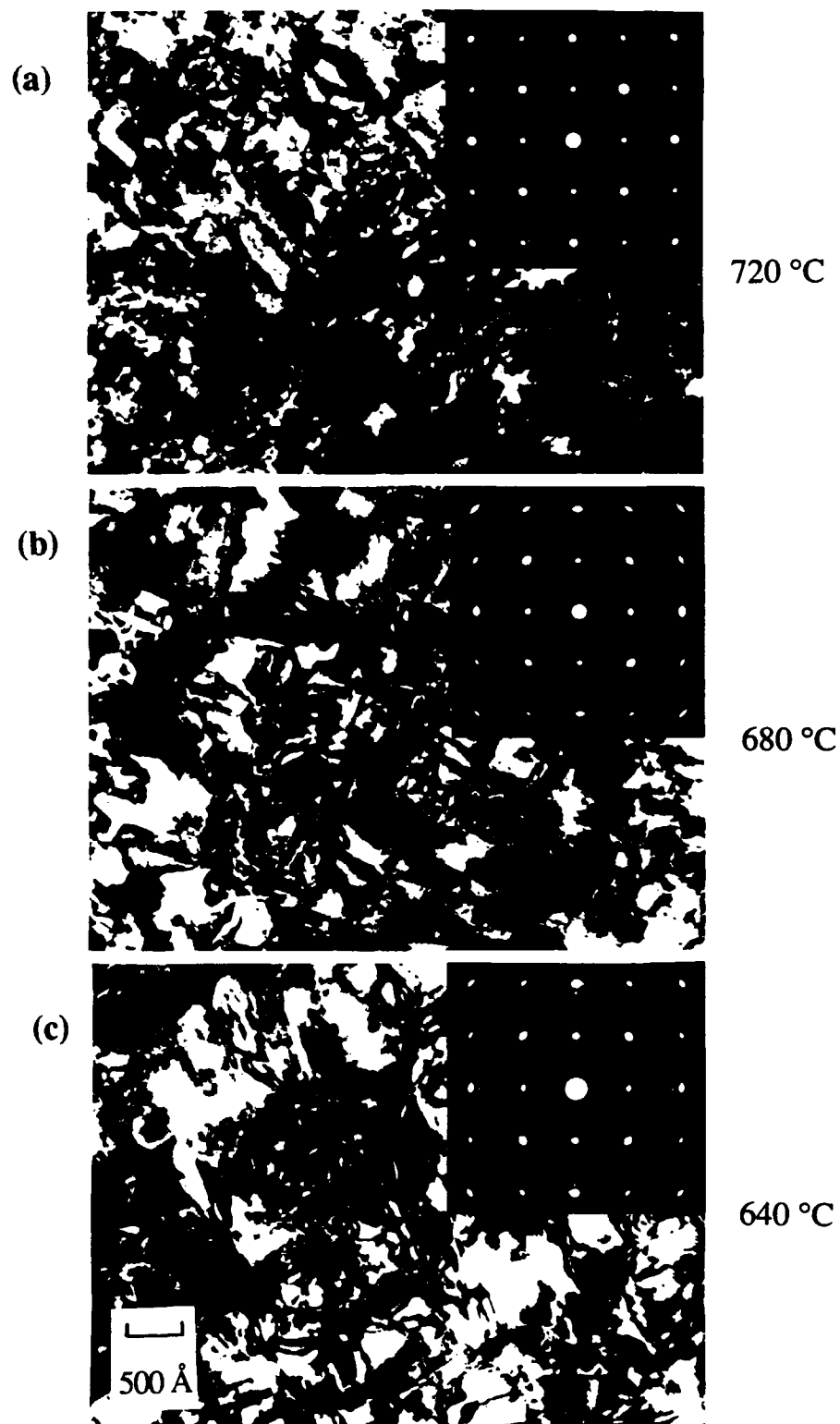


Figure 6.4. Plan-view TEM micrographs and electron diffraction patterns of $\text{YBa}_2\text{Cu}_3\text{O}_{7-\delta}$ films deposited at (a) 720°C, (b) 680°C, and (c) 640°C, all with 5 mTorr O_2 .

density of possible surface precipitates. The SEM analysis was performed with a JOEL JSM-840 operated with an electron beam energy of 10 keV. Scanning tunneling microscopy (STM) has been used to measure the surface roughness, with an atomic-scale resolution (vertically). The STM analysis was performed using a Digital Instruments Nanoscope II system, with a tip bias of 500 mV, and a tunneling current of 0.20 nA.

Results of the STM analysis of the surface morphology are shown in Fig. 6.5(a-e), as a function of the growth temperature and the film thickness. Each photograph represents a 1000 nm x 1000 nm area. Evidence of the screw dislocation growth mode reported for off-axis magnetron sputter-deposited YBCO films²³ and laser-ablation deposited films²⁴ is observed for the films deposited at 680°C (b,e) and 720°C (a,d), but is not evident in the film deposited at 640°C (c). Note that the characteristic width (or length) of the surface features increases with increasing substrate temperature, and with increasing film thickness. In Fig. 6.6, line profiles of single STM traces are shown, revealing the height of vertical steps. The film deposited at 720°C shows step heights of about one unit cell (5 steps = 5.86 nm). The smallest steps in the films deposited at 680°C and 640°C film are also about one c-axis unit, but some steps appear to be two unit-cell heights. In each trace, the position of the highest marker is at the top of a growth spiral. The average roughness of the 1600Å films deposited at 720°C, 680°C, and 640°C are ± 0.95 nm, ± 2.04 nm, and ± 0.97 nm, respectively, obtained from the STM scans shown in Figs. 6.5(a), 6.5(b), and 6.5(c). (The average roughness is defined as the mean vertical distance from a centerline drawn through the profile).

The STM scans shown in Fig. 6.5 reveal the fine-scale features of the surface morphology, and indicate the presence of the screw dislocation growth mode previously reported by Hawley et al.²³. Note that as the growth temperature decreases, the characteristic width of the growth spirals decreases, and at 640°C there is no clear evidence that growth is controlled by the screw dislocation mechanism. Also note that at this temperature, the T_c decreases and the c-axis parameter increases, as shown in Table 6.2. The T_c decrease and c-axis expansion indicate

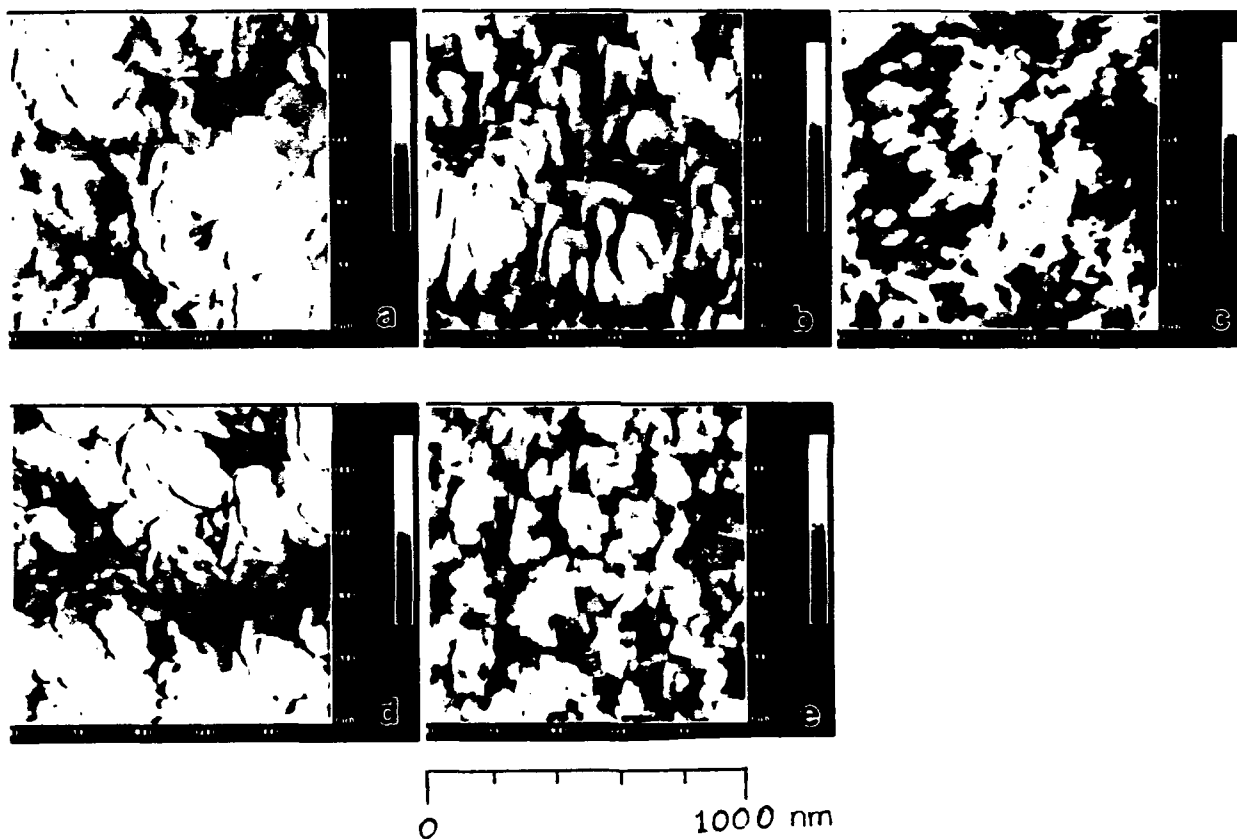


Figure 6.5. STM images of the surface morphology of 1600 Å thick films deposited at (a) 720°C, (b) 680°C, and (c) 640°C; and of 200 Å films deposited at (d) 720°C and (e) 680°C.

Table 6.2 Properties of 1600 Å thick $\text{YBa}_2\text{Cu}_3\text{O}_{7-\delta}$ films on (100) MgO, deposited with 1 mTorr O_2 .

Substrate temperature (°C)	T_c (K)	ΔT_c (K)	c-axis length (Å)	cation composition Y:Ba:Cu
720	84.4	5.0	11.712	1.12:1.87:3.02
680	84.7	1.7	11.724	1.18:1.71:3.11
640	81.3	3.4	11.731	1.19:1.72:3.09

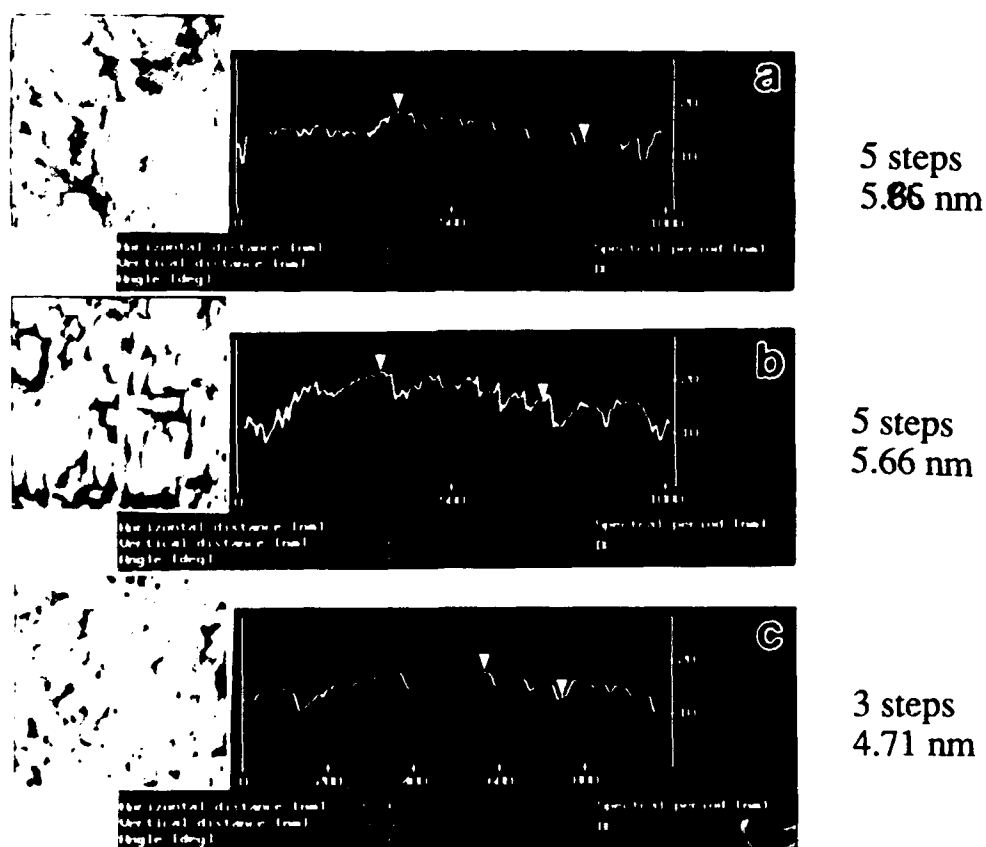


Figure 6.6. Line profiles of single STM traces, showing the height of individual surface steps. Profiles are for films deposited at (a) 720°C, (b) 680°C, and (c) 640°C.

that at this temperature, the surface mobility is insufficient to allow equilibrium growth of the superconducting phase. Following this reasoning, it appears that the occurrence of the screw dislocation growth mechanism is an indicator of favorable growth conditions (for co-deposited, c-axis YBCO films under the conditions of most vacuum deposition techniques). Therefore, complete elimination of surface steps may not be possible in these types of films. Two possible ways to eliminate these steps (i.e., eliminate the screw dislocation growth mode) would be to 1) deposit a-axis films, or 2) deposit c-axis films layer-by-layer. YBCO is not layered in the a-axis direction, and relatively smooth a-axis films have been reported.³⁶ Depositing a-axis films essentially requires co-deposition (and strict control of temperature and O₂ pressure), and sequential deposition could be used to produce layer-by-layer c-axis films.

Although the screw dislocation growth mode is evident in these ion-beam sputter-deposited films, the surface morphology is significantly smoother than that of off-axis sputtered films reported previously.²³ The off-axis films reported previously (for YBCO on (100) MgO at 705°C) have growth spirals which are more completely developed, and have many more steps per-unit-length than the films reported here. It is possible that the morphology difference can partly be attributed to the higher oxygen partial pressure used in that study (60 mTorr). The other factor which could account for the smoother surfaces of the ion-beam sputtered films is the energetic bombardment present during growth. During ion-beam sputtering, the pressure is low enough that sputtered and reflected species arrive at the film surface without significant energy loss.³² During off-axis sputtering, the high gas pressure and off-axis geometry ensure that atoms arrive with near-thermal energies. It is known that ion bombardment during growth can have significant effects on film nucleation and microstructure,³⁷ affecting electrical, optical, and mechanical properties. It is possible that with appropriate low energy ion-bombardment, the density of surface steps could be reduced further. The bombardment would need to be of low enough energy not to produce implantation, excessive resputtering, or atomic defects, but high enough to increase the surface mobility of

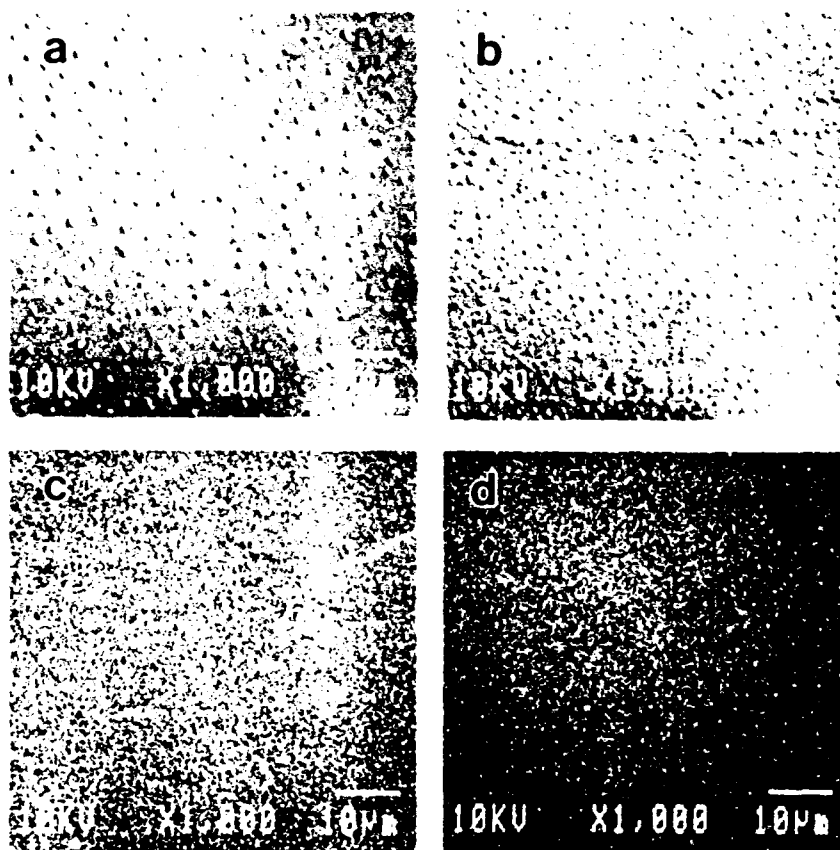


Figure 6.7. SEM micrographs of $\text{YBa}_2\text{Cu}_3\text{O}_{7-\delta}$ films deposited at (a) 720°C , (b) 680°C , and (c) 640°C ; and at (d) 680°C but Cu deficient.

adatoms.

SEM photographs of these films reveal the presence of surface precipitates distributed across the film surface, shown in Fig. 6.7(a-d). Energy dispersive X-ray analysis reveals that these precipitates are copper-rich. Note that the size and areal density of these precipitates is a strong function of the substrate temperature. The film shown in Fig. 6.7(d) was grown under nominally the same conditions as that shown in Fig. 6.7(b) (i.e., 680°C and 1 mTorr O₂). However, the film related to Fig. 6.7(d) has a much lower density of precipitates than the others. RBS analysis reveals that the Y:Ba:Cu composition of this film is 1.13:1.93:2.93. This is closer to the stoichiometric composition than the other films, but is slightly Cu-deficient (at no expense to the critical temperature).

The surface precipitates observed by SEM, determined to be Cu-rich using EDX analysis, must be eliminated. It is clear from Fig. 6.7 that the substrate temperature affects both the areal density and size of the precipitates, for a given film composition. One explanation is that at higher substrate temperatures, the surface diffusion length increases, resulting in larger precipitates spaced farther apart, as we observe. The film shown in Fig. 6.7(d), deposited at 680°C with 1 mTorr O₂, has a significantly smaller amount of precipitates than the others. The only difference observed between this film and the others shown in Fig. 6.7 is its composition, measured to be 1.14:1.93:2.93 for Y:Ba:Cu. This composition is much closer to being stoichiometric than the others, while being slightly Cu-deficient. This reveals the importance of film composition in determining the surface precipitate density. So, although the deposition temperature (and the oxygen pressure) affect the precipitate density and size, the film composition is a controlling factor. It appears that a slight Cu deficiency is required to eliminate these precipitates. This general trend was observed in co-evaporated films reported by Chew et al.,³⁸ although they also mention that 'pitting' can occur in Cu-deficient films. (The reason for the composition difference of the film in Fig. 6.7(d), compared to the others shown in Fig. 6.7 (listed in Table 6.2), is not known for certain. However, this film was deposited many runs before the others, and slight changes in the target surface

may have occurred. There is no indication of any effects on the films' resistivity or T_C .)

If multilayered superconductor devices are to be successful, any surface precipitates must be eliminated, as well as minimizing the roughness caused by occurrence of the screw dislocation growth mode. It would be virtually impossible to grow continuous layers on the order of 1 nm thick on surfaces dominated by the screw dislocation growth mechanism. These surface morphology issues appear to be common for codeposited YBCO films using vacuum deposition techniques.

6.5 Conclusions

In this part of our study, we have demonstrated that both the O_2 pressure and the substrate temperature can affect the T_C and lattice parameter of $YBa_2Cu_3O_{7-\delta}$ films. We have also shown how the substrate temperature affects the degree of epitaxy on (100) MgO substrates, and the film surface morphology. In general, our results are similar to those obtained by researchers using other sputtering techniques, although our films appear to be slightly smoother. Film properties can only be considered 'optimal' when the electrical properties are good, and any surface precipitates are eliminated. The elimination of surface precipitates is still an issue which has not been successfully solved by any researchers depositing $YBa_2Cu_3O_{7-\delta}$ films.

Chapter 7

Multi-layered film structures

In this chapter, our results of multilayered film structures are presented. Cross-sectional TEM analysis is the main technique employed to verify the structural integrity of each layer. Three multilayer structures are presented here: $\text{YBa}_2\text{Cu}_3\text{O}_{7-\delta}$ / MgO / $\text{YBa}_2\text{Cu}_3\text{O}_{7-\delta}$ (on MgO substrates); $\text{YBa}_2\text{Cu}_3\text{O}_{7-\delta}$ / KNbO_3 (on MgO); and $\text{YBa}_2\text{Cu}_3\text{O}_{7-\delta}$ / YSZ / Si_3N_4 (on Si). The $\text{YBa}_2\text{Cu}_3\text{O}_{7-\delta}$ films discussed in this chapter were all deposited using a single, rotating, composite $\text{YBa}_2\text{Cu}_3\text{O}_{7-\delta}$ target.

7.1 $\text{YBa}_2\text{Cu}_3\text{O}_{7-\delta}$ / MgO / $\text{YBa}_2\text{Cu}_3\text{O}_{7-\delta}$ structures on MgO substrates

These superconductor-insulator-superconductor structures were deposited in order to study the feasibility of depositing Josephson junctions using $\text{YBa}_2\text{Cu}_3\text{O}_{7-\delta}$ and ion beam sputtering. The structures were deposited completely *in situ*. After depositing the first $\text{YBa}_2\text{Cu}_3\text{O}_{7-\delta}$ layer, a magnesium target was positioned directly in front of the $\text{YBa}_2\text{Cu}_3\text{O}_{7-\delta}$ target, and an MgO film was produced by reactive sputtering. The Mg target was then pulled away (with the ion beam off), allowing for the deposition of the next $\text{YBa}_2\text{Cu}_3\text{O}_{7-\delta}$ layer. The layer thicknesses were monitored using a quartz crystal resonator. MgO was chosen as an insulator layer for several reasons. MgO is proven as a chemically compatible material to $\text{YBa}_2\text{Cu}_3\text{O}_{7-\delta}$, and thin MgO layers have successfully been used to fabricate low- T_c Josephson junctions.

Several experiments were performed to examine the multilayer integrity as a function of MgO thickness. Figure 7.1 shows a cross-sectional TEM micrograph of a structure having an 80 Å MgO layer. In Fig. 7.1(a), a low magnification image is shown, and in 7.1(b) an atomic resolution image is shown. (These film layers were deposited at 680°C with 0.4 mTorr oxygen, and a 1200 eV krypton ion beam.) Note that the top and bottom $\text{YBa}_2\text{Cu}_3\text{O}_{7-\delta}$ layers are c-axis oriented, although the MgO layer reveals separate grains of different orientations. We believe that

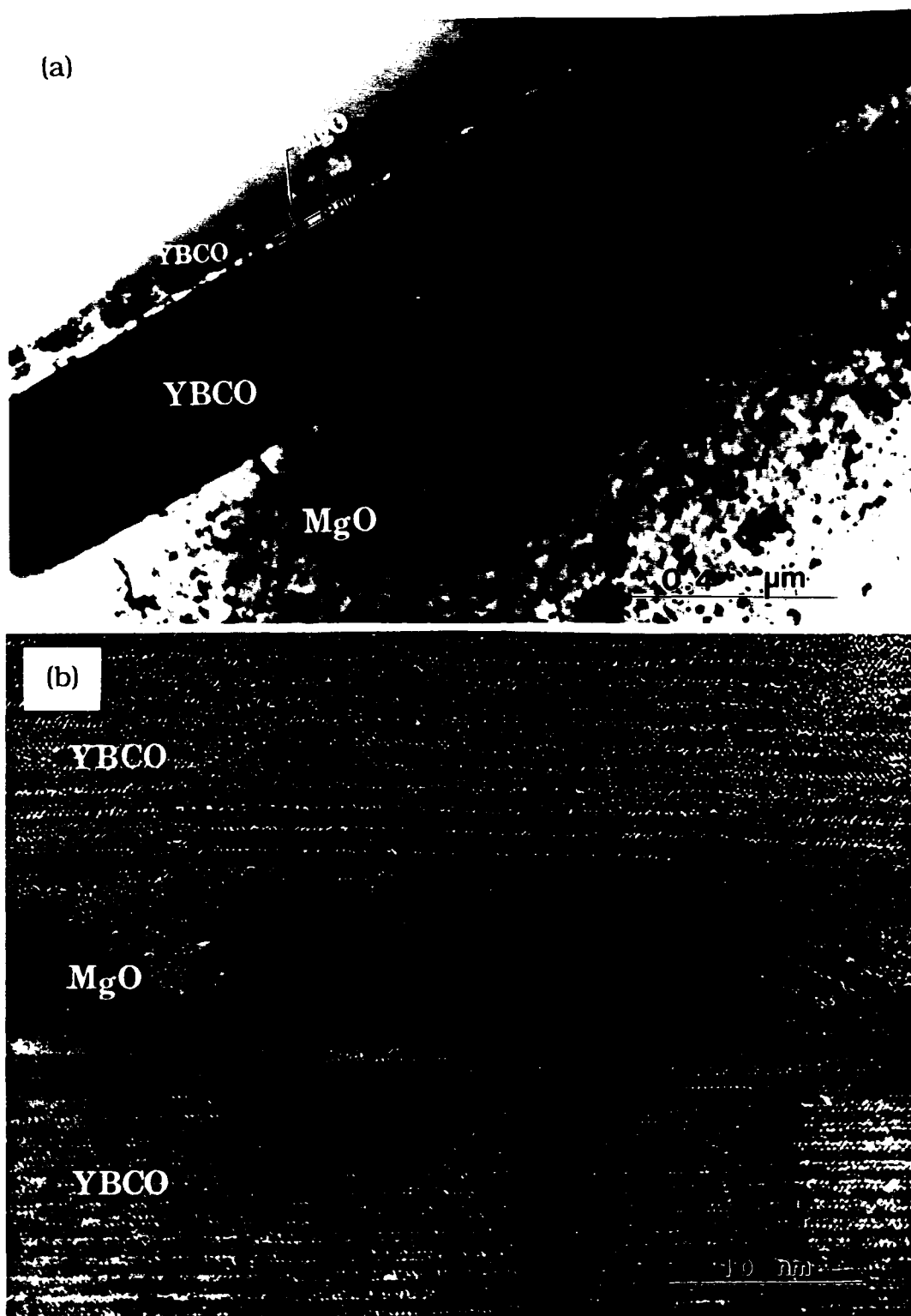


Figure 7.1. Cross sectional TEM micrograph of a YBa₂Cu₃O_{7-δ} / MgO / YBa₂Cu₃O_{7-δ} structure, at (a) low magnification and (b) high mag., atomic resolution. The MgO layer is about 80 Å thick.

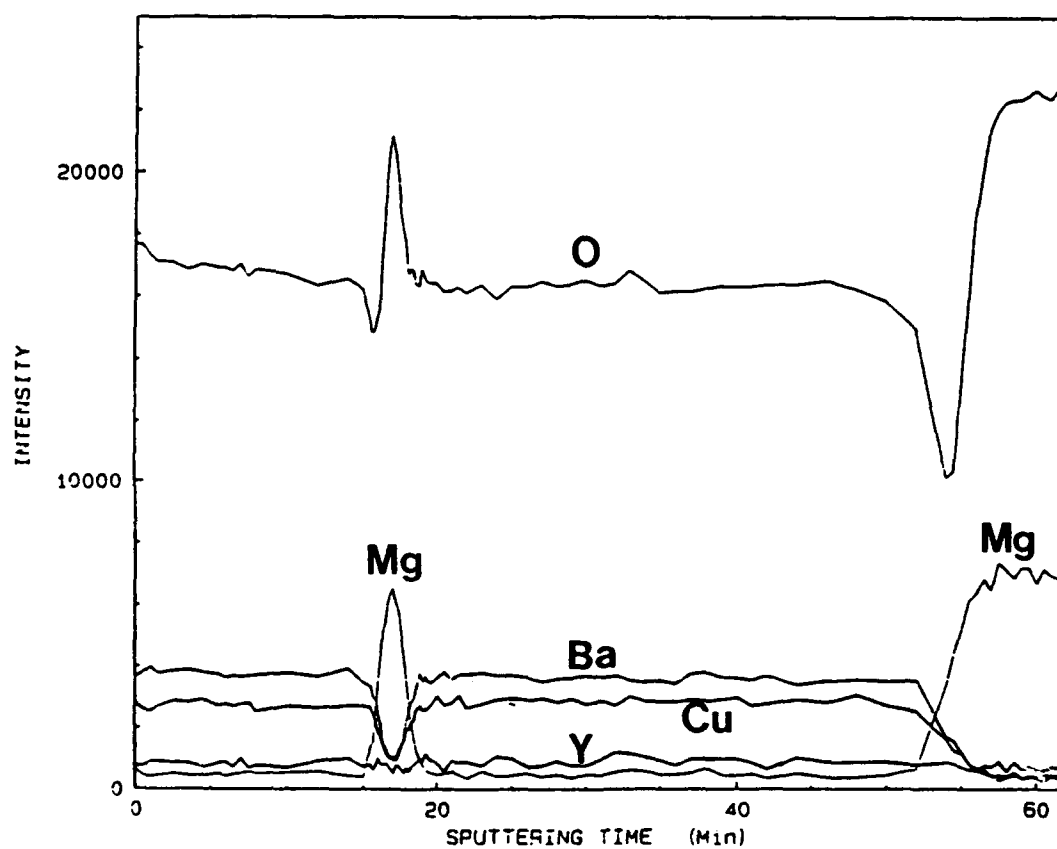


Figure 7.2 AES sputter-depth profile of a YBa₂Cu₃O_{7-δ} / MgO / YBa₂Cu₃O_{7-δ} structure, with an 80 Å thick MgO layer.

the fast lateral growth of the $\text{YBa}_2\text{Cu}_3\text{O}_{7-\delta}$ a-b planes can explain this occurrence. The Auger electron spectroscopy (AES) sputter-depth profile of this sample is shown in Fig. 7.2, verifying that the Mg has not interdiffused with the $\text{YBa}_2\text{Cu}_3\text{O}_{7-\delta}$ (a sputter-depth profile will never have completely sharp interfaces due to ion mixing and surface roughness effects).

Presently, attempts to grow thinner MgO layers (50 Å and 20 Å) have been unsuccessful. Cross-sectional TEM revealed that layers were not continuous in this thickness range. More work is necessary to study the optimum deposition conditions for MgO films. Although some groups have reported epitaxial MgO films on $\text{YBa}_2\text{Cu}_3\text{O}_{7-\delta}$,³⁹ many groups are concentrating on more complex insulating layers such as SrTiO_3 ⁴⁰ and $\text{PrBa}_2\text{Cu}_3\text{O}_{7-\delta}$.⁴¹ Although no group has obtained S/I/S junctions with $\text{YBa}_2\text{Cu}_3\text{O}_{7-\delta}$, these better lattice matched materials are probably the best hope. However, for other multilayer device structures not requiring an extremely thin insulating layer, we have shown that MgO may be appropriate.

7.2 $\text{YBa}_2\text{Cu}_3\text{O}_{7-\delta}$ / KNbO_3 layers on MgO substrates

This particular layer combination was investigated for a number of reasons. KNbO_3 is cubic, with a lattice parameter falling between those of $\text{YBa}_2\text{Cu}_3\text{O}_{7-\delta}$ and MgO. Therefore, a better lattice match is obtained by depositing $\text{YBa}_2\text{Cu}_3\text{O}_{7-\delta}$ on KNbO_3 as compared to on MgO directly. KNbO_3 also has promising ferroelectric and electrooptic properties; showing compatibility with $\text{YBa}_2\text{Cu}_3\text{O}_{7-\delta}$ is a first step towards device integration. KNbO_3 films used for this study were deposited by computer-controlled ion beam sputter-deposition in this laboratory, but in another deposition chamber. X-ray diffraction and plan-view TEM show that these films grow epitaxially on (100) MgO. For a complete description of deposition conditions, see Graettinger et al.²⁸

The $\text{YBa}_2\text{Cu}_3\text{O}_{7-\delta}$ films were deposited using a 500 eV Xe ion beam, a substrate temperature of 680°C, and an O_2 pressure of 10 mTorr. We chose this substrate temperature to minimize the possibility of interdiffusion, but still give reasonable $\text{YBa}_2\text{Cu}_3\text{O}_{7-\delta}$ electrical properties.

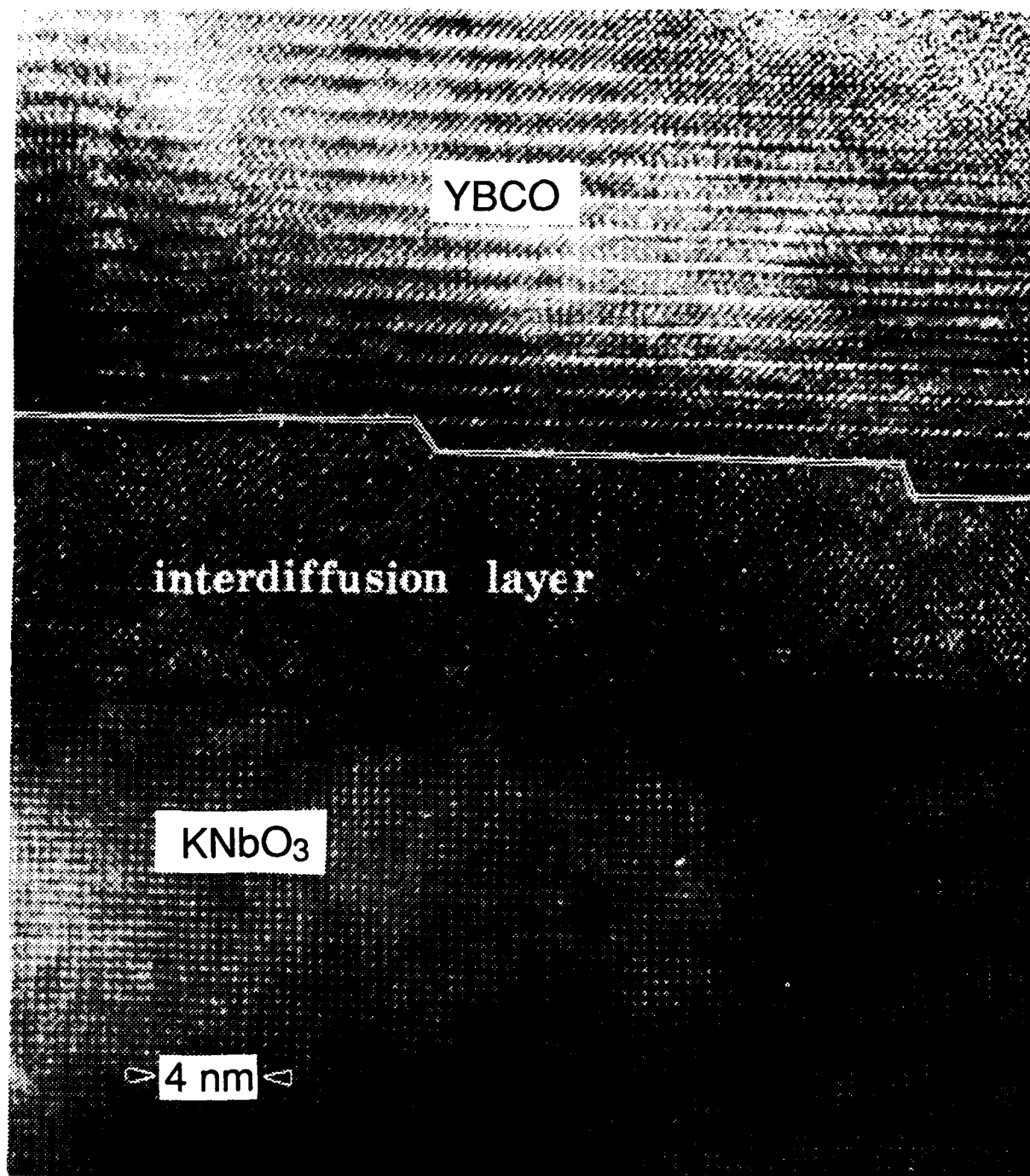


Figure 7.3. Cross sectional TEM micrograph of a $\text{YBa}_2\text{Cu}_3\text{O}_{7-8}$ / KNbO_3 structure on MgO . Both films are epitaxially oriented with respect to the MgO . Notice that a thin epitaxial reacted layer separates the two layers.

A cross-sectional TEM micrograph of this structure is shown in Fig. 7.3. This reveals that both films are epitaxially oriented, although there is a thin reaction layer between the two films. The orientation is confirmed by the X-ray diffraction pattern shown in Fig. 7.4. The 00 l peaks of YBa₂Cu₃O_{7- δ} appear, as do the h 00 peaks of the KNbO₃ (preceded by a 'K' in the figure). In Fig. 7.5, the susceptibility of this YBa₂Cu₃O_{7- δ} film is shown as a function of temperature, revealing a T_c of 85 K. Although the transition is not extremely sharp, it reveals that the superconducting properties are still reasonably good. An RBS spectrum is shown in Fig. 7.6. Note that the K peak is symmetric and has a nice, flat top. This reveals that no significant K diffusion into the MgO or YBa₂Cu₃O_{7- δ} has occurred. (The Nb and Cu signals overlap, which gives some uncertainty in the obtained film compositions.)

This successful demonstration of the integration of these materials opens up the possibility for fabrication of integrated HTSC-ferroelectric and/or electrooptic thin-film-based devices.

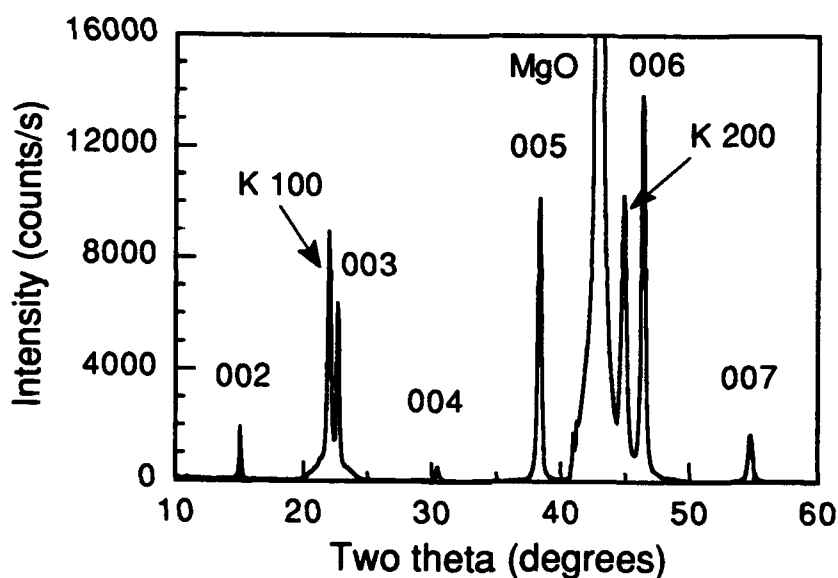


Figure 7.4 X-ray diffraction pattern of epitaxial YBa₂Cu₃O_{7- δ} on KNbO₃ on (100)MgO. Peak labels preceded by 'K' represent KNbO₃; the others are for YBa₂Cu₃O_{7- δ} .

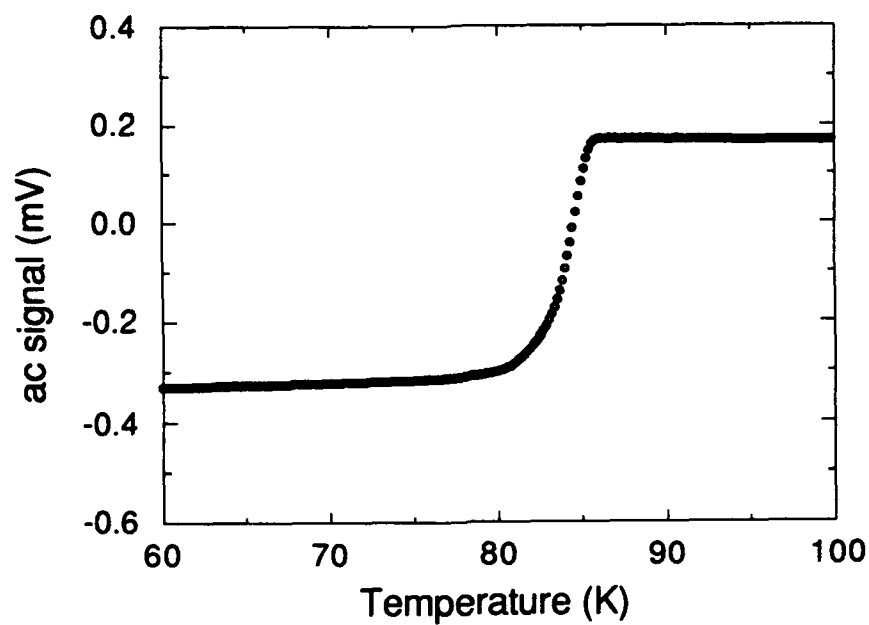


Figure 7.5 T_c of $\text{YBa}_2\text{Cu}_3\text{O}_{7-\delta}$ film on KNbO_3 , measured by the susceptibility change.

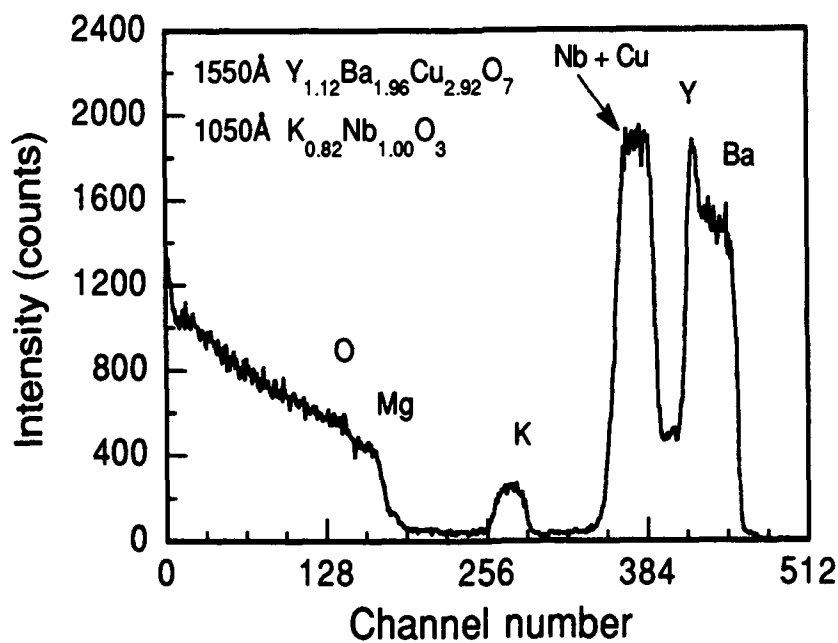


Figure 7.6 RBS spectrum of $\text{YBa}_2\text{Cu}_3\text{O}_{7-\delta}$ film on KNbO_3 on (100) MgO .

7.3 $\text{YBa}_2\text{Cu}_3\text{O}_{7-\delta}$ / YSZ / Si_3N_4 structures on Si substrates

$\text{YBa}_2\text{Cu}_3\text{O}_{7-\delta}$ films were deposited on YSZ (polycrystalline)/ Si_3N_4 (amorphous) films on silicon substrates in order to demonstrate their potential for use as bolometers. The substrates (with YSZ and Si_3N_4 films) were obtained from Honeywell Corporation; this particular substrate is necessary for optimum bolometer sensitivity.⁵ The requirement for the $\text{YBa}_2\text{Cu}_3\text{O}_{7-\delta}$ film is that it have a reasonably large temperature coefficient of resistance [$\text{TCR} = (1/R) \cdot (\delta R / \delta T)$] at the device operating temperature (for example, 77K).

After ion-beam sputter-deposition of the $\text{YBa}_2\text{Cu}_3\text{O}_{7-\delta}$ film (at 700°C with 5 mTorr O_2), the integrity of the structure was examined using cross-sectional TEM analysis. The electron micrograph in Fig. 7.7 reveals the fairly sharp interfaces between the layers. The thin YSZ layer prevents interdiffusion between $\text{YBa}_2\text{Cu}_3\text{O}_{7-\delta}$ and Si, while the Si_3N_4 layer serves as a thermal isolation membrane for each bolometer 'pixel' in the final device.⁵ The electrical properties of the $\text{YBa}_2\text{Cu}_3\text{O}_{7-\delta}$ layer are shown in Fig. 7.8. The superconducting transition onset is at 87 K, with zero resistance at 66 K. A bolometer operating at 77 K (LN_2 temperature) would have a TCR of ~ 0.15 , quite acceptable for device design specifications. The x-ray diffraction pattern of this film (Fig. 7.9) reveals that the $\text{YBa}_2\text{Cu}_3\text{O}_{7-\delta}$ grew c-axis oriented, even though the YSZ was polycrystalline. (It has proven very difficult for any researchers to deposit the highest quality $\text{YBa}_2\text{Cu}_3\text{O}_{7-\delta}$ on non-single crystal substrates.)



Figure 7.7 Cross-sectional TEM micrograph showing the $\text{YBa}_2\text{Cu}_3\text{O}_{7-8}$ / YSZ / Si_3N_4 structure on Si. The YSZ (the thinnest layer) is 600 Å thick.

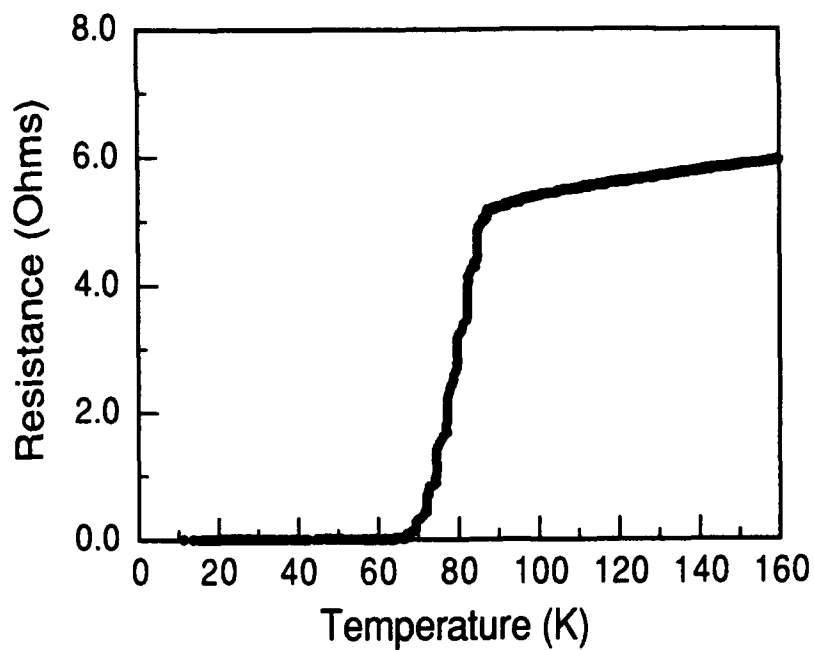


Figure 7.8 Resistance measurement of $\text{YBa}_2\text{Cu}_3\text{O}_{7-\delta}$ film on YSZ.

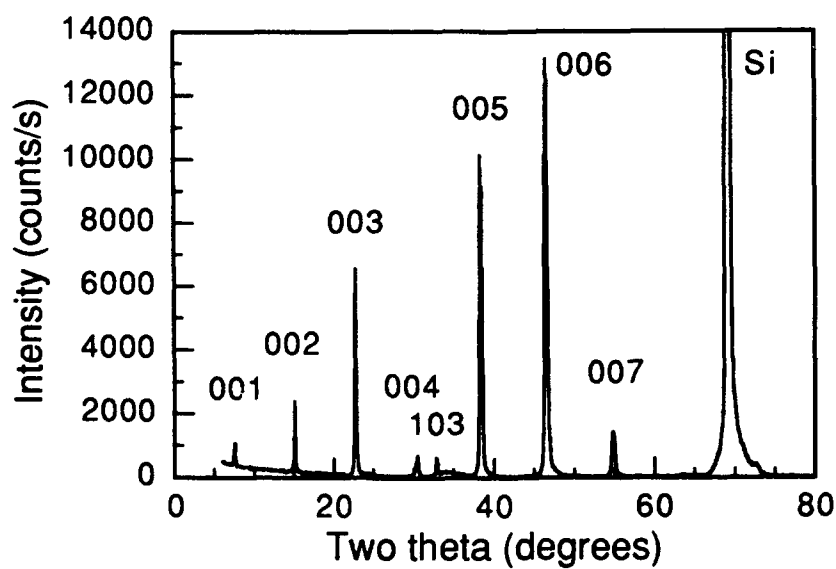


Figure 7.9 X-ray diffraction pattern of $\text{YBa}_2\text{Cu}_3\text{O}_{7-\delta}$ film on YSZ.

7.4 Conclusions

In this chapter, our results show that ion-beam sputter-deposition can be successfully used to deposit layered structures. Sputtering targets are easily interchanged *in situ* because the plasma source and target are independent when using ion-beam sputtering. We demonstrated successful $\text{YBa}_2\text{Cu}_3\text{O}_{7-8}$ film growth on KNbO_3 films on MgO , and on $\text{YSZ} / \text{Si}_3\text{N}_4$ films on Si .

$\text{YBa}_2\text{Cu}_3\text{O}_{7-8} / \text{MgO} / \text{YBa}_2\text{Cu}_3\text{O}_{7-8}$ structures were fabricated having 80 Å MgO layers. This demonstrates a possibility for producing multi-level SC devices on one wafer. Very thin (<60 Å) MgO layers were studied for Josephson junction applications, but were discontinuous, presumably due to the deposition conditions. Because ion beam sputtering is a fairly energetic technique, it is likely that very thin (~10 Å) layers would suffer due to bombardment-induced interface mixing effects. However, this question has not been definitively answered.

Chapter 8

Demonstration of uniform $\text{YBa}_2\text{Cu}_3\text{O}_{7-\delta}$ deposition over 4" diam (unheated) silicon wafers

The deposition of superconducting films with uniform thickness and composition over large area substrates is crucial for the fabrication of many superconducting^{5,42} and hybrid superconducting / semiconducting devices. Although high quality films of $\text{YBa}_2\text{Cu}_3\text{O}_{7-\delta}$ (and other high- T_c materials) have been deposited *in situ* using techniques such as pulsed laser ablation,⁴³ and off-axis magnetron sputtering,⁴⁴ it has been proven difficult to deposit uniform films over large areas due to certain limitations characteristic of these deposition techniques. A detailed discussion of the difficulties related to large-area deposition is given in Ref. [45].

8.1 Experimental

A 3-cm diameter Kaufman-type ion source is used to sputter a (commercially obtained) stoichiometric $\text{YBa}_2\text{Cu}_3\text{O}_{7-\delta}$ target (10 cm diameter, 99.9% pure, 75% dense). Xenon was chosen as the ion source working gas in order to minimize energetic reflected atoms. A Xe flow of 1.6 sccm is used, resulting in a Xe pressure of 1.33×10^{-4} Torr. An oxygen gas flow of 2 sccm, added directly to the chamber during deposition, results in an O_2 pressure of 8.2×10^{-5} Torr. Films were deposited using a Xe^+ ion beam energy of 800 eV, and a beam current of 25 mA. The sputtering power used is fairly low (20 Watts), so excessive target heating is avoided (the target is not actively cooled). Films were deposited on 100 mm diameter Si wafers to determine the coating thickness and compositional uniformity over this area. The substrate temperature reaches about 150°C due to radiative heating from the ion source and target.

The system geometry for the large-area deposition is shown in Fig. 8.1. The ion beam is incident at 20° from the target normal. The substrate is positioned such that its center is positioned at a 30°

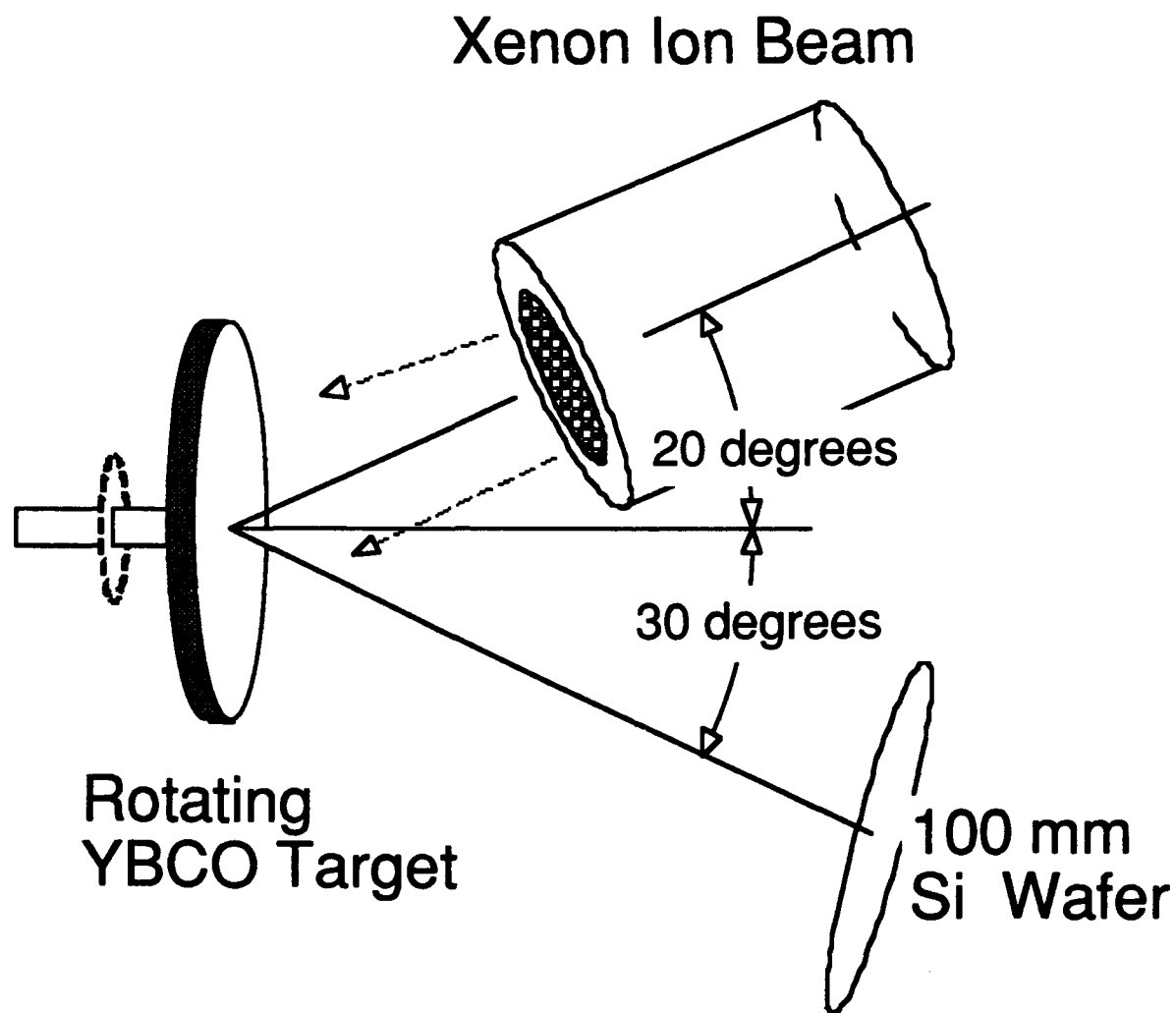


Figure 8.1. Schematic of the system geometry used for the ion-beam sputtering of a rotating, composite $\text{YBa}_2\text{Cu}_3\text{O}_{7-\delta}$ target, and deposition onto a 100 mm (4") diameter Si wafer.

angle with respect to the target normal, resulting in a 130° scattering angle (see Fig. 8.1). This deposition geometry allows the depositing flux distribution to be ~centered on the substrate, while maximizing the scattering angle of incident reflected Xe atoms (thus minimizing their energy). Constant target rotation (30 rpm) is used during deposition to eliminate the development of a rough surface topography, which can alter the sputtered flux distribution.²¹ The beam to target distance is about 9 cm, and the target to substrate distance is nearly 22 cm. With this geometry, and the previously mentioned sputtering conditions, a deposition rate of about 0.85 nm/min. is obtained.

Analysis of the film thickness and composition was performed using Rutherford backscattering spectrometry (RBS). A 2 MeV He^+ beam energy was used (incident at a 6° tilt from the substrate normal), with the detector positioned at a 165° scattering angle. Spectra were recorded at the wafer center, and at 9, 18, 27, 36, 45, and 48 mm distances from the center in the $\pm X$ and Y directions, as shown on the wafer diagram in Fig. 8.2. Because these films are amorphous as deposited, the film density is not precisely known. Therefore, the film thickness obtained using RBS may not be extremely accurate, but the resolution will be unaffected, therefore percent changes in measured film thickness are still representative.

8.2 Results and discussion

To map out the thickness and composition across the 100 mm Si wafer, spectra were obtained at 9 mm intervals across the wafer (except for the outermost points at 48 mm from center), as shown in the wafer diagram in Fig. 8.2. The X -direction represents the horizontal direction with positive X moving away from the ion source (as shown in Fig. 8.1). The positive Y -direction is vertically upward. A typical RBS spectrum of an as-deposited YBCO film on Si is shown in Fig. 8.3. Use of an RBS simulation fit reveals the film thickness (181 nm) and cation composition ($\text{Y}_{1.04}\text{Ba}_{1.98}\text{Cu}_{2.98}$). The measured thickness distribution across the wafer

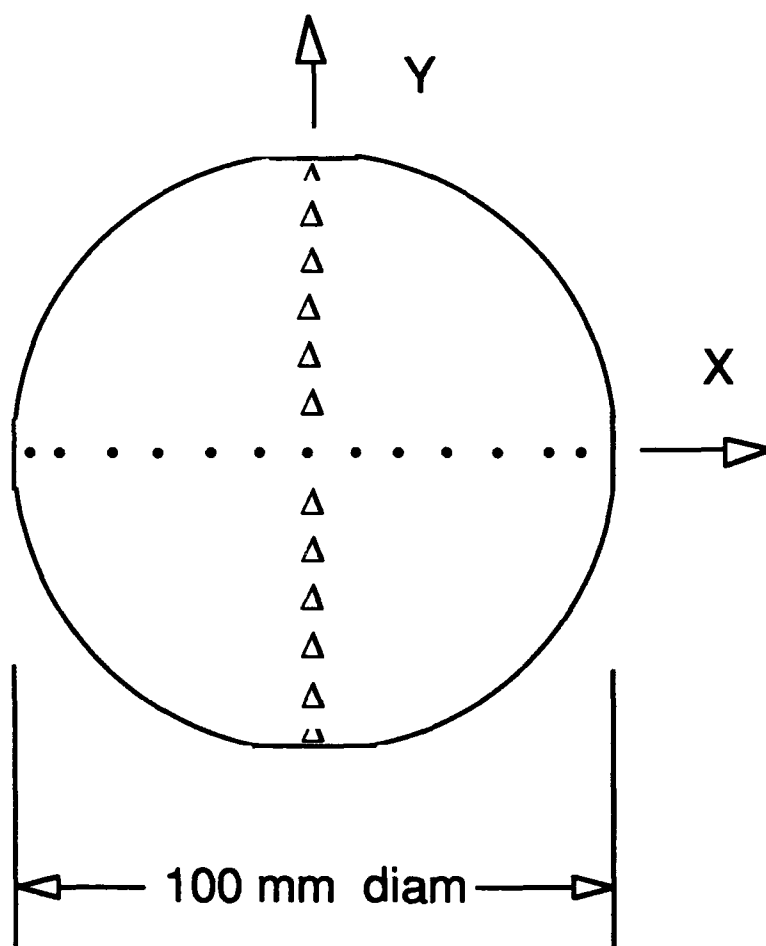


Figure 8.2. Wafer diagram showing the points at which RBS spectra were obtained to determine film thickness and composition. In relation to Fig. 8.1, the positive X-direction points away from the ion source, and the Y-direction points vertically upward.

is shown in Fig. 8.4, with the symbols representing the experimental data, and the solid line a cosine distribution, found to approximately fit the functional distribution of the depositing flux. The solid circles represent data obtained horizontally across the wafer (X-direction), with the open circles representing positions measured along the vertical plane. A thickness variation of $\pm 2.9\%$ was measured within a 3" diameter area. The cation composition distribution is shown in Fig. 8.5 (scaled to a sum of 6 cations per molecular formula). The solid symbols represent the composition along the X-direction, and the open symbols represent the composition obtained in the Y-direction (where no solid points are seen, they are overlapped by open symbols). The compositional variation of the Y, Ba, and Cu atoms within a 3" diameter area is found to be $\pm 0.9\%$, $\pm 5.2\%$, and $\pm 3.4\%$, respectively.

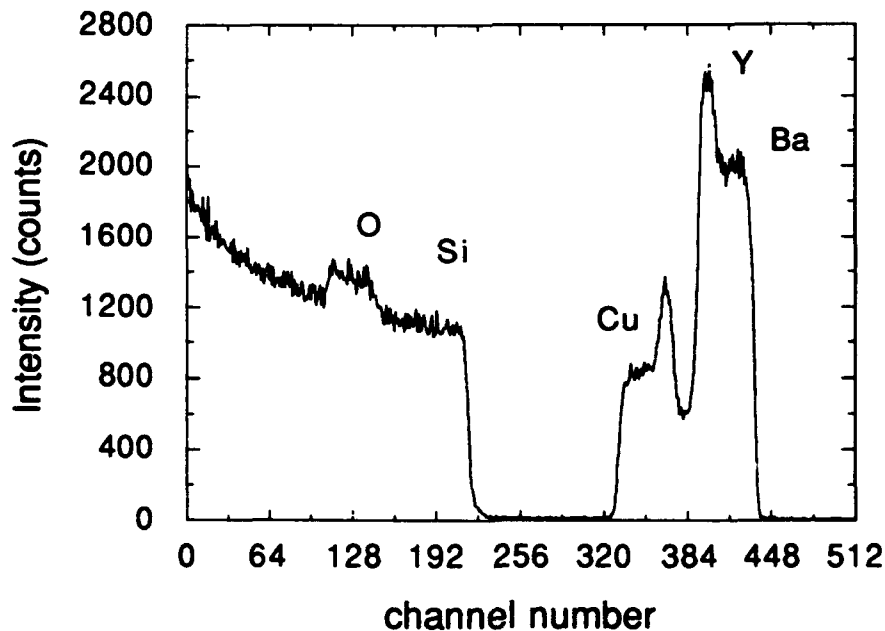


Figure 8.3. Typical RBS spectrum of the one position on the wafer. A spectrum simulation reveals that the film is 181 nm thick, with a cation composition ratio of $\text{Y}_{1.04}\text{Ba}_{1.98}\text{Cu}_{2.98}$.

Values of the thickness and composition variations across both the X and Y directions, over both 3" and 4" diameter areas are listed in Table 8.1. Note from the table, and from Figs. 8.4 and 8.5, that the variations are much larger in the X-direction than in the Y-direction.

The film thickness and compositional uniformity data shown in Table 8.1 and Figs. 8.4 and 8.5 reveals the applicability of ion-beam sputtering for deposition over large areas. The sputtered flux distribution is observed to follow a cosine relation, similar to what would be expected.¹⁸ Notice that no substrate movement is required to obtain this uniformity.

The film composition is fairly uniform over the 100 mm wafer, although the composition of each element, particularly Ba and Cu, shows a variation across the wafer. The slight deficiency of Ba over the entire substrate area is likely due to resputtering of the depositing film by reflected Xe and energetic sputtered species.

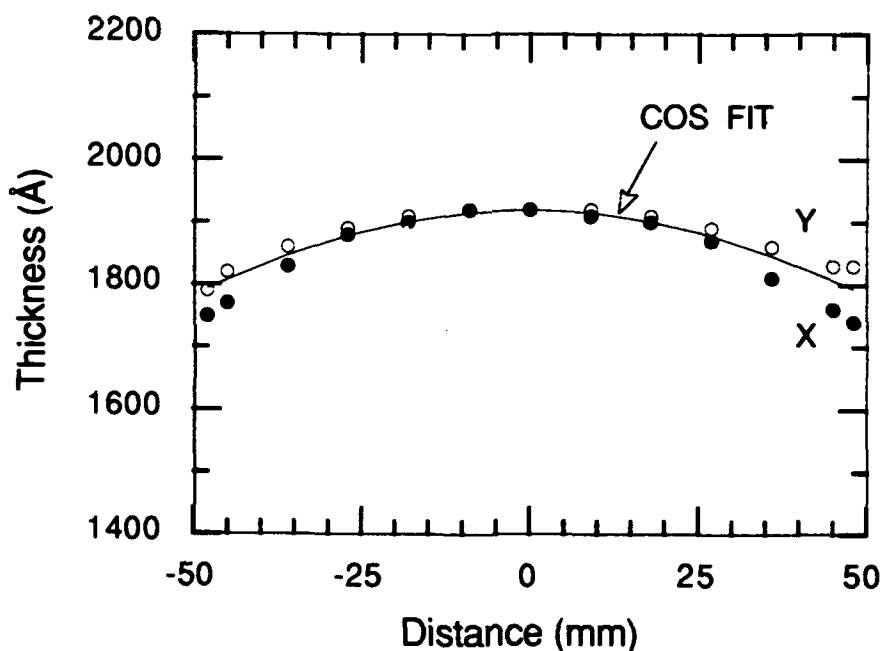


Figure 8.4. Film thickness distribution across the 100 mm (4") wafer measured using RBS. The solid circles and the open circles correspond to positions measured along the X and Y directions, respectively.

However, resputtering can be ruled out as a cause for the observed compositional variation shown in Fig. 8.5. Resputtering would reduce both the Ba and Cu preferentially, but some film areas are rich in Cu compared to the Y composition. Also, the fact that the deficiencies in Cu and Ba appear at (horizontally) opposite sides of the substrate eliminate resputtering as the mechanism responsible. We believe that the observed compositional variation (most pronounced along the X-direction) is caused by a difference in the angular flux-distribution of the sputtered Y, Ba, and Cu. Differences in the angular distribution of the sputtered species would arise because the ion beam is not incident normal to the target, and the masses of Y, Ba, and Cu differ. The developing collision cascade will then be nonuniform, since the energy transferred to different elements will depend on the mass of their neighbors. The composition data along the X-direction indicate

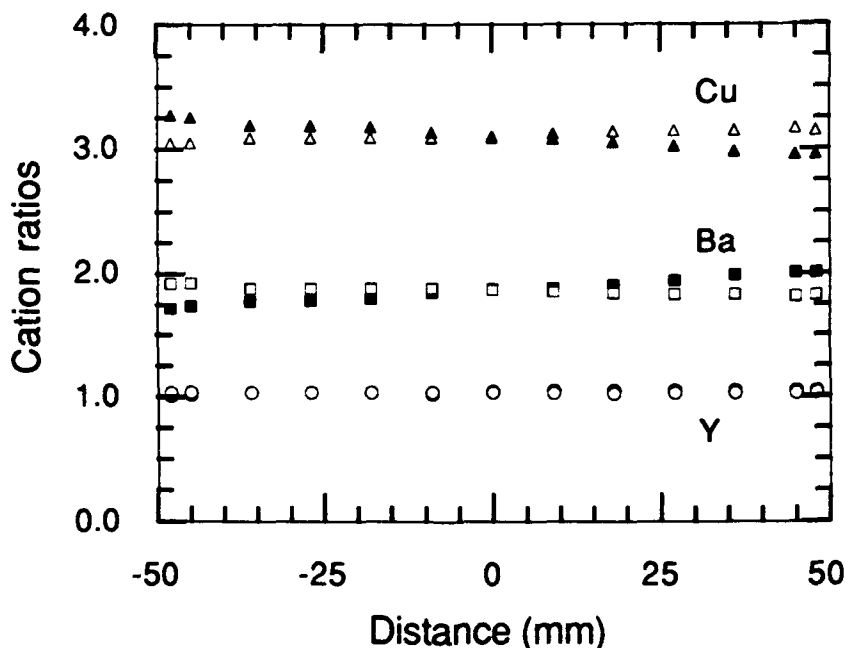


Figure 8.5. Cation composition ratios across the 100 mm (4") wafer measured using RBS. Compositions shown are for positions indicated on the wafer diagram, along both the X (solid symbols) and Y (open symbols) directions.

Table 8.1. Film thickness and compositional variations along the horizontal (X) and vertical (Y) directions for 3" and 4" diameter substrate areas.

Percent variation	Thickness	Composition		
		Y	Ba	Cu
3" diam area				
X-direction	±2.9 %	±0.9 %	±5.2%	±3.4 %
Y-direction	±1.6 %	±0.7 %	±1.3 %	±0.8 %
4" diam area				
X-direction	±4.7 %	±1.7 %	±7.1 %	±4.2 %
Y-direction	±3.4 %	±0.7 %	±2.9 %	±1.8 %

that the Cu distribution peaks closest to the target normal, followed by the Y, with the Ba distribution peaking farthest from the target normal (in the positive X-direction). Table 8.1 reveals that less of a difference in the film composition is observed in the Y-direction. This is expected, since the ion beam is ~normal to the target vertical.

Continuous substrate rotation could be used to improve the composition uniformity, but would not eliminate the drop in thickness at the outer edge of the substrate. To improve the coating uniformity, or to deposit over even larger areas, the process is readily scaleable using a larger diameter ion beam, and a larger area target. The main difficulties involved when scaling the process to larger areas pertain to the use of *in situ* deposition. Because the sticking coefficients of Ba and Cu decrease with increasing substrate temperature, we find that nonstoichiometric targets are required to deposit stoichiometric films when depositing on

heated substrates (although stoichiometric targets produce ~acceptable results). Composition control can also be accomplished by sequentially sputtering from multiple elemental targets, which we are presently studying. Other difficulties pertaining to the use of *in situ* deposition on large substrates lie in uniformly heating large substrates in vacuum, and providing a uniform oxygen activity over the substrate. These issues must be addressed regardless of the deposition technique used. (As we showed in Chap. 6, obtaining a uniform oxygen flux at the substrate shouldn't be a problem, since we could operate with a background chamber pressure of 1 mTorr oxygen.)

One possible way to avoid these issues altogether is to deposit on unheated substrates, and to obtain the superconducting phase using an appropriate post-deposition anneal. Recent results indicate that very high quality films can be obtained using annealing temperatures and O₂ pressures similar to those used during *in situ* deposition.⁶

8.3 Conclusions

In this report, we have shown that ion-beam sputtering of a stoichiometric YBa₂Cu₃O_{7-δ} target can readily be used to uniformly coat large area substrates. Using a 3 cm diameter ion source and a 10 cm diameter target, films have been deposited which have a thickness uniformity over a 3" diameter area of ±2.9%, and a compositional uniformity of ±0.9% Y, ±5.2% Ba, and ±3.4% Cu. Scaling up the process to improve uniformity and increase the coating area for ambient temperature film deposition is straightforward. The scale-up for deposition using heated substrates, and possibly active oxygen sources, is more difficult, but can be accomplished. Deposition onto unheated substrates is much easier from a processing standpoint, especially if both sides of the wafer need coating, and would be viable for certain applications if suitable post-deposition annealing treatments can be exploited.

Chapter 9

Project summary and conclusions

In this project we have studied the processing issues and properties of $\text{YBa}_2\text{Cu}_3\text{O}_{7-\delta}$ thin films deposited using ion-beam sputtering. The project involved constructing a deposition system specifically designed for computer-controlled ion-beam sputter-deposition from multiple targets. The processing-property relationships of *in situ* deposited $\text{YBa}_2\text{Cu}_3\text{O}_{7-\delta}$ thin films have been studied, using either a single $\text{YBa}_2\text{Cu}_3\text{O}_{7-\delta}$ compound target or multiple targets (Y, BaF, and Cu).

Deposition from either a single $\text{YBa}_2\text{Cu}_3\text{O}_{7-\delta}$ target or from multiple elemental targets have been shown to be feasible for producing superconducting $\text{YBa}_2\text{Cu}_3\text{O}_{7-\delta}$ films. Under presently optimized conditions, films deposited on (100) MgO have a T_c of 85 K, and a J_c (12 K) of 1×10^7 A/cm². We have determined that the processing conditions which are critical for obtaining good film properties include: 1) the ion beam energy and gas type (500 eV Xe); 2) the substrate temperature ($\geq 680^\circ\text{C}$); and 3) the oxygen pressure at the substrate (≥ 1 mTorr). These are parameters which we have definitely determined to be critical. It is likely that other yet undetermined parameters are also important for optimization of the T_c .

Growth of $\text{YBa}_2\text{Cu}_3\text{O}_{7-\delta}$ films using the multiple target approach, although shown to be feasible, does not seem to be advantageous over single-target deposition. (However, we also have to recognize that due to particular research program needs, we were forced to spend less time investigating the deposition process when using multiple elemental targets.) Unlike other compounds, the properties of $\text{YBa}_2\text{Cu}_3\text{O}_{7-\delta}$ thin films do not seem to be hindered by being significantly off-stoichiometric. Therefore, the use of a single target provides a close-enough film composition to obtain good film properties, with good reproducibility. Also, the oxygen flux to the substrate is critical. With single-target sputtering, the oxygen flux remains constant throughout the deposition; but with sequential deposition, the oxygen flux varies,

since some of the oxygen comes from the target surface. As shown by results from other researchers, single target sputtering of $\text{YBa}_2\text{Cu}_3\text{O}_{7-\delta}$ has emerged as a more reliable technique than multi-source approaches, although there may be particular applications where a multi-target approach is advantageous.

The growth of several multi-layered structures has been successfully demonstrated in order to show the versatility of the ion-beam sputtering technique. We have deposited 1) $\text{YBa}_2\text{Cu}_3\text{O}_{7-\delta}$ / (80 Å) MgO / $\text{YBa}_2\text{Cu}_3\text{O}_{7-\delta}$ structures on (100) MgO , 2) $\text{YBa}_2\text{Cu}_3\text{O}_{7-\delta}$ on KNbO_3 on (100) MgO , and 3) $\text{YBa}_2\text{Cu}_3\text{O}_{7-\delta}$ on YSZ / Si_3N_4 on silicon. The $\text{YBa}_2\text{Cu}_3\text{O}_{7-\delta}$ / MgO / $\text{YBa}_2\text{Cu}_3\text{O}_{7-\delta}$ structure demonstrates the feasibility for producing single-chip, multi-layered superconductor devices. Integrating $\text{YBa}_2\text{Cu}_3\text{O}_{7-\delta}$ with electrooptic KNbO_3 films opens an opportunity for new device types, and growth of the $\text{YBa}_2\text{Cu}_3\text{O}_{7-\delta}$ on YSZ has acceptable properties for use in bolometer devices.

We have also investigated the use of ion-beam sputter-deposition for coating large substrate areas. We have demonstrated (on unheated substrates) that over a 4" diameter area, a thickness and compositional uniformity of about $\pm 5\%$ is obtained. Ways to improve the uniformity have been identified. Further investigation is therefore warranted to fully optimize the ion-beam sputter-deposition techniques to produce high quality, reproduceable $\text{YBa}_2\text{Cu}_3\text{O}_{7-\delta}$ thin films.

Chapter 10

Acknowledgments

This research effort was carried out, for the most part, by the following research team: Dr. Daniel J. Lichtenwalner (post-doctoral researcher), Clifford N. Soble II, René R. Woolcott Jr., and Dr. Michael S. Ameen (post-doctoral researcher, presently at MRC Corporation, NY).

Other important contributors include Dr. H.S. (Alex) Rou and Dr. Kim Christensen (for TEM analysis), and Thomas M. Graettinger (for the design of some system components).

Useful insights and discussions from Dr. A.R. Krauss (Argonne National Laboratory), Dr. Nalin Parikh (University of North Carolina - Chapel Hill), Dr. David Haase (NCSU Physics Dept.), and Richard Chapman and Roland Adu-Poku (Microelectronics Center of North Carolina) are greatly appreciated.

Chapter 11

References

1. M.K. Wu, J.R. Ashburn, C.J. Torng, P.H. Hor, R.L. Meng, L. Gao, Z.J. Huang, Y.Q. Wang, and C.W. Chu, *Phys. Rev. Lett.* **58**, 908 (1987).
2. T. Venkatesan, X.D. Wu, B. Dutta, A. Inam, M.S. Hegde, D.M. Hwang, C.C. Chang, L. Nazar, and B. Wilkens, *Appl. Phys. Lett.* **54**, 581 (1989).
3. W.G. Lyons, R.R. Bonetti, A.E. Williams, P.M. Mankiewich, M.L. O'Malley, J.M. Hamm, A.C. Anderson, R.S. Withers, A. Meulenberg, and R.E. Howard, *IEEE Trans. Magn.* **27**, 2537 (1991).
4. R.H. Ono, J.A. Beall, M.W. Cromar, T.E. Harvey, M.E. Johansson, C.D. Reintsema, and D.A. Rudman, *Appl. Phys. Lett.* **59**, 1126 (1991).
5. T.G. Stratton, B.E. Cole, P.W. Kruse, R.A. Wood, K. Beauchamp, T.F. Wang, B. Johnson, and A.M. Goldman, *Appl. Phys. Lett.* **57**, 99 (1990).
6. R. Feenstra, T.B. Lindemer, J.D. Budai, and M.D. Galloway, *J. Appl. Phys.* **69**, 6569 (1991).
7. V. Matijasevic, P. Rosenthal, K. Shinohara, A.F. Marshall, R.H. Hammond, and M.R. Beasley, *J. Mat. Res.* **6**, 682 (1991).
8. P.K. Gallagher, H.M. O'Bryen, S.A. Sunshine, and D.H. Murphy, *Mat. Res. Bull.* **22**, 995 (1987).
9. M.F. Barba, P. Ortega, E. Saiz, and J.S. Moya, *Mat. Lett.* **10**, 149 (1990).
10. D. Dimos, P. Chaudhari, J. Mannhart, and F.K. LeGoues, *Phys. Rev. Lett.* **61**, 219 (1988).
11. R. Gross, P. Chaudhari, M. Kawasaki, M.B. Ketchen, and A. Gupta, *Appl. Phys. Lett.* **57**, 727 (1990).
12. S.A. Wolf, V.Z. Kresin, *IEEE Trans. Magn.* **27**, 852 (1991).
13. P.G. Blauner, J.S. Ro, Y. Butt, and J. Melngailis, *J. Vac. Sci. Technol. B* **7**, 609 (1989).
14. J.T. Kucera, J.D. Perkins, K. Uwai, J.M. Graybeal, and T.P. Orlando, *Rev. Sci. Instrum.* **62**, 1630 (1990).

15. D.D. Berkley, B.R. Johnson, N. Anand, K.M. Beauchamp, L.E. Conroy, A.M. Goldman, J. Maps, K. Mauersberger, M.L. Mecartney, J. Morton, M. Tuominen, and Y-J. Zhang, *Appl. Phys. Lett.* **53**, 1973, 1988).
16. S.I. Shah and P.F. Carcia, *Appl. Phys. Lett.* **51**, 2146 (1987).
17. O. Auciello, M.S. Ameen, A.R. Krauss, A.I. Kingon, and M.A. Ray, *Mat. Res. Soc. Sym. Proc.* **157**, 287 (1990).
18. J.P. Biersack and W. Eckstein, *Appl. Phys. A* **34**, 73 (1984).
19. D.J. Lichtenwalner, A.C. Anderson, and D.A. Rudman, *J. Vac. Sci. Technol. A* **7**, 102 (1989).
20. H. Asano, M. Satoh, and T. Konaka, *Appl. Phys. Lett.* **58**, 2981 (1991).
21. J. Roth, in Proc. of the Symposium on Sputtering, ed. by P. Varga, G. Betz, and F.P. Viehböck, Vienna, Austria (1980).
22. J. Geerk, G. Linker, and O. Meyer, *Mat. Sci. Reports* **4**, 193 (1989).
23. M. Hawley, I.D. Raistrick, J.G. Beery, and R.J. Holton, *Science* **251**, 1587 (1991).
24. H.U. Krebs, Ch. Krauns, X. Yang, and U. Geyer, *Appl. Phys. Lett.* **59**, 2180 (1991).
25. A.C. Westerheim, L.S. Yu-Jahnes, and A.C. Anderson, *IEEE Trans. Magn.* **27**, 1001 (1991).
26. J.H. James, B. Dwir, M. Affrante, A. Münzer, T. Naucner, B.J. Kellet, and D. Pavuna, *Supercond. Sci. Technol.* **4**, S136 (1991).
27. A.I. Kingon, M.S. Ameen, O. Auciello, K.D. Gifford, H. Al-Shareef, T.M. Graettinger, S.H. Rou, and P.D. Hren, *Ferroelectrics* **116**, 35 (1991).
28. T.M. Graettinger, S.H. Rou, M.S. Ameen, O. Auciello, and A.I. Kingon, *Appl. Phys. Lett.* **58**, 1964 (1991).
29. G. Selvaduray and C. Zhang, *J. Mat. Res.* **7**, 283 (1992).
30. H. Ozkan, F.G. Karioris, E.R. Vance, J. Eridon, and L. Cartz, *Nucl. Instrum. Methods B* **46**, 291 (1990).
31. D.J. Lichtenwalner, Ph.D. dissertation, Massachusetts Institute of Technology (1990).
32. R.E. Somekh, *J. Vac. Sci. Technol. A* **2**, 1285 (1984).
33. H.S. Kwok and Q.Y. Ying, *Physica C* **177**, 122 (1991).

34. C.N. Soble II, Masters dissertation, North Carolina State University (1992).
35. D.S. Misra and S.B. Palmer, *Physica C* **176**, 43 (1991).
36. C.B. Eom, A.F. Marshall, S.S. Laderman, R.D. Jacowitz, and T.H. Geballe, *Science* **249**, 1549 (1990).
37. J.J. Cuomo and S.M. Rossnagel, *Nucl. Instrum. Methods B* **19/20**, 963 (1987).
38. N.G. Chew, S.W. Goodyear, J.A. Edwards, J.S. Satchell, S.E. Blankinsop, and R.G. Humphreys, *Appl. Phys. Lett.* **57**, 2016 (1990).
39. K. Sakuta, K. Asano, T. Awaji, S. Hashiguchi, and T. Kobayashi, *Jpn. J. Appl. Phys.* **29**, 1668 (1990).
40. L.P. Lee, K. Char, M.S. Colclough, and G. Zaharchuk, *Appl. Phys. Lett.* **59**, 3051 (1991).
41. C.B. Eom, A.F. Marshall, J.-M. Triscone, B. Wilkens, S.S. Laderman, and T.H. Geballe, *Science* **251**, 780 (1991).
42. W.G. Lyons and R.S. Withers, *Micro. J.* **33**, 85 (1990).
43. X.D. Wu, R.E. Muenchausen, S. Foltyn, R.C. Estler, R.C. Dye, C. Flamme, N.S. Nogar, A.R. Garcia, J. Martin, and J. Tesmer, *Appl. Phys. Lett.* **56**, 1481 (1990).
44. N. Newman, K. Char, S.M. Garrison, R.W. Barton, R.C. Taber, C.B. Eom, T.H. Geballe, and B. Wilkens, *Appl. Phys. Lett.* **57**, 520 (1990).
45. D.J. Lichtenwalner, C.N. Soble II, R.R. Woolcott Jr., O. Auciello, and A.I. Kingon, *J. Appl. Phys.* **70**, 6952 (1991).

Chapter 12

Publication and presentation list

12.1 Publications

1. "Study of the surface morphology and growth mode of of *in situ* ion-beam sputter-deposited $\text{YBa}_2\text{Cu}_3\text{O}_{7-\delta}$ thin films", D.J. Lichtenwalner, O. Auciello, R.R. Woolcott Jr, C.N. Soble II, R. Adu-Poku, R. Chapman, S.H. Rou, J. Duarte, and A.I. Kingon, to be published in J. Vac. Sci. Technol. A **10**(4), July/Aug. (1992).
2. "Uniform deposition of $\text{YBa}_2\text{Cu}_3\text{O}_{7-\delta}$ films over large areas using ion-beam sputtering", D.J. Lichtenwalner, C.N. Soble II, R.R. Woolcott Jr, O. Auciello, and A.I. Kingon, J. Appl. Phys. **70**, 6952 (1991).
3. "Development of an automated dual ion beam assisted process for superconducting oxide film deposition", C.N. Soble II, M.S. Ameen, S.H. Rou, R.R. Woolcott Jr, O. Auciello, A.I. Kingon, and A.R. Krauss, Nucl. Instrum. Methods B **59/60**, 155 (1991).
4. "Computer-controlled ion-beam deposition systems for high T_c superconductor and other multi-component oxide thin films and layered structures", A.R. Krauss, O. Auciello, A.I. Kingon, M.S. Ameen, Y.L. Liu, T. Barr, T.M. Graettinger, S.H. Rou, C.S. Soble II, and D.M. Gruen, Appl. Surf. Sci. **46**, 67 (1990).
5. "Studies on ion-scattering and sputtering processes relevant to ion-beam sputter-deposition of multicomponent thin films", O. Auciello, M.S. Ameen, A.R. Krauss, A.I. Kingon, and M.A. Ray, Mat. Res. Soc. Sym. Proc. **157**, 287 (1990).

6. "Studies on ion scattering and sputtering processes in ion-beam sputter-deposition of high T_c superconducting films: the optimization of deposition parameters", M.S. Ameen, O. Auciello, A.I. Kingon, A.R. Krauss, and M.A. Ray, Amer. Inst. Phys. Conf. Proc. **200**, 79 (1990).
7. "A review of basic phenomena and techniques for sputter-deposition of high-temperature superconducting films", O. Auciello, M.S. Ameen, A.R. Krauss, A.I. Kingon, and D.J. Lichtenwalner, Surf. Mod. Technol. **4**, 109, ed. by T.S. Sudharsan et al., TMS publishers, Warrendale, PA (1991).
8. "A critical analysis of deposition techniques and basic phenomena related to high-temperature superconducting thin films", O. Auciello, A.R. Krauss, A.I. Kingon, and M.S. Ameen, Scanning Microscopy **4**, 203 (1990).
9. "Computer-controlled ion-beam sputter-deposition of multicomponent oxides", A.I. Kingon, M.S. Ameen, O. Auciello, C.N. Soble II, T.M. Graettinger, and S.H. Rou, Amer. Cer. Soc. Conf. Proc. (1990).
10. "Ion-beam sputter-deposition of $YBa_2Cu_3O_{7-\delta}$: beam-induced target changes and their effect on deposited film composition", O. Auciello, M.S. Ameen, T.M. Graettinger, S.H. Rou, C.N. Soble II, and A.I. Kingon, Amer. Inst. Phys. Conf. Proc. **182**, 61 (1989).
11. " $YBa_2Cu_3O_{7-\delta}$ films deposited by a novel ion-beam sputtering technique", A.I. Kingon, O. Auciello, M.S. Ameen, S.H. Rou, and A.R. Krauss, Appl. Phys. Lett. **55**, 301 (1989).

12.2 Presentations

1. "Study of the surface morphology and growth mode of of *in situ* ion-beam sputter-deposited $\text{YBa}_2\text{Cu}_3\text{O}_{7-\delta}$ thin films", presented by O. Auciello, 38th National Sym. of the American Vacuum Society, Seattle WA (1991).
2. "Microstructure and properties of $\text{YBa}_2\text{Cu}_3\text{O}_{7-\delta}$ thin films synthesized using ion-beam sputter-deposition", poster presentation by R.R. Woolcott Jr. and C.N. Soble II, Materials Research Society Fall meeting, Boston (1991).
3. "Development of an automated dual ion beam assisted process for superconducting oxide film deposition", presented by C.N. Soble II, conference on Ion Beam Modification of Materials (IBMM), Knoxville, TN (1990).
4. "Studies on ion scattering and sputtering processes in ion-beam sputter-deposition of high T_c superconducting films: the optimization of deposition parameters", poster presentation by M.S. Ameen and O. Auciello, 36th National Sym. of the American Vacuum Society, Boston (1989).
5. "A critical analysis of deposition techniques and basic phenomena related to high-temperature superconducting thin films", presented by O. Auciello (invited), Scanning Electron Microscopy International Conference, Utah (1989).
6. "Computer-controlled ion-beam sputter-deposition of multicomponent oxides", presented by A.I. Kingon (invited), Amer. Ceramic Society Annual Symposium, Indianapolis, IN (1988).